iScience

CellPress
OPEN ACCESS

Review

Advanced perspectives on MXene composite nanomaterials: Types synthetic methods, thermal energy utilization and 3D-printed techniques

Yuanlong Cui,[1,*] Jie Zhu,[2] Hui Tong,[1] and Ran Zou[3,*]

SUMMARY

MXene, 2D material, can be synthesized as single flake with 1 nm thickness by using phase change material, polymer and graphene oxide. Meanwhile, the MXene and its composite derivative materials have been applied widely in electro-to-thermal conversion, photo-to-thermal conversion, thermal energy storage, and 3D printing ink aspects. Furthermore, the forward-looking utilization of the MXene nanomaterials in hydrogen energy storage, radio frequency field application, CO_2 capture and remediation of environmental pollution, is explored. This article reveals that the efficiencies of the photo-to-thermal and electro-to-thermal energy conversions with the MXene nanomaterials could reach about 80–90%. In parallel, it is demonstrated that the MXene printed ink has the excellent rheological property and high viscosity and stability of liquid, which contribute to arranging the multi-dimensional architectures with functional materials and controlling the flow rate of the MXene ink in the range of 0.03–0.15 mL/min for speedily printing and various printing structures.

INTRODUCTION

Human-induced climate change has caused more energy consumption and serious environmental damage.[1] At present, frontier research on energy-saving technology and environmental protection solution face challenges in the efficiency, stability, durability and function of significant materials.[2,3] As a result, the development of multi-functional materials with exceptional performance contributes to increasing energy conversion/storage and decreasing greenhouse gas emission. Since the development of single layer graphene, two-dimensional (2D) materials have attained marvelous concern owing to their distinctive properties involved in their bulk form. In terms of the mechanical, optical, electrical and thermal physical properties, the extraneous properties of graphene, mechanically exfoliated from graphite, designated via thinning down the thickness of three-dimensional (3D) nanomaterials to 2D atomically thin sheets, can be amended deeply.[4–6] This ground-breaking finding critically proliferates the focus on the characterizations and synthesis of high quality 2D nanomaterials beyond graphene.[4] Herein, the graphene has been regarded as a reference for all 2D materials and unfolded the potential to explore even more. Recently, there are fascinating 2D nanomaterials like silicene,[7,8] borophene,[9] germanene,[10] layered double hydroxides,[11,12] transition metal dichalcogenides (TMDs),[13–15] transition metal oxides (TMOs),[16,17] adding a big diversity with peculiar property to this 2D nanomaterial family, which are still escalating rapidly.

MXene history

The MXene is made from a bulk crystal called MAX phases which are layered, hexagonal carbides and nitrides, and have the common formula: M_{n+1} A X_n, where n = 1 to 3, M is an early transition metal, A is an A-group (mostly groups 13 and 14) element and X is either carbon and/or nitrogen. One of the most broadly studied materials is Ti_3AlC_2. When the Al from Ti_3AlC_2 is extracted, a novel 2D material called 'MXene' is produced which consists of transition metal carbides, nitrides and carbonitrides,[18,19] and the $Ti_3C_2T_x$ as the most typical representative has attracted an ever-increasing exploration attention.[20] Figure 1 presents a schematic diagram of the MXene development progress from 2011 to 2021.[21]

The first MXene was proposed based on the selective etching of aluminum (Al) from Ti_3AlC_2 using hydrofluoric (HF) acid approach in 2011.[22] Subsequently, various sorts of MXenes were produced in 2012 including $Ti_3C_2T_x$, Ti_2CT_x, V_2CT_x, Nb_2CT_x, $Nb_4C_3T_x$ and $Ta_4C_3T_x$,[23,24] and became a large family of

[1]School of Architecture and Urban Planning, Shandong Jianzhu University, 1000 Fengming Road, Jinan 250101, China

[2]Department of Architecture and Built Environment, The University of Nottingham, Nottingham NG7 2RD, UK

[3]School of Management Engineering, Shandong Jianzhu University, 1000 Fengming Road, Jinan 250101, China

*Correspondence: cuiyuanlong22@sdjzu.edu.cn (Y.C.), zouran19@sdjzu.edu.cn (R.Z.)

https://doi.org/10.1016/j.isci.2022.105824

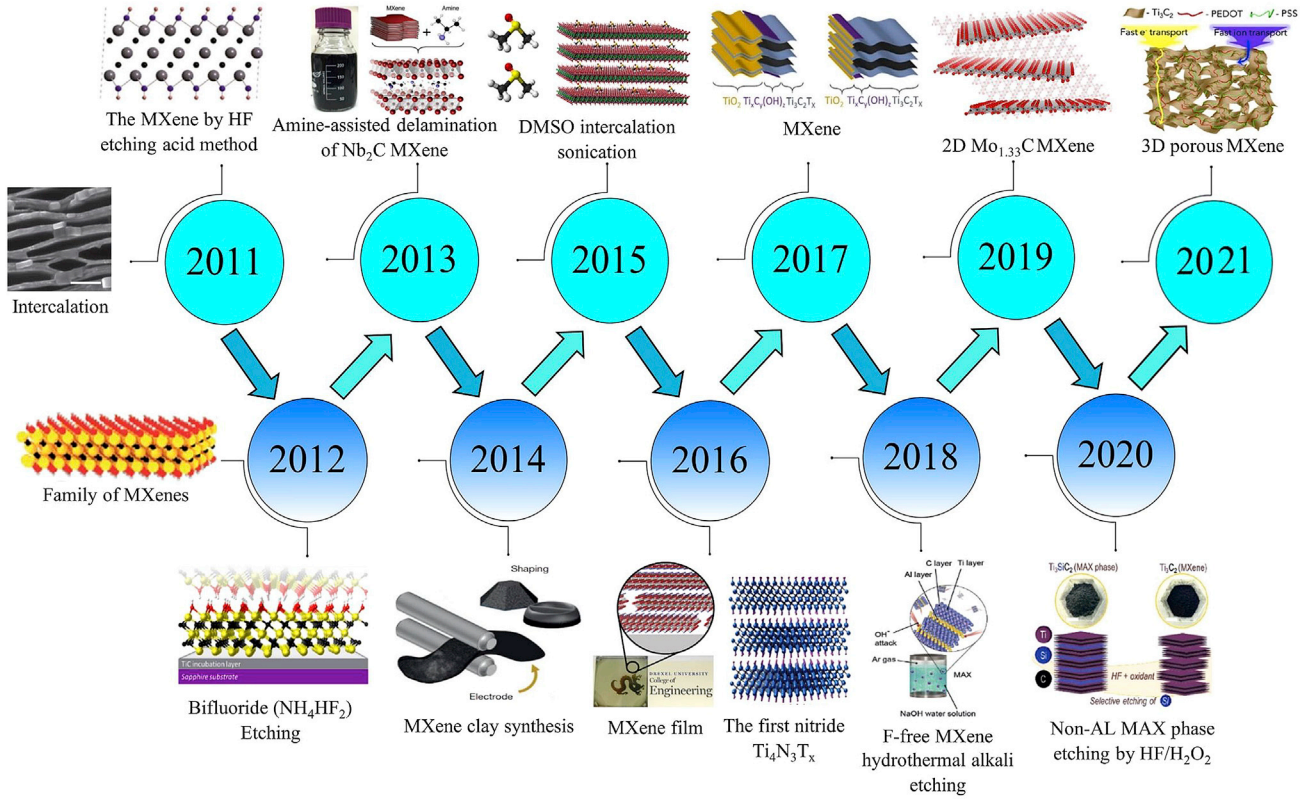

Figure 1. Schematic diagram of timeline development of MXene from 2011 to 2021[21]
Reproduced with permission from (Alhabeb et al., 2014), Copyright 2017 American Chemical Society.

transition metal carbonitrides and carbides.[25] A single layer of MXene was first compounded in 2013 by using the intercalation and delamination with organic molecule modes.[26] Afterward, in 2014, the MXene was etched by a mixture of LiF and HCl[27] and ammonium bifluoride[28] in place of highly concentrated and hazardous hydrofluoric acid solution. In 2015, large scale delamination of MXene was achieved via the amine-assisted[29] and tetrabutylammonium hydroxide (TBAOH) methods[30] whereas the two ordered double-transition metal MXenes were proposed by using the dimethyl sulfoxide (DMSO) intercalation.[31] In 2016, the transparent thin MXene film was fabricated based on the spray coating method[32,33]; meanwhile, the first nitride MXene, $Ti_4N_3T_x$, was proposed by using fluoride molten salt etching method.[34] In 2017, the MXene with ordered divacancies ($Mo_{1.33}CT_x$) was realized by removing both Al and Sc atoms from a chemically in-plane ordered quaternary MAX phase.[35] Also, the oxidation stability of the MXene solution was studied to fabricate novel composite MXene for various applications.[36] In 2018, the F-free MXene was attained via hydrothermal alkali etching.[37] In addition, the MXene from non-Al MAX (Ti_3SiC_2) was described by using hybrid of the HF and H_2O_2 as etchant.[38] Afterward, different researches were reported in 2019, such as adopting MXene-metal oxides, MXene-polymers and MXene-carbon for various applications, representing composite MXene as cutting-edge hybrid material for multidisciplinary applications.[39–41] Specifically, the porous MXene/conducting polymer materials for flexible alternating current (AC) filtering electrochemical capacitors were investigated.[39] Acetonitrile was utilized as the solvent to exclude the anodic oxidation of MXene during the deposition of polymer poly (3,4-ethylenedioxythiophene) (PEDOT) onto MXene film.[40,41] In 2020, the possibility of producing F-terminated MXene by a water-free etching manner based on ammonium dihydrogen fluoride and polar organic solvent was obtained. This water-free etching of the MXene could make it possible to utilize MXene and its nanocomposites within different water-sensitive applications.[42] In 2021, a 3D porous MXene@ rGO (graphene oxide) film as flexible electrode was fabricated through self-propagating method.[43]

As the nanoscale precursor MXene materials have two vital characteristics, i.e., various structures and unique properties. Figure 2 exhibits different nanostructures of the MXene materials like nanoflowers,[44–46]

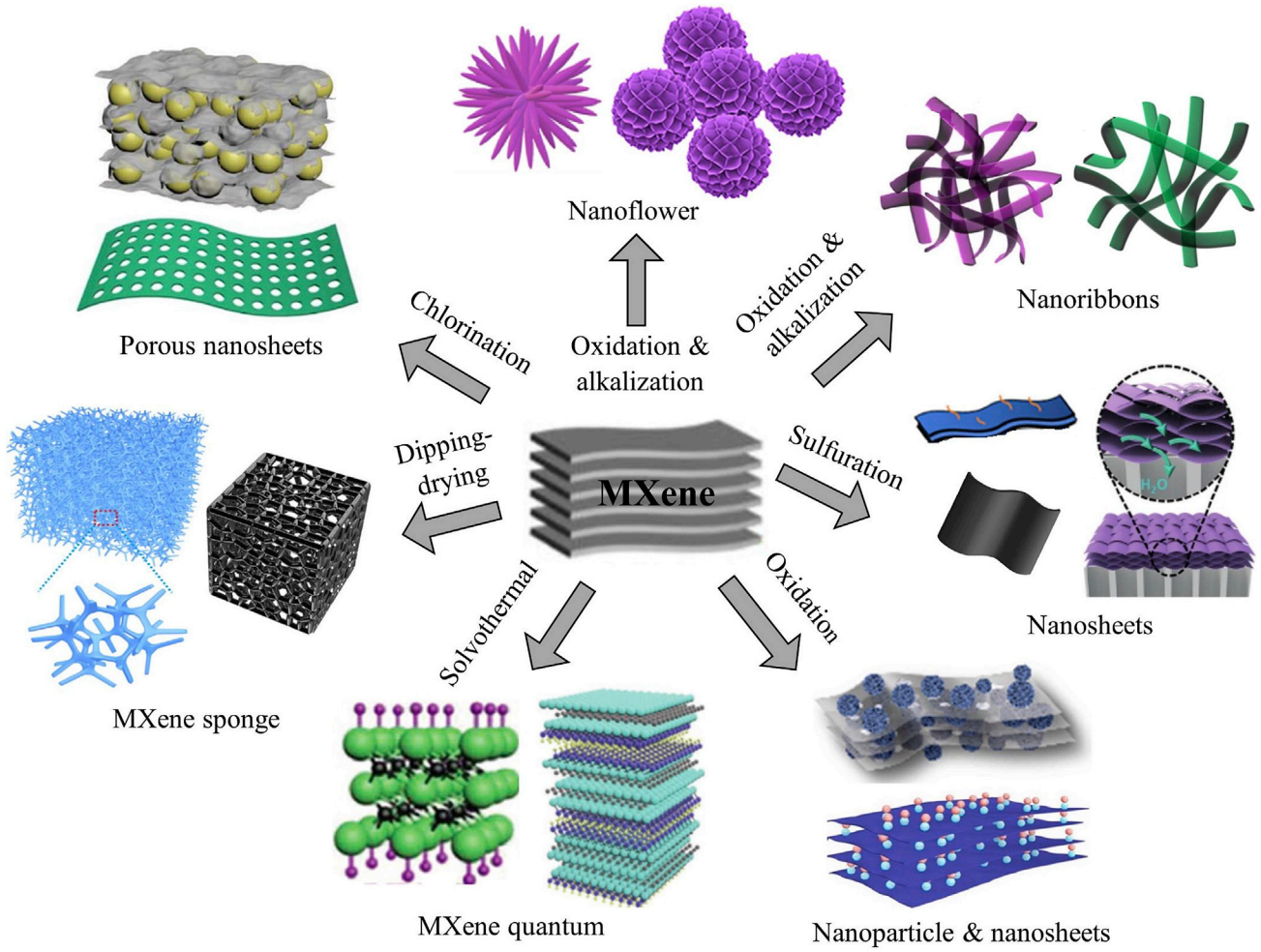

Figure 2. Different structures of MXene derivative materials[47,49,53,55,58]

Reproduced with permission from (Dong et al., 2017), Copyright 2017 American Chemical Society; (Xu et al., 2018), Copyright 2018 Wiley; (Zhao et al., 2019), Copyright 2019 Wiley-VCH GmbH, Weinheim; (Yue. et al., 2018), Copyright 2018 Elsevier; (Zhang et al., 2019), Copyright 2019 Elsevier.

nanoribbons,[47,48] quantum dot,[49,50] nanosheets,[51,52] porous nanosheets,[53,54] MXene sponge[55,56] and nanosheets and nanoparticles.[57,58] The synthesis solutions, involving oxidation and alkalization, sulfuration, solvothermal chlorination and dipping-drying, can be used to obtain these structures. Until now, the MXene-based materials were largely classified into MXene composite materials including MXene@ PCM, MXene@ polymer, MXene@ graphene oxide, MXene@ carbon nanotubes, MXene@ metal and MXene-based mixture solutions like MXene@ oil, MXene@ ionic liquid and MXene@ water, which are associated with the unique 2D structure of MXene precursors. This indicates that the MXene has great potential to synthesize other materials. Because Gogotsi's group synthesized successfully the first MXene material in 2011, it was paid much attention in light of its structure, chemical, magnetic, electronic and mechanical properties.[22,59] Similar to graphene, the MXene has good flexibility, 2D morphology and especial layered structure. In addition, the MXene material could be exfoliated to become a single nanosheet via ultrasonic approach, which has sufficient accessible surfaces. This indicates that it could supply an excellent substrate to realize zero-dimensional nanoparticles, 1D nanowires, combining with 2D nanosheet to obtain 3D hybrid structure.

MXene properties

The MXenes have versatile intrinsic properties, like an outstanding metallic conductivity that derives from additional density of electron at the Fermi Level,[60] hydrophilicity because of plentiful water-loving polar surface terminations,[25] and readily solution process ability without any requirement of dispersing agents.[20]

This unique structure and excellent properties make them favorable in different utilizations involving electromagnetic interference (EMI) shielding,[61–63] terahertz shielding,[64–66] optoelectronics,[33] flexible and transparent electrodes,[32,67] sensors,[68] thermal heaters,[69] light-emitting diodes (LEDs),[70,71] antibacterial films,[72] ion batteries storage,[73,74] additive for lubricating,[75] supercapacitors,[76] catalyst[77] and water treatment.[78] Except mechanical, optical and electronic properties, the MXene displays great thermal physical properties, which spends much interest in the field of heat transfer. Bao et al.[79] investigated thermal physical properties of ethylene glycol (EG) based nanofluids by adding 5 vol % of single and multi-layer MXenes, and concluded that thermal conductivities of the two types could be improved 64.9 and 53.1%, respectively. Meanwhile, when the volume concentration is below 1%, the MXene exhibits a great self-lubricating property, and single layer MXene@ EG nanofluid has no obvious sedimentation within one month and keeps good stability. Lu et al.[80] compounded a polyethylene glycol (PEG) @ MXene with PCM material, and found that its thermal conductivity is 7.2 times higher compared to the pure PEG's. Aslfattahi et al.[81] introduced the MXene in PCM to increase thermal physical properties. Their results display that the thermal conductivity could be enhanced by 16% when the MXene concentration is 0.3 wt % within the PCM. Jin et al.[82] made the MXene@ PVA (polyvinyl alcohol) films via multi-layered casting, and demonstrated that its thermal conductivity is about 23 times greater in comparison with the PVA's because of continuous MXene layer. In the meantime, it is stability in terms of the MXene dispersed in aqueous solution owing to its inherent hydrophilicity.[83,84] Nowadays, about 70 MAX phases are revealed, merely a few MXenes could be developed via the chemical etching method.[85] $Ti_3C_2T_x$ is the initial and the most representative MXene which attributes to its high aspect ratio, high thermal conductivity and outstanding hydrophilicity indicating it is a promising candidate in the world of the nanoparticle materials.

Moreover, the MXene has good application prospect because of attractive mechanical properties including tensile loading, fracture toughness and young modulus. Specifically, tensile strength is the maximum stress which is the limit between rupture and plasticity zones. It is found that the tensile strength of MXene mainly depends on the film thickness. Luo et al.[86] demonstrated that the elastic modulus and tensile strength decrease from 17 GPa to 8 GPa and 61 MPa–36 MPa, respectively, when the thickness of MXene film is improved from 2.3 μm to 17 μm. Wang et al.[87] assembled MXene into different polymer materials for ameliorating the tensile strength of MXene, and found that the tensile strength of the MXene composite materials could reach up to 436 MPa when the thickness of MXene film is 1.2 μm. This is ascribed to the capability of hydrogen bonding to break and amend in the procedure of cyclic stretching, thus absorbing much more energy compared to ionic bonding. Meanwhile, the fracture toughness of MXene is regarded as a significant factor to describe the capacity of the composite materials to resist fracture. Liang et al.[88] demonstrated that the fracture toughness of ceramic is enhanced by 7.6 $MaPa \cdot m^{1/2}$ with the introduction of 3 wt % MXene, which is 36% greater compared to ceramics without any additives. Cai et al.[89] concluded that the fracture toughness of Al_2O_3 is increased by 300% owing to the addition of 2 wt % MXene. Wozniak et al.[90] demonstrated that the fracture toughness of SiC has a dramatically enhancement by 5 $MPam^{1/2}$ at 1.5 wt % of MXene in SiC, which is 2.7 times as high as the value of SiC. Furthermore, Young's modulus of MXene composite materials are utilized to measure the stiffness and resist to elastic deformation under loading. To be more specific, Firestein et al.[91] concluded that the Young's modulus of MXene nanosheet could reach 80–100 GPa when it is in the direction perpendicular to the Ti_3C_2. Yu et al.[92] introduced AZ91D magnesium (Mg) into the MXene, and revealed that the dynamic Young's modulus of MXene composite materials is reduced as the material surface temperature increases. Monastyreckis et al.[93] implemented a simulation investigation on adding MXene into epoxy materials for ameliorating the Young's modulus, and verified that the MXene@ epoxy with 30 vol % nanosheets contributes to boosting the Young's modulus from 1.5 to 8.2 GPa, indicating approximately 8.4 times compared to pure epoxy materials. Herein, the detailed mechanical property comparison of the MXene composite materials is exhibited in Table 1.

MXene stability

2D transition-metal nitrides and carbides (MXene) have attracted great attention because of the optical, electrochemical, chemical and electronic properties. Nevertheless, it is vital in terms of structural integrity and stability of the MXene, this is because that the MXene may experience different heat-treating processes in the preparation stage.[98] In particularly, the thermal instability is a significant issue that rigorously obstacles the huge industrial scale application of MXene materials.[99] Consequently, it is imperative to investigate the stability and elaborate the varying of MXene structure and properties based on various environmental factors. Seredych et al.[59] conducted the stability investigation of three kinds of MXene ($Ti_3C_2T_x$,

Table 1. Comparison of mechanical properties

Items		Mechanical properties			
Reference	Material	Tensile strength	Fracture toughness	Young modulus	Hardness
Luo et al.,[86]	$Ti_3C_2T_x$	36 to 61 MPa	N/A	8 to 17 GPa	N/A
Wan et al.,[87]	$Ti_3C_2T_x$	Up to 436 MPa	8.39 $MPam^{1/2}$	14.0 GPa	N/A
Liang et al.,[88]	MXene@ Si-B-C-N	207.9 to 233.7 MPa	5.62 to 7.62 $MPam^{1/2}$	102.3 to 146.6 GPa	N/A
Fei et al.,[89]	MXene@ SiC	30.58 to 160.51 MPa	1.52 to 6.55 $MPam^{1/2}$	1.82 to 13.90 GPa	1.82 to 13.90 GPa
Wozniak et al.,[90]	MXene@ Al_2O_3	N/A	3 to 5 $MPam^{1/2}$	N/A	25 GPa
Firestein et al.,[91]	Ti_3C_2	Up to 670 MPa	N/A	80-100 GPa	N/A
Yu et al.,[92]	MXene@ AZ91D (Mg)	165 to 215 MPa	N/A	42 to 69 GPa	N/A
Monastyreckis et al.,[93]	MXene@ PVA and	86.2 to 91 MPa	N/A	Up to 22 GPa	N/A
	MXene@ epoxy	34.8 to 80.3 MPa	N/A	Up to 66 GPa	N/A
Ye et al.,[94]	MXene@ Al_2O_3–silicone	0.117 MPa	N/A	N/A	N/A
Chen et al.,[95]	MXene@ Mo	N/A	117.4 to 123.3 $MPam^{1/2}$	N/A	N/A
Luo et al.,[96]	MXene@ CNF	142.2 MP	9.48 $MPam^{1/2}$	1.96 GPa	N/A
Hatam-Lee et al.,[97]	$Ti_{n+1}C_nO_2$ and $Ti_{n+1}N_nO_2$	9 to 24 MPa	14 to 72 $MPam^{1/2}$	130 to 520 GPa	N/A

Mo_2CT_x and Nb_2CT_x), and demonstrated that the $Ti_3C_2T_x$ is more thermally stable compared with Nb_2CT_x and Mo_2CT_x with few atomic layers, and Mo_2CT_x is less thermally stable compared with Nb_2CT_x. Li et al.[100] thought that the thermal stability of MXene could be sustained in the range from 20 to 800°C under argon (Ar) atmosphere condition. Meanwhile, Wang et al.[101] revealed that the thermal stability of MXene could reach up to 1200°C based on the same condition. To sum up, the thermal stability of MXene mainly relies on its composition, size and environmental condition.[102] It is found that the larger dimension of MXene contributes to enhancing the thermal stability and different types of MXene derivative materials display diverse stabilities based on the same condition,[20] whereas it is readily to occur the oxidation reaction when the MXene films are exposed to the atmospheric air environment.[103,104] Variation categories of degradation might rigorously destruct the structure integrity, which further restricts the lifespan and prevents the useful properties of MXene derivatives for future applications.[105] Specifically, Zhang et al.[36] synthesized the MXene flakes to avoid the oxidation reactions, and concluded that the MXene flake could sustain the 2D morphology with very clean edges and a neat surface. Kim et al.[106] made the UV–vis spectra of the MXene dispersion into water and deposited for 30 days, and revealed that the gradual progression of MXene dispersion oxidation, which is verified via an emerging peak of titanium dioxide (TiO_2) when the size is about 250 nm. Xia et al.[107] described the process of MXene oxidation based on an indoor temperature, where dispersion of synthesized MXene is reserved in tin (Sn)-wrapped vials to disregard the probability of light-induced oxidation. It is quite challenging to hinder the reaction of the MXene oxidation, particularly when they are transported from laboratory to industry for producing commercial goods. Consequently, the MXene derivative materials could facilitate the scientific community to explore the mechanisms and oxidation kinetics, which are conducive to exploiting novel solutions for refining the oxidation stabilities.

Currently, there are various approaches, such as the synthesis of minimal defective layered MXenes, polymeric composites of MXenes, organic dispersions or medium of MXenes and storage conditions for aqueous dispersion, which are utilized to ameliorate the oxidation stability and mechanical strength of the MXenes. The choice of the raw materials plays a vital role on the stability and conductive property of the MXenes.[108] Specifically, when the MXene ($Ti_3C_2T_x$) is synthesized by using graphite-based carbon raw material, it exhibits high conductivity reaching 4400 S/cm with good stability for approximately 10 days, by comparison, when the MXene ($Ti_3C_2T_x$) is produced based on the TiC-based carbon raw material, its conductivity is only 3480 S/cm and maintains 4.8 days' stability. Likewise, when the lampblack carbon source is utilized to make the MXene, the conductivity is merely 1020 S/cm with less 5.1 days of stability. Herein, it is indicated that the structure, oxidation stability and physiochemical MXenes properties are affected because of the quality of the MAX phase and steps of synthesis.[109] In addition, adding polymer into the MXene material is a favorable approach not only to enhance its oxidation stability, but also to ameliorate mechanical strength of the MXene structure. Specifically, Lee et al.[110] improved the oxidation stability through adding polydopamine composite materials. It is demonstrated that about 10wt %

concentration of the polydopamine contributes to decreasing the shrinkage resistance caused by the interlayer gap at elevated temperatures. Meanwhile, it is found that the MXene@ dopamine composite material could avert the penetration of humidity and oxygen, which is attributed to the binding between the hydroxyl groups of MXene flakes and catechol groups of dopamine. Huang and Mochalin[111] concluded that based on the oxygen and argon (Ar) atmospheric conditions, it has great stability when the MXene is dispersed into isopropanol. Zhang et al.[36] explored an efficient solution to ameliorate the oxidation stability of MXene by judging oxidation degrees based on various circumstances. It is found that the MXene oxidation stability is affected by the synergistic effect of low temperature and storage environment, which are conducive to prolonging and delaying the oxidation reactions. It is also demonstrated that the small flakes oxidize quicker compared to the larger ones, which is prevented in an argon (Ar) condition when the temperature is low. Zhao et al.[112] discovered the interaction between the particles of oxidation kinetics, and indicated that the pH value of acidic dispersions has a significant influence on the oxidation stability of the MXene. The professional and systematic assessments promote to extend the understanding of MXenes composite materials and enhance the potential utilization range. When the spotlight of the MXene derivative materials is boosted in light of its various structures, outstanding properties and potential utilizations, it is timely to have a progress summarization on the state-of-the-art of MXene composite materials.

To sum up, the MXenes have intrinsically outstanding volumetric capacitance and conductivity because they are molecular sheets made out of the nitrides and carbides of transition metals. It has already been verified that the MXenes could be applied ranging from energy conversion to medicine and optoelectronics fields. Therefore, some authors have summarized the MXene synthesis methods, properties and composites of MXenes, and investigated various fields of applications. Specifically, Zhan et al.[113] made an overview with regard to the synthesis solutions including one-step, etching, hydrothermal, and intensive layer delamination methods, but the multi-layered casting and two-step technique methods are not mentioned. Gong et al.[114] provided a summary in light of the synthesis approaches, properties, and performances of MXene@ polymer. Meanwhile, George and Kandasubramanian[115] and Faruk et al.[116] reported various applications of the MXene@ polymer composite materials in the biomedical aspects involving the antimicrobial medical bandaging and bone regeneration. Ma et al.[117] illustrated the latest developments of the MXene composite materials for wearable device applications including the facial expression, human motions and signature recognitions. Mahmud et al.[118] also explored the development of the MXene-based heterostructures and nano-hybrids which can be utilized in batteries, supercapacitors, electromagnetic absorption as well as environmental and water treatment. However, these above-mentioned researches have not explored thermal energy conversions like photo-to-thermal, electro-to-thermal, and thermal energy storage. Meanwhile, the advanced MXene-based 3D printing techniques have not been referred to as well. As a result, this article has laid emphasis on providing a bird's eye view on various categories of the MXene composite nanomaterials for thermal energy utilizations and 3D-printed techniques. In addition, it elaborates some perspectives for the opportunities and challenges in current research and viewpoints for future applications including the hydrogen energy storage, radio frequency fields application, carbon dioxide capture, remediation of environmental pollution analysis and recycled MXene composite materials. It is expected that this article could provoke the interests of researchers and build a vital avenue in terms of the MXene derivative material development for different application fields.

OVERVIEW OF MXENE COMPOSITE NANOMATERIALS

MXenes, such as $Ti_3C_2T_x$, fabricated with active terminal groups (-OH, F and =O) on its surface, contribute to interacting with polymers via hydrogen bonding and enhancing the low mechanical strength. In addition, the novel MXene composite materials, including MXene@ phase change material (PCM), MXene@ polymer, MXene@ graphene oxide (GO), MXene@ carbon nanotubes, MXene@ metal nanoparticles, and MXene-based mixture solutions involving MXene@ oil, MXene@ ionic liquid (IL), and MXene@ water, contribute to enhancing the specific heat capacity, thermal energy storage capacity, thermal and electrical conductivities as illustrated in the following section.

Types of MXene nanomaterials

MXene composite nanomaterials

MXene@ phase change materials. Phase change materials (PCMs), like conventional paraffin wax (PW) and polyethylene glycol (PEG), have very high energy storage capacity, repeated utilization, relaxed process control and cooling capacity.[119–121] This is because they can absorb and/or release an extraordinary

amount of latent heat because of a phase transition occurring within a specified temperature range. Moreover, the PEG has become a hotspot because of its moderate phase transition temperature, low expense and high phase transition enthalpy[122,123] and hydrophilic characteristics utilized in the physical energy cycle.[124,125] In fact, PEG is normal hydrophilic PCM employed in the physical energy cycle,[126,127] which owns high affinity with MXene and can serve as the medium for energy conversion and storage. However, PCM has the low thermal conductivity that causes a heat transfer resistance, and there is a risk of leakage during the process of the phase transition.[128,129] Henceforth, it is proved that the MXene@ PCM not only increases significantly its thermal conductivity and energy conversion ability, but also decreases the density of the composite nanomaterials.[130–132] To be more specific, Aslfattahi et al.[81] successfully synthesized the novel composite nanomaterials by adding MXene into the PCM (PW 70) to boost the thermo-physical properties. Their results reveal that the thermal conductivity and specific heat capacity of MXene@ PW 70 could be enhanced about 16 and 43% respectively at the concentration of 0.3 wt % of MXene. This is because of its 2D geometry, high surface area, negligible thickness of MXene flakes and particular planar structure. Meanwhile, Lin et al.[133] compounded a lightweight and high stable MXene@ polyethylene glycol (PEG) aerogel to investigate its structure property and thermal stability. As shown in Figure 3A, about 29–32 mg/cm^3 density of MXene@ PEG aerogel is synthesized by a mild wet chemical method under 70°C for avoiding oxidation and structural degradation of MXene. It is found from a scanning electron microscope (SEM) image that the MXene@ PEG aerogel has a cellular structure and its skeleton gradually varies from loose to dense; meanwhile, the porosity reduces with the declining of the MXene content as exhibited in Figure 3B. This is because the rigidity of the MXene as the heterogeneous components induces straightforwardly porous structure. Furthermore, in the light of the thermal stability, the actual solidification and fusion enthalpies of MXene@ PEG aerogels contributes to realizing comparatively high values of 141.51 and 167.72 J/g, respectively. Lu et al.[80] added the MXene into the PEG as a new composite phase change working substance for boosting its thermal properties, and actual photo of MXene@ PEG is exhibited in Figure 3C. To guarantee long-term utilization, the MXene@ PEG must have good reusability and thermal reliability, and the differential scanning calorimetry (DSC) curves could be consistent before and after 100 thermal cycles as described in Figure 3D. In addition, it can be concluded from Figure 3E that the MXene@ PEG thermal conductivity could reach 2.052 W/m·K, which is around 7.2 times compared to the pure PEG 0.285 W/m·K. On the other hand, the electrical conductivity of pure PEG is around 10^{-11} S/m, whereas the MXene@ PEG reaches 10.41 S/m. This indicates that the MXene@ PEG derivative material has higher thermal and electrical properties compared to the traditional PCM, which can help to enhance the light-to-thermal conversion efficiency and thermal energy storage ability. Fan et al.[134] developed a MXene@ PEG material to improve thermal energy storage efficiency at the UV-Vis-NIR region. As indicated in Figure 3F, the pure PEG, control group and MXene@ PEG with different concentrations of PEG are laid up within three constant temperatures. It can be observed that when the temperature is 95°C, the pure PEG and control group melted completely, whereas the MXene@ PEG (90%) had only a slight leakage. By comparison, the MXene@ PEG (80%) and MXene@ PEG (85%) could sustain their primitive shapes without any leakage. In addition, the DSC curves of the pure PEG, 80 and 85% loadings of the MXene@ PEG are given in Figure 3G, the melting temperature of the MXene@ PEG ranges from 61.3 to 62.1°C. This means that the MXene nanosheet has no influence on the phase change temperature of PEG. This can increase thermal energy storage efficiency up to 94.5% based on the actual solar radiation, which is higher than that of the normal PCM. Mo et al.[135] proposed a 3D porous material by combining PEG, MXene, and polyvinyl alcohol (PVA) to constitute high-performance MXene derivative material. It can be seen from Figure 3H that thermal conductivity of the MXene@ PVA/PEG reaches 0.428 W/(mK) which is 4.2 times greater compared to the PEG 2000's, resulting in an increasing of 423.8%. In addition, the phase change enthalpy of MXene@ PEG/PVA derivative material could reach 131.1 J/g with 96.5% efficiency, indicating high photo-to-thermal conversion efficiency and thermal energy storage capability.

MXene@ polymer. Introducing reinforced polymer elements into MXene to attain conductive polymer composites (CPCs) is a viable solution to solve the issues of oxidation and brittleness.[136,137] To be more specific, Jin et al.[82] fabricated the MXene@ poly vinyl alcohol as alternating multi-layered film structure to enhance thermal conductivity.

The SEM image in Figure 4A displays an excellent layer structure alternating continuous MXene and PVA layers. It can be obtained from Figure 4B that thermal conductivities of the MXene@ PVA-AM-7.5, 13.9 and 19.5 films could reach 2.31, 3.34 and 4.57 W/m·K, resulting in the increases of 1055, 1570, and 2275%, respectively, compared to the pure PVA 0.20 W/m·K. In addition, the MXene layer is conducive to

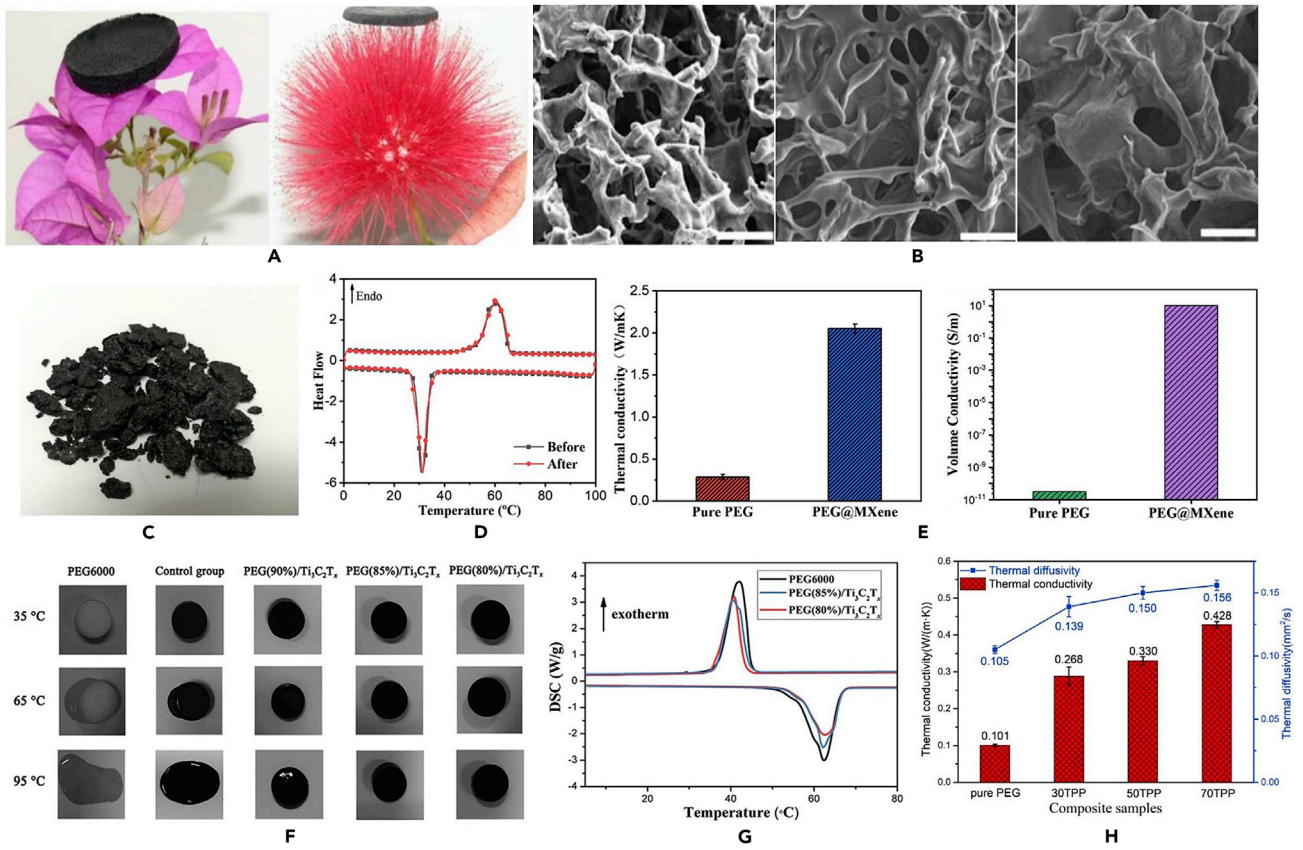

Figure 3. Synthesis of MXene@ PCM nanomaterials

(A) Actual images of the light weight of MXene@ PEG aerogels.

(B) SEM image of skeleton variation from lose to dense.[133] Reproduced with permission from (Lin et al., 2020), Copyright 2019 Elsevier.

(C) Actual photo of MXene@ PEG.

(D) DSC curves of MXene@ PCM after 100 thermal cycles.

(E) Thermal and electrical conductivities of MXene@ PEG.[80] Reproduced with permission from (Aslfattahi et al., 2020), Copyright 2020 Elsevier.

(F and G) Macroscopic morphology of pure PEG and different contents of the MXene@ PEG; (G) DSC curves.[134] Reproduced with permission from (Fan et al., 2019), Copyright 2019 The Royal Society of Chemistry.

(H) Thermal diffusivity and thermal conductivity variation of the different contents of MXene@ PEG/PVA.[135] Reproduced with permission from (Mo et al., 2021), Copyright 2020 Elsevier.

decreasing the interfacial thermal resistance between different layers and supplying an expressway in terms of the photo conduction as exhibited in Figure 4C. Meanwhile, the thermal conductivity of the MXene@ PVA material is significantly enhanced when the thickness of MXene layer is added. Gund et al.[39] added the poly (3,4-ethylenedioxythiophene) polystyrene sulfonate (PSS) into MXene for improving charge storage capability based on the optimum composition and thickness, which has extreme flexibility and durability. As exhibited in Figure 4D a spray-coating method is utilized to deposit active materials involving MXene, Au-coated polyethylene terephthalate (PET) and the bending, the rolling and folding structures are obtained through varying the amount and concentration of sprayed colloidal dispersion. Xu et al.[138] fabricated the MXene@ PVA polymer foam as EMI shielding material which has lightweight and superior absorption. The fabrication process of the MXene@ PVA foam is explained in Figure 4E, and it is found that 10.9 mg/cm^3 of MXene@ PVA foam could stand on a dandelion because of its ultralow density. Also, the MXene@ PVA derivative material exhibits strong mechanical property which contributes to affording more than 5,000 times bigger than its own weight because of the strong hydrogen bonding between MXene surface and PVA molecular chains. In addition, it can be observed from the SEM images that when the thickness of MXene@ PVA film is 300 μm, its porosity could reach 88.3%, by comparison, when the thickness is 100 μm, it has a porosity of 64.9%. This demonstrates that the MXene@ PVA material is an ordered lamellar structure which could diminish the multi-reflection of the reflected electromagnetic wave

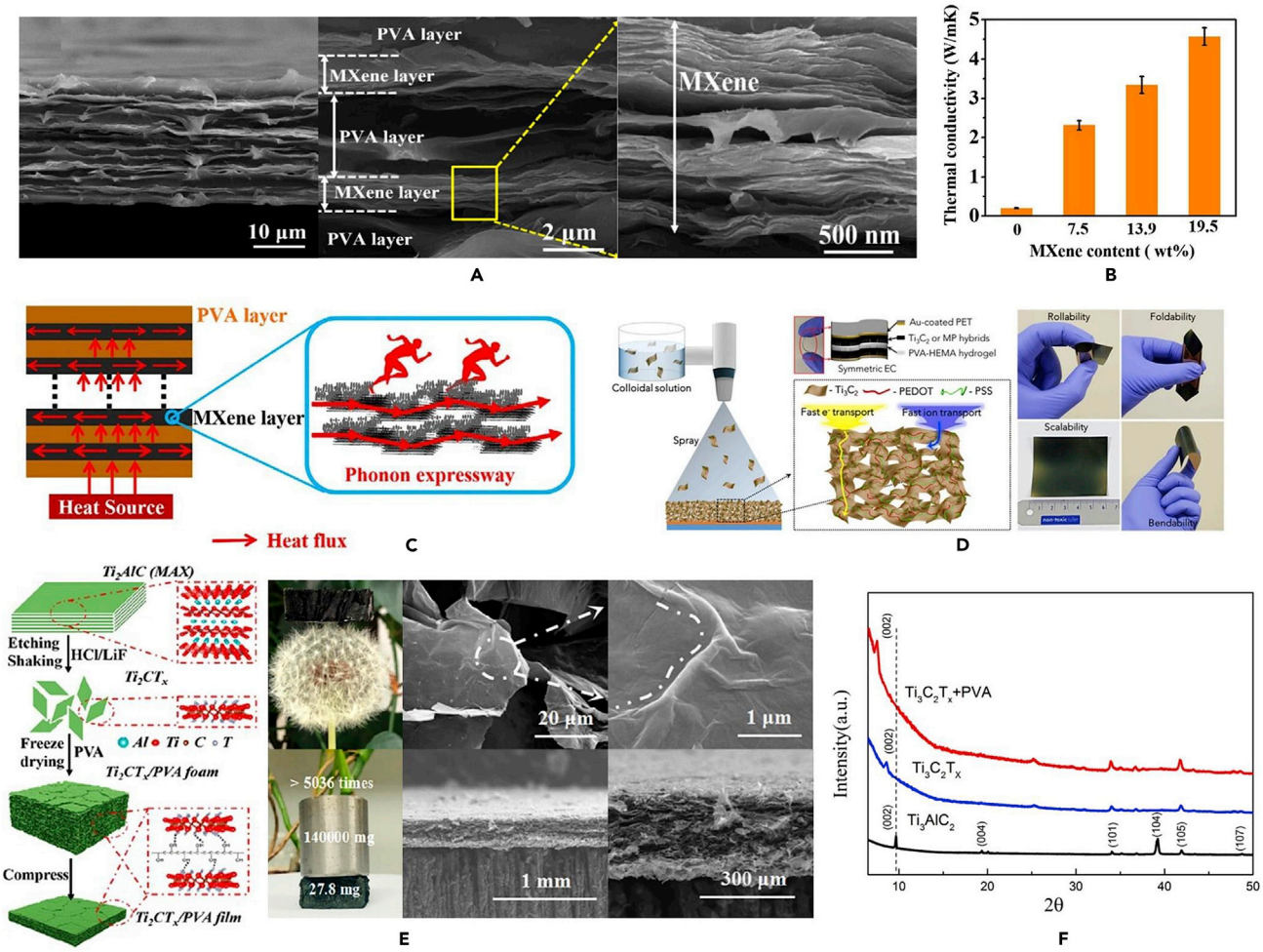

Figure 4. Synthesis of MXene@ PVA nanomaterials

(A) SEM images of MXene@ PVA-AM-19.5 film structure layer.

(B) Thermal conductivity variation at different MXene contents.

(C) Heat transfer process within the MXene@ PVA multi-layered films.[82] Reproduced with permission from (Jin et al., 2020), Copyright 2019 Elsevier.

(D) Fabrication of MXene@ PEDOT and physical properties.[39] Reproduced with permission from (Gund et al., 2020), Copyright 2019 Wiley-VCH GmbH.

(E) Preparation process of MXene@ PVA, MXene@ PVA foam standing on a dandelion, supports more than 5,000 times its own weight.[138] Reproduced with permission from (Xu et al., 2019), Copyright 2019 American Chemical Society.

(F) Fabrication process of MXene@ PVA chemical structure and phase shift variation with different angles.[139] Reproduced with permission from (Liu et al., 2018), Copyright 2018 American Chemical Society.

in pores. Liu et al.[139] added strong Ti-O bonds by cladding on the surface of the MXene without changing the crystal structure largely as shown in Figure 4F, and concluded that thermal conductivity of the MXene@ PVA could reach 47.6 W/(m·K), which is even higher than those of some metals and most of the other 2D materials. Furthermore, the peak of phase shifts varies with angles from 9.6 to 8.6° for MXene and 7.8° for MXene@ PVA, implying the rising of the lattice parameter.

Notably, 1D aramid nanofibers (ANFs), derived from the poly (*p*-phenylene terephthalamide) (PPTA) fiber, display excellent thermal stability, excellent performance and strong interfacial adhesion. Also, they are pretty stable within water, which contributes to the self-assembly process. Hence, addition of ANFs into MXene can assist obtaining a desirable equilibrium of the entire performance, thus spreading their potential applicability. Specifically, Xie et al.[140] successfully developed an ultrathin and strong mechanical MXene@ ANF composite paper for investigating the structure elements and ameliorating the electrical conductivity properties. The interior structure of the MXene@ ANF material is fixed based on the hydrogen bonding as described in Figure 5A. The cross-section multi-layered structure of MXene@ ANF material with

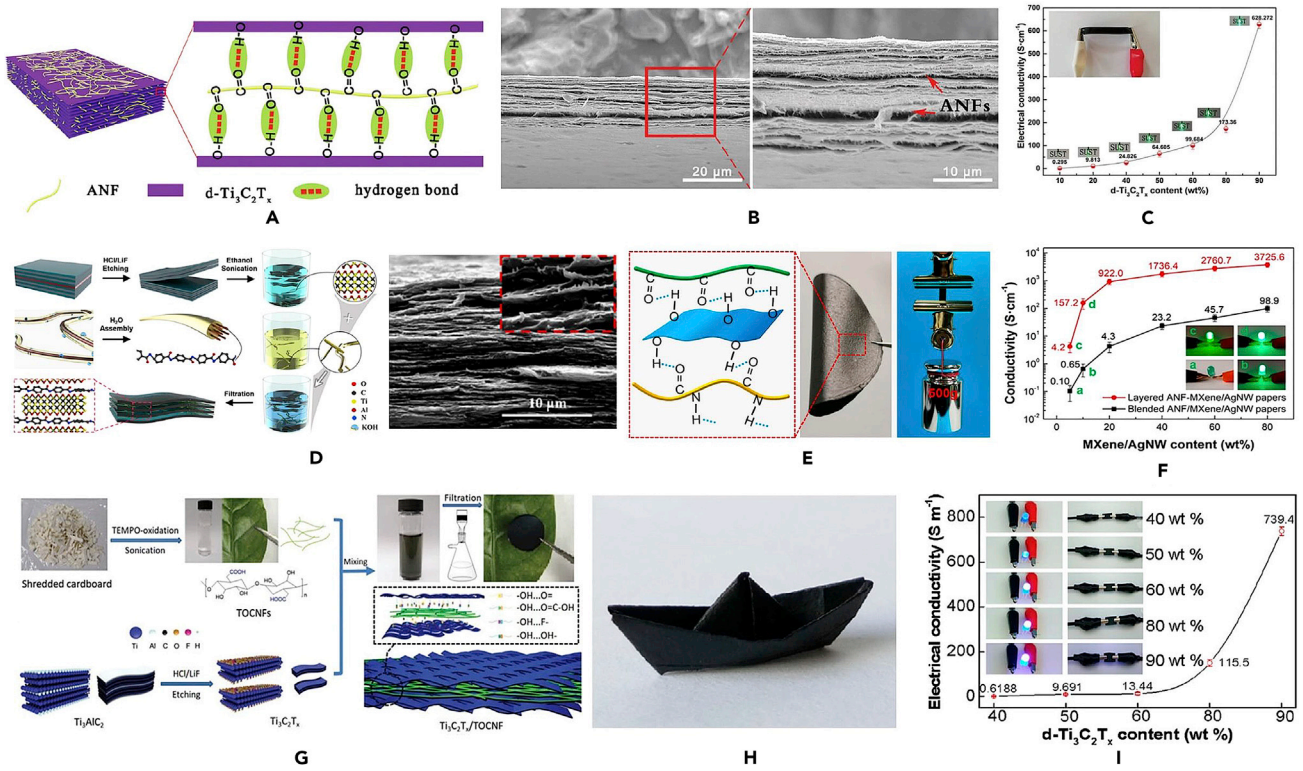

Figure 5. Synthesis of MXene@ nanofiber nanomaterials

(A) Interior structure of MXene@ ANF composite paper.

(B) SEM image of MXene@ ANF cross-section multi-layered structure.

(C) Electrical conductivity variation with the MXene content.[140] Reproduced with permission from (Xie et al., 2019), Copyright 2019 The Royal Society of Chemistry.

(D) Synthesis process of MXene@ ANF film.[141] Reproduced with permission from (Lei et al., 2020), Copyright 2020 American Chemical Society.

(E) Digital images of the MXene@ ANF/AgNW nanomaterial paper possessing ultra-flexibility and withstanding a weight of 500g.

(F) Electrical conductivity variation with the MXene ANF/AgNW content.[142] Reproduced with permission from (Ma et al., 2020), Copyright 2020 American Chemical Society.

(G) Synthesis procedure of the MXene@ TOCNF film.[143] Reproduced with permission from (Zhan et al., 2019), Copyright 2019 The Royal Society of Chemistry.

(H) Digital image of a small boat prepared by folding the MXene@ CNF paper which displays good flexibility.

(I) Electrical conductivity variation with the MXene content.[144] Reproduced with permission from (Cao et al., 2018), Copyright 2018 American Chemical Society.

a large specific surface area is exhibited in Figure 5B. This is conducive to not only assuring stress transfer but also benefitting the reconstruction of the hydrogen bond and improving the mechanical property.

Results from Figure 5C demonstrate that electricity conductivity of the MXene@ ANF materials is enhanced ranging from 0.295 S/cm to 628.272 S/cm when the MXene content varies from 10 wt % to 90 wt %. Lei et al.[141] compounded an ultrathin, super-flexible, metal-level robust and extremely stable MXene@ ANF film via the sonication process as depicted in Figure 5D. The SEM image exhibits a quite orderly multi-layered structure of MXene@ ANF, which is similar to the result from Xie et al.[140] and indicates the MXene@ ANF has a "brick-and-mortar" structure because of the abundant hydrogen-bond attached on the surface of 2D MXene nanosheets and carbon-oxygen groups of 1D rigid rod-like ANF. Meanwhile, Ma et al.[142] introduced silver nanowire (AgNW) into the MXene@ ANF as a nanomaterial to improve itself properties. The SEM images in Figure 5E demonstrate that the double layered nanocomposite films could be folded in half and withstand a weight of 500 g without any fracture or crack, representing the brilliant mechanical and flexibility properties. Meanwhile, the electrical conductivity of MXene@ ANF/AgNW nanomaterial could be enhanced with the rising of the MXene@ AgNW content as shown in Figure 5F. This is because that the numerous junction points are produced between the AgNW and ANF for attaining more efficient conductive network. This means that the double layered MXene@ ANF/AgNW has significantly boosted the

electrical conductivity attributing to the conductive networks of the highly efficient MXene@ ANF/AgNW. Furthermore, it is notable that the cellulose nanofiber (CNF) derived from natural plants has been widely used as a promising flexible substrate to reinforce filler owing to a number of merits like excellent mechanical strength, flexibility, biodegradability, and hydrophilicity. To be more specific, Zhan et al.[143] illustrated the fabrication process of the MXene@ CNF film as exhibited in Figure 5G, and proved that the MXene nanoflakes with rich surface functional groups strongly interact with CNF via hydrogen bonding. Owing to the effect of the synergistic toughening from MXene and CNF, the MXene@ CNF composite material exhibits favorable toughness and strength, and there is no fracture or crack on the material surface when the MXene@ CNF is folded into a complex shape like a small boat as shown in Figure 5H.[144] In addition, the MXene@ CNF composite material displays a superior electrical conductivity, which is enhanced considerably with the MXene content within the MXene@ CNF material. Compared with other polymer materials, CNF is one type of insulating polymer with 1D nanofiber structure resulting in less insulating contacts with 2D conductive MXene nanosheets.

Polydimethylsiloxane (PDMS) as an interface material matrix has been widely used for thermal management[145] and as dielectrics for flexible devices[146] because of its highly flexibility, non-toxicity, low cost, and easy modeling capability. Therefore, some research has been focused on mixing the PDMS with the MXene to improve thermal physical property. For example, Wang et al.[147] introduced the PDMS (Figure 6) into a 3D interconnected MXene structure by the ice-template assembly approach to ameliorate internal thermal physical property, and the whole fabrication process of the 3D MXene@ PDMS is shown in Figure 6A. In the composite MXene@ PDMS nanomaterials as indicated in Figure 6B, the heat is transferred along the MXene flakes because the MXene displays much higher thermal conductivity compared with the PDMS. Meanwhile, the interconnection bond could decrease the interface thermal resistance of MXene skeleton, which conduces to the improvement of the MXene@ PDMS thermal conductivity. In addition, it is discovered from (C) that the thermal conductivity of the MXene@ PDMS increases with the temperature in the range from 25 °C to 125 °C. This can suppress the interfacial thermal resistance among the MXene and provide large pressure for the interlinkage of 3D-MXene skeleton at a high temperature. Yang et al.[148] fabricated the MXene@ PDMS/graphene nanomaterial as a stretchable and flexible strain sensor by adding the MXene@ graphene film into PDMS substrates as presented in Figure 6D. The SEM images in Figure 6E present the cracks of the MXene@ PDMS/graphene which are enlarged in the range from 0 to 52.6% from the upper layer to the bottom layer when the scope of the tensile strain varies from 0 to 70%. This means that the upper layer of the MXene@ PDMS/graphene material is easy to produce the cracks to dissipate stresses because of its brittleness; by comparison, the bottom layer of the MXene@ PDMS/graphene material could sustain the conductive pathways. Liu et al.[149] investigated the dielectric constants of the MXene@ PDMS nanomaterials at various friction layers, and concluded from Figure 6F that the dielectric constant rises from 2.65 to 5.74 attributing to the higher surface charge density of MXene@ PDMS nanomaterial.

In comparison with the CNF and ANF materials, the polyvinylidene fluoride (PVDF) has high optimal dielectric properties and strong polar C–F bonds, so this provides EMI shielding materials with high performance. Meanwhile, the PVDF shows a brilliant film-forming ability in the process of scalable solution, which could readily obtain a compact hierarchical brick-and-mortar structure. Specifically, Li et al.[150] developed the MXene@ PVDF to obtain a fold-endurance, flexible and big region film as shown in Figure 6G. The area and thickness of the MXene@ PVDF could be flexibly adjusted via altering the coating area and blade gap, meanwhile, the MXene@ PVDF material shows a brilliant electrical conductivity ranging from 21.1 to 214.6 S/cm and high EMI shielding effectiveness of 19,504.8 dB cm^2/g under extremely cold condition. Furthermore, the natural rubber (NR) is a rigid bulk material that is suitable for stretchable electronics in comparison to other polymer materials. Therefore, Luo et al.[151] prepared a MXene@ NR film as an interconnected 3D network to attain excellent electrical conductivity, and demonstrated from Figure 6H that the electrical conductivities could reach 500 S/m for 3.1 vol % and 1400 S/m for 6.71 vol % of the MXene loading within the MXene@ NR. This indicates that the MXene@ NR could provide significant reinforcement to the NR matrix, affording obviously enhanced tensile strength. Xu et al.[152] fabricated a novel MXene@/PANI (polyaniline) material to ameliorate electrochemical performance of the MXene-based electrodes, and revealed that the MXene@/PANI displays an outstanding cycling stability with high capacitance retention of 91.6% and a high capacitance of 556.2 F/g. VahidMohammadi et al.[153] reported an approach for fabricating the MXene@ PANI material via the oxidant-free polymerization, and demonstrated that the volume capacitance of the MXene@

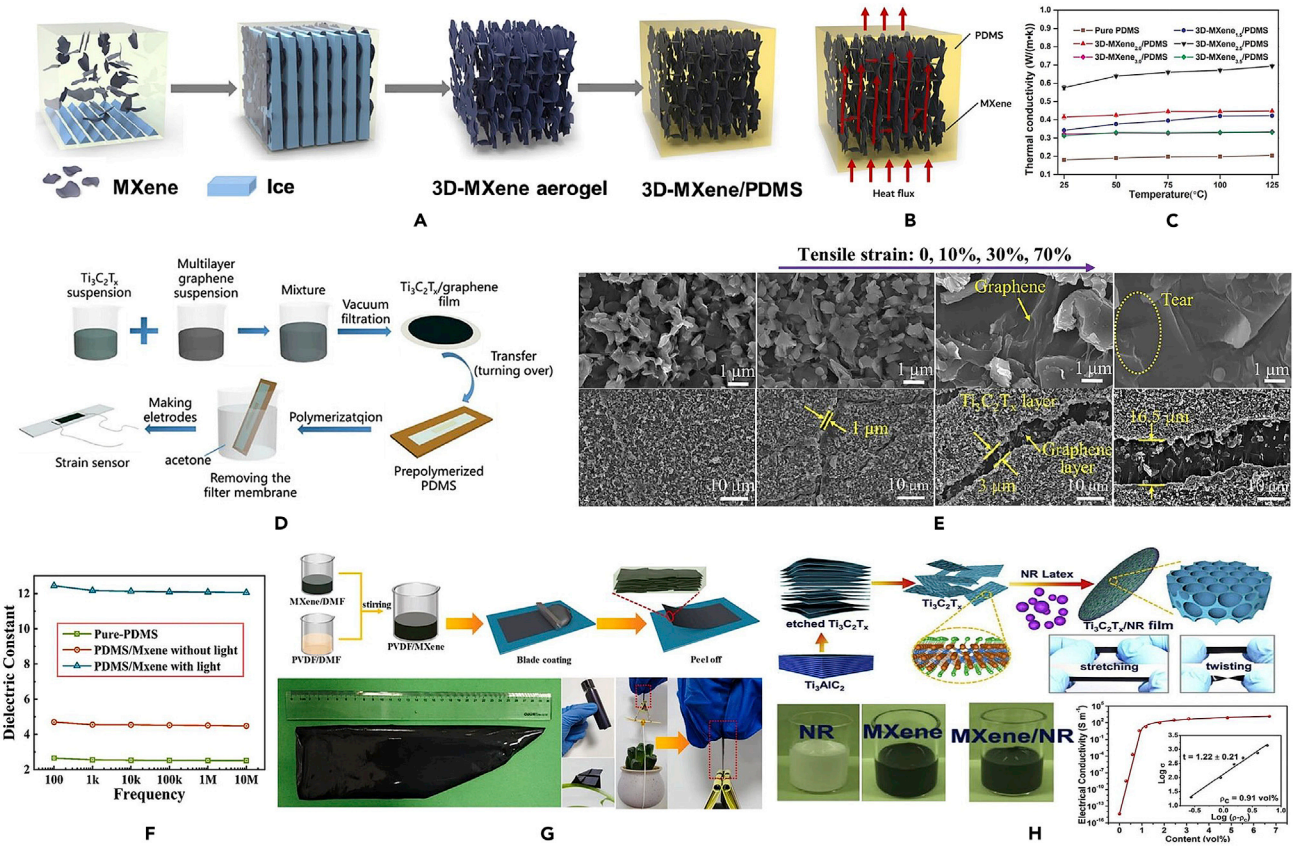

Figure 6. MXene@ novel polymor nanomaterials

(A) Synthesis process of MXene@ PDMS.

(B) MXene@ PDMS materials.

(C) Thermal conductivity variation with temperature.[146] Reproduced with permission from (Lin et al., 2012), Copyright 2012 American Chemical Society.

(D) Schematic diagram of the fabrication of the MXene@ PDMS/graphene strain sensor.

(E) SEM images of the MXene@ PDMS/graphene based strain sensor.[147] Reproduced with permission from (Wang et al., 2020), Copyright 2019 Elsevier.

(F) Dielectric constant of different triboelectric layers at different states.[148] Reproduced with permission from (Yang et al., 2019), Copyright 2019 Elsevier.

(G) Preparation process of MXene@ PVDF film and digital photo of the MXene@ PVDF film.[149] Reproduced with permission from (Liu et al., 2021), Copyright © 2021 Elsevier.

(H) Synthesis of MXene@ NR and electrical conductivity.[150] Reproduced with permission from (Li et al., 2021), Copyright 2021 Elsevier.

PANI could reach 1682.3 F/cm^3 with a brilliant cycle performance. Zhang et al.[154] fabricated an MXene@ PPy (polypyrrole) material through HCl-LiF *in-situ* etching method, and concluded that the supercapacitor and specific capacitance of the MXene@ PPy could reach 21.61 Wh/kg and 458 F/g, respectively, which contribute to obtain a stable microstructure and outstanding energy storage material.

Polymer materials have been utilized widely for different fields because of their vital advantages like flexible processibility, light weight and ease to realize great performance. Unfortunately, polymers are largely made of C, O and H components, which exhibit high flammability and inevitably bring a massive threat to life safety. Consequently, the flame retardant improvement of polymer materials has been a concentration topic in both industrial and academic fields.[155,156] There are currently two major approaches including physical blending and chemical reactions to enhance the fire resistance for polymer matrix.[157] The "labyrinth effect" is induced because of dispersed 2D nanomaterials for extending airflow path in matrix and forming high quality char. This contributes to effectively obstructing further combustion of polymer materials. Herein, introduction of MXene into the polymer materials is conducive to ameliorating fire-resistance and thermal stability to avoid catching fire. Specifically, Wang et al.[158] fabricated the MXene@ polyimide (PI) aerogel that exhibits excellent fire-resistant performance, and found that it plays a significant role in restraining the degradation of PI. Hai et al.[159] demonstrated that the MXene@ polyester resin (UPR)

materials could act the physical obstruction influence of MXene on exposure to flame and has a better flame retardancy compared with MAX. Li et al.[160] synthesized MXene@ montmorillonite (MMT) nanosheets to form the strong hydrogen bond interactions for constructing a lamellar nacre-like nanostructure, and revealed that the insertion of the MMT contributes to preventing the oxidation of MXene at high temperature and improving long-term fire resistance of the MXene.

MXene@ graphene oxide. Graphene oxide (GO) has been widely utilized as an electrode material for supercapacitors because of its high electrical conductivity. This can remove the self-restacking of both MXene and GO via the formation of a structure with alternating MXene@ GO layers. Wei et al.[161] developed the MXene@ GO composite lamellar film for dyes molecular separation, organic solvent permeation and highly efficient water. Their results reveal that the composite MXene@ GO film displays ultrahigh flux for organic solvents and water as well as over 90% of excellent dyes molecular separation performance in both aqueous and organic solutions. In the meantime, the MXene@ GO film could ensure a long-time stability operation for a series of dyes. Yan et al.[162] fabricated a flexible MXene@ reduced graphene oxide (rGO) film based on the electrostatic self-assembly approach, and discovered that the maximum volumetric power density of the supercapacitor could reach up to 74.4 kW/L whereas the ultrahigh volumetric energy density is 32.6 Wh/L, which is much higher than MXene based other materials in aqueous electrolytes. Because the hybrid structure and electrochemical performance of the MXene@ GO film are ameliorated, this film has a potential for portable and micro sized combined thermal energy storage device applications based on high performance and ultrahigh volumetric capacitance.

MXene@ carbon nanotubes. He et al.[163] synthesized a composite MXene@ CNTs (carbon nanotubes) material to further enhance the catalytic and conductivity performance of $CoMoP_2$, and found that the electrical conversion efficiency of MXene@ CNTs material could reach 10.64%, which is higher compared to the Noble metal platinum of 7.04%. Cai et al.[164] introduced the carbon nanotubes/polyaniline (CNT/PANI) into the MXene to improve the storage capability, and concluded that the capacitance of the MXene@ CNT/PANI could achieve the maximum value of 429.4 F/g, which is much higher than that of the CNT/PANI (260.3 F/g). Wang et al.[165] developed the MXene@ CNT to improve the electrocatalyst performance of the lithium polysulfide battery based on the tensile strain effect, and found that the MXene@ CNT exhibits a high capacity of 1451 mAh/g and rate capability up to 8 cycles.

MXene@ metal nanoparticles. Recently, metal nanoparticles have been widely discovered because of the unique catalytic, electrical, magnetic and optical properties. Hu et al.[166] introduced the transition metal nanoparticle (TMNP) including Fe, Co and Ni in the MXene as novel composite materials for improving the storage capacity of Li–S batteries, and confirmed that the Li–S cell using the MXene@ Co catalyst is conduced to delivering a higher capacity of 788 mAh/g compared to pure MXene materials. Wen and Yang[167] developed a novel composite MXene@ Pt (Platinum) material as biosensor for sensitive analysis of pyruvate in human serum, and indicated that the biosensor has a high sensitivity with low interfering substances including uric acid and glucose.

MXene-based mixture solutions

MXene@ oil. Synthetic or mineral high temperature oils are widely used as heat transfer fluids in many applications. In particular, vegetable oils are mainly utilized in the food sector, but also in other industries.[168] Vegetable oil based MXenes as effective coolants and lubricants have been utilized in different thermal systems for achieving sustainable advancement of clean energy efficiency; they have a more enjoyable eco-balance and a critical availability with seven times cheaper price compared to the traditional thermal oil.[169] To be more specific, Samylingam et al.[170] synthesized the MXene@ olein palm oil (OPO) as thermal fluid for enhancing thermal conductivity, viscosity, and solar absorption capability in a solar PV/T system. Six different concentrations of the MXene@ OPO nanofluids are formulated in this study. This thermal property is mainly affected by the motion of free particles and molecular vibrations, and it is enhanced by the suspended nano-sized particles' Brownian motion. Moreover, the 2D materials of MXene act as nano-fillers, which enable efficient heat transfer from fluids because of higher thermal conductivity and bigger surface area. Both the formation of liquid layering and the rising of particle movement increase the nanofluid thermal conductivity. Meanwhile, the thermal conductivity is also influenced by the size of nanoparticles within the base fluid. When the size reduces, the thermal conductivity increases. This kind of behavior of nanoparticle is found true for the MXene@ OPO nanofluid with increasing concentrations. Meanwhile, Parashar et al.[171] investigated the dynamic viscosity of the

MXene@ OPO for regression analysis based on the artificial neural networks (ANNs) model, and demonstrated that the dynamic viscosity reduces when the temperature is increased. In the meantime, the dynamic viscosity of the MXene@ OPO can be significantly boosted for both low and high temperature scopes, and the concentration has little influence on the dynamic viscosity. This indicates that the MXene@ OPO has the potential of being used as thermal working fluid, especially at higher temperature range from 60 to 100°C.

Soybean oil (SO) is one of the base fluids with better heat transfer capacity and high decomposition temperature, and it is widely available, non-toxic, biodegradable, and possesses a wide range of viscosity. Rubbi et al.[172] formulated the MXene@ SO as coolant within a solar PV/T system because of its good heat transfer property. The SO has the chemical composition of long-carbon chained triglycerides and several types of lipids. Results demonstrate that the maximum improvements of thermal conductivity and viscosity could reach 60.82% at 55°C and 13.28% at 25°C for both 0.125 wt % of MXene nanoparticles. This indicates that the intermolecular interactions of the MXene@ SO significantly affect the thermal conductivity. The enhancement of viscosity with addition of particle is because of the structure of MXene nanosheets which increases resistance force between the different layers of the oil. It is also found that larger surface area and higher aspect ratio of MXene nanosheets have considerable influences on the thermal conductivity of the nanofluid suspension. Silicone oil-based nanofluids have the high operating temperature up to nearly 400°C which permits it to medium-to-high temperature applications. Aslfattahi et al.[90] prepared three different concentrations of MXene@ silicone oil to enhance thermal physical properties and explore its stability utilized in the concentrated photovoltaic thermal collector system, and concluded that the viscosity of the MXene@ silicone oil is decreased by 37% when the temperature varies from 25 to 50°C for various concentrations of MXene with SO. Addition of MXene flakes has minor influence on the decomposition of formulated nanofluid, and the thermal stability of MXene@ silicone oil could be kept at 320°C for any of the samples. In summary, introducing more MXene nanoparticles into the SO contributes to boosting PV module electrical efficiency owing to better cooling of MXene@ SO derivative materials. Moreover, the addition of the MXene nanoparticles into the SO could improve the overall solar energy system performance when the solar concentration ratio is high, indicating the MXene materials are more suitable to be employed at high temperature levels and solar concentrations.

MXene@ ionic liquid. Ionic liquids (ILs) are the novel purely ionic, salt-like materials that are liquid at unusually low temperatures. The ILs have a wealth of advantages involving high thermal conductivity and stability, high dissolution capacity, low melting point, non-volatility as well as non-toxicity. Therefore, adding the nanoparticles into the ILs contributes to improving the heat transfer for applications with high temperature. Das et al.[173] developed a novel MXene@ ionic liquid (IL) aqueous binary solution to study its thermal conductivity, and concluded that the concentration of MXene nanomaterial has vital influence on the thermal conductivity of composite material. Specifically, when the concentration of the MXene is set up as 0.2 wt %, the thermal conductivity of the composite MXene@ IL can be improved by around 47%. Compared to the MXene@ water/alumina and MXene@ palm oil, the heat transfer coefficient could be improved by 2 and 12.6%, respectively. Moreover, it is demonstrated that the viscosity of MXene@ IL nanofluids can be decreased when the shear stress of the material is reduced. This is because the reduction of temperature is conducive to strengthening the intermolecular forces between MXene particles and IL solution. Lower viscosity is one of the key concerns for thermal fluid application because higher viscosity may add the pressure drop, resulting in high pumping power demand. Furthermore, Bakthavatchalam et al.[174] developed a MXene@ IL with diethylene glycol (DEG) and ionic, and illustrated that when the average temperature is 60°C, the thermal conductivity is enhanced from 24.83 to 57.45% as the concentration varies from 0.1 wt % to 0.4 wt %. The thermal stability and conductivity and of the MXene@ IL could be ameliorated by increasing the concentration and temperature of the MXene nanoparticle.

MXene@ water. To resolve the MXene into pure water, Wang et al.[175] added the sodium citrate as an anionic and antioxidant surfactant into the MXene@ water to improve the anti-oxidation ability, and concluded that the addition of sodium citrate contributes to dramatically enhancing the stability and oxidation resistance of the MXene nanofluid. Abdelrazik et al.[176] analyzed the effects of two different types of surfactants, sodium dodecylbenzenesulfonate (SDBS) and cetyltrimethylammonium bromide (CTAB), on the transmittance spectra rate and absorption spectra rate. It is found that the surfactant category plays a significant role on the transmittance spectra of the MXene nanofluid. In addition, it is indicated that

the MXene disperses better in the presence of SDBS, and achieves the better stability of the MXene@ water via using the SDBS surfactant.

Synthesis strategies of MXene nanomaterials

The synthesis methods of the composite MXene nanomaterials play a vital role in obtaining stability in chemical structure, high thermal physical properties, and energy conversion efficiency. Six types of synthesis approaches, viz., bottom-up synthesis method, top-down synthesis method, direct vacuum impregnation, freeze-drying, two-step technique, and toluene dilution methods, are summarized in the following section.

Bottom-up synthesis method

The bottom-up preparation technique involves different approaches that are recently proposed such as chemical vapor deposition (CVD) in the temperature ranging from 1000 to 1300 to formulate Ti_3SiC_2. Specifically, Xu et al.[177] developed the Mo_2C membranes by using the CVD method, and found that the stack could be heated up to 1085°C inside hydrogen; afterward, the molybdenum carbide (Mo_2C) crystals are formed via the flow of the methane. Yang et al.[178] utilized the CVD method to obtain the ultrafine platinum NP-decorated 3D hybrid nanocomposite, and concluded that the composite material has high catalytic activity and long-term stability. Geng et al.[179] investigated control approach in terms of the morphology of Mo_2C crystals via the CVD method, and revealed that the shapes and thickness of Mo_2C fractal crystals could be attained through altering the concentration of methane. Nevertheless, this CVD technique is not suitable to prepare the MXene owing to thin layers generated rather than single layer, high expense and low production output.

Top-down synthesis method

The top-down method includes etching and exfoliation, which is largely employed to prepare the MXene materials. Ghidiu et al.[28] first introduced this technique using LiF and HCl on the conversion from Ti_3AlC_2 to MXene. Hu et al.[180] adopted the etching method to rapidly obtain the 2D MXene materials, and demonstrated that the MXene could be sustained at a stability status from 300 to 800 °C because of air oxidation reaction. Natu et al.[181] and Omomo et al.[182] exfoliated Ti_3AlC_2 by using the polar organic molecule dimethyl sulfoxide (DMSO) and tetrabutylammonium hydroxide (TBAOH), respectively, which can be widely employed for exfoliation of the MXene.

Direct vacuum impregnation method

Liu et al.[119] synthesized the MXene@ PEG by using direct vacuum impregnation approach. To be more specific, solid PEG and MXene powder are placed into a vacuum oven to attain the adsorption saturation when the temperature is 80°C for 12 h under high vacuum. Then, the residue of the PEG is separated via using the filter paper that is altered regularly until no PEG leakage from the sample. Wang et al.[120] compounded the MXene and carbon foam (CF) as a new material to achieve high-performance electromagnetic wave absorption by using the vacuum impregnation and freeze-drying methods. In the synthesis process, three CF specimens are dissolved into three impregnation MXene suspension solutions with different concentrations, and the weight gain rate is utilized to investigate the contents of adsorbed MXene, and found that the higher the weight gain rate, the more MXene are adsorbed in specimens. To decrease the sheet resistance, Seok et al.[121] fabricated a polypropylene (PP) membrane and used MXene as a filter to control the membrane thickness via vacuum filtration method, and concluded that the membrane thickness over 5 mm could cause a dramatic reduction in the sheet resistance below 1–5 Ω/sq.

Freeze-drying method

Lin et al.[133] mixed the MXene colloid with the PEG solution by warming at 70°C under stirring for one day, and then several ice crystals tend to expel the MXene and PEG nanosheets and compel them assemble between numerous ice crystals. Finally, the porous MXene@ PEG aerogel is obtained via freeze-drying method to take out the ice crystals via sublimation. Furthermore, Mo et al.[135] also synthesized a novel composite PCM by using the polyvinyl alcohol (PVA), polyethylene glycol (PEG) and MXene based on the vacuum impregnation and freeze-drying approaches. The MXene@ PVA foam is firstly attained by a freeze-drying process with ice as the sample. 3 mg/mL PVA solution and few-layered MXene suspension are mixed with different volume ratios. The suspension is frozen at −18°Cat −65°C for 24 h. Subsequently, the series MXene@ PVA samples with different mass are immersed into the PEG to complete infiltration PEG under vacuum condition for 2 h.

Other synthesis methods

Apart from the above mentioned two traditional synthesis techniques, some other approaches have been applied to synthesize composite based-MXene nanomaterials, such as multi-layered casting method,[82] two-step technique,[172] and toluene dilution method.[90] To be more specific, Jin et al.[82] prepared an MXene@ PVA alternating multi-layered membrane by using the multi-layered casting method. The aqueous PVA solution is firstly casted onto an iron substrate, and then the MXene aqueous is also casted onto the PVA layer and dried at 45 °C to form an MXene layer. Repeat casting of MXene and PVA in succession of 11 cycles, finally, a MXene@ PVA multi-layered film with 5-layer of MXene and 6-layer of PVA is attained. In addition, Rubbi et al.[172] synthesized the MXene@ SO by using the two-step technique method owing to large scale production and cost effective. In the synthesis process, the MXene powder is dispersed into the SO and stirred around 30 min at 700 rpm via a magnetic stirrer, and heated at 70°C temperature to make the mixture homogeneous into the base fluid. Then, the suspensions of MXene@ SO need to be sonicated for 30 min by an ultrasonic probe sonicator to agitate the intermolecular forces between SO and MXene flakes. Meanwhile, the ultrasonic probe sonication contributes to boosting the stability and homogeneity of the suspensions through breaking clusters. By comparison, Aslfattahi et al.[85] introduced the MXene flakes into the silicone oil to obtain a high viscosity composite nanomaterial based on the Toluene diluted method. The Toluene is utilized as a dilator to compound the MXene@ SO on a 120°C hot plate, and stirred for 30 min to realize the original volume of SO without any solvent. Table 2 summarizes and compares base-MXene composite types and synthetic methods.

THERMAL ENERGY CONVERSION AND STORAGE

Different kinds of composite MXene nanomaterials have been utilized to extensively explore for thermal energy conversion including photo-to-thermal, electro-to-thermal, thermal energy storage. Current advances in energy conversion application are introduced, mainly, solar thermal PV/T application, solar water desalination, solar photo-thermal electrode, wearable device, light-driven actuator, smart hydrogel and biomedical applications.

Photo-to-thermal energy conversion

MXene has been regarded as the photo-to-thermal material that is able to harness solar energy, and attracted huge attention over the past decades. An ideal of photo-to-thermal material should display a broadband and efficient absorption because of their bandgap structures and inherent electronic. It is essential that the material thermal properties and optical are thought to realize an efficient photo-to-thermal conversion. The optical properties of materials, such as heat transfer loss, matching of a material's absorption spectrum to incident light and absorption coefficient, have a vital effect on the material choice and light-to-heat conversion optimization. Except for the inherent properties of the utilized material, other features including mechanical integrity, thermal stability, and expense, should also be factored in for practical engineering. Photo-to-thermal conversion efficiency is a direct index to determine the light energy utilization of direct absorption solar collector. Light-to-heat, also known as photo-to-thermal conversion, including collecting and converting solar irradiation based on photo-to-thermal materials into heat as terminal energy for beneficial usage. Specifically, Fan et al.[134] discovered the efficiency of the photo-to-thermal storage and conversion on the basis of the MXene@ PEG composite materials, and concluded that the storage efficiency could reach the maximum value of 94.5% when the 20 wt % of MXene is introduced into PEG. Samylingam et al.[170] investigated the thermal efficiency of a solar PV/T unit combined with MXene@ olein palm oil (OPO), and revealed that the system efficiency is increased by 11.2%, compared with Al_2O_3 aqueous solution resulting in around 40% of the PV surface temperature decrease. Wang et al.[175] performed an experimental analysis of a solar PV/T unit combined with graphene and MXene materials, and demonstrated that the system thermal energy conversion efficiency with the MXene@ water can reach 63.35%, which is 4.34% higher compared to the graphene material's. Wang et al.[183] utilized the MXene@ water nanofluid as the thermal fluid in the solar collector system to analyze the photo-to-thermal conversion performance. Results demonstrate that the thermal conversion efficiency based on thin-layer MXene@ water nanofluid is 91.9% with 0.02 wt % of MXene mass fraction, which is higher than that of multi-layer MXene@ water nanofluid. This is because of the influence of the localized surface plasmon resonance induced by MXene flakes, which contributes to enhancing the optical absorption performance of the MXene@ water. Rubbi et al.[172] concluded that the thermal effectiveness of the PV/T system using MXene@ SO nanofluid is 84.25% with 0.07 kg/s mass flow rate. Das et al.[173] investigated the effect of the MXene@ IL on the performance of the solar PV/T system, and demonstrated that the thermal efficiency could be

Table 2. MXene synthesis methods and applications

Reference	MXene-derivation		Synthesis method	Synthesis condition	Applications
Liu et al.,[119]	MXene@ PCM	MXene@ PEG	Vacuum curing process	• Stirred at 70 °C to fully dissolve. • Keep at 60 °C for 12 h in a vacuum drying oven. • Mass ratio of PEG: Epoxy = 7:3.	EMI shielding effectiveness
Lin et al.,[133]		MXene@ PEG	Stirring	• 150 mg/mL of PEG solution+ 17.6 mg/mL of MXene colloid. • 70 °C under stirring for 24 h+ freeze drying for 56 h.	Solar energy utilization
Lu et al.,[85]		MXene@ PEG	Direct vacuum impregnation method	• 3.0 g of LiF +40 mL of 12 M HCl. • Maintain at 80 °C for 12 h.	Thermal energy utilization
Fan et al.,[134]		MXene@ PEG	Vacuum curing process	• Ultrasonic processing for 1 h. • Under vacuum 0.05 Mpa.	Thermal energy storage
Mo et al.,[135]	MXene@ Polymor	MXene@ PVA	Freezing drying process with ice	• Ultrasonication for 2 h. • The suspension is frozen at −18°C. • Freeze-dried in a freeze dryer under 0.1 Pa pressure at −65°C for 24 h.	Thermal energy utilization
Jin et al.,[82]		MXene@ PVA	Multi-layered casting method	• Dried at 45 °C to obtain a PVA layer. • Drying under a vacuum at 70 °C for 6 h.	Electrical devices application
Gund et al.,[39]		MXene@ PSS	Scalable processing method	• The mass ratio of the MXene with PSS = 1:2.	Electrochemical capacitors application
Xu et al.,[138]		MXene@ PVA	Freeze-drying approach with ice	• The total volume is defined as 2.5 mL and 20 mg/mL of PVA solution. • Freeze-dried for 2-day within a freeze dryer.	5G cellular network communication technology

(*Continued on next page*)

Table 2. *Continued*

Reference	MXene-derivation		Synthesis method	Synthesis condition	Applications
Xie et al.,[140]	MXene@ Nanofiber	MXene@ ANF	Sonicating, filtering and vacuum-assisted filtration	• 1.0 g of PPTA fibers, 1.5 g of KOH and 20 mL of water. • Dried at 105 °C for 15 min.	Electromagnetic interference shielding application
Lei et al.,[141]		MXene@ ANF	Ultrasonic treatment and mechanical emulsification	• 5g of KOH, 7.5 g of PPTA fibers and 500 mL of DMSO. • 2 g of MAX, 2 g of LiF and 9 M 40 mL of HCl solution. • 35 °C under magnetic stirring for 24 h.	Electromagnetic interference shielding application
Ma et al.,[142]		MXene@ ANF	Vacuum filtration and hot-pressing method	• 1.0g of Kevlar 49 thread, 1.5 g of KOH and 500 mL of DMSO. • 1.0g of MAX powder +1.0 g of LiF +20 ML of HCl via stirring at 35 °C for one day. • The weight ratio of MXene and AgNW is set to 10:1. • Dried under hot-pressing at 60 °C and 1 MPa.	Electromagnetic interference shielding application
Zhan et al.,[143]		MXene@ CNF	Stirring and vacuum assisted filtration process	• 5 g of LiF+5 g of Ti3AlC2 powder +9 M HCl solution; via stirring at 35 °C for one day. • Sonicating for 1 h and centrifugation at 3500 rpm for 1 h.	Wearable and portable electronics applications

(*Continued on next page*)

Table 2. *Continued*

Reference	MXene-derivation		Synthesis method	Synthesis condition	Applications
Wang et al.[147]	MXene@ other materials	MXene@ PDMS	Vacuum-assisted impregnation method	• 2.0 g of LiF +2.0 g of Ti3AlC2 powder + 40 mL of HCL. • Stirring under 45 °C for one day and sonication for 40 min. • Infiltrating for 1 h, and curing at 100 °C for 1 h.	Thermal management, energy harvesters, and sensors
Yang et al.,[148]		MXene@ PDMS	Electrochemical method and vacuum filtered and dried	• 1.0 g of Ti3AlC2 powder +12 mL DMSO via stirring for 18 h. • Dried at 50 °C in an oven.	Strain sensors application for human body
Liu et al.,[149]		MXene@ PDMS	Spin-coating method	• The weight ratio of MXene and PDMS is 1:4. • Keep the temperature at 80 °C for 6 h.	Light power and sensors application
Li et al.,[150]		MXene@ PVDF	Oil bath stirring	• 10 g of MAX powder +10 g of LiF powders+ 200 mL of 9 M HCl. • Stirring at 35 °C for one day. • Oil bath stirring at 60 °C for one day.	Wearable EMI shielding application
Luo et al.,[151]		MXene@ NR	Vacuum filtration approach	• MXene@ NR keeps at 170 °C and 10 MPa for 20 min.	Foldable electronics application
Wei et al.,[161]	MXene@ GO	MXene@ GO	Modified Hummer's method + vacuum filtration method	• 1.98 g of LiF+ 3 g of Ti3AlC2 + 30 mL 6M HCL. • Stirring continuously at 300 rpm at 80 °C for 5 days.	Water and organic solvents treatment application
Yan et al.,[162]		MXene@ rGO	Probe sonication	• Hydrazine decline of graphene oxide at 90 °C for one day.	Portable and highly integrated supercapacitors application

(*Continued on next page*)

Table 2. *Continued*

Reference	MXene-derivation		Synthesis method	Synthesis condition	Applications
Samylingam et al.,[170]	MXene@ Oil	MXene@ OPO	Stirring and ultrasonic probe sonicating	• 3g MAX+ 3g of LiF +30 mL HCL. • Stirring at 40 °C for two days. • 30 min at 700 rpm via a hot plate.	Solar PV/T system application
Rubbi et al.,[172]		MXene@ SO	Magnetic stirring and ultrasonic probe sonicating	• The weight fractions ranges from 0.025 to 0.125 wt %. • Stirring for 30 min at 700 rpm using a magnetic stirrer.	Solar PV/T system application
Aslfattahi et al.,[85]		MXene@ SO	Diluted approach via Toluene	• 54 mg of MXene +60 mL of SO + 60 mL of Toluene. • Stirred with 400 rpm at 50 °C for 30 min using a hot plate. • Half an hour via ultrasonic probe sonicator.	Concentrated PV/T system application
Das et al.,[173]	MXene@ IL	MXene@ IL aqueous binary solution	Ultrasonic probe sonicating	• Magnetic stirring for half an hour at 45 °C. • Stirring using hot plate magnetic for 1 h at 50 °C and 700 rpm.	Solar PV/T system application
Bakthavatchalam et al.,[174]		MXene@ IL with DEG and ionic	Magnetic stirring, ultrasonic sonicating and two-step method	• Magnetic stirring for 30 min at 40 °C, 1000 rpm.	Solar PV/T system application
Wang et al.,[175]	MXene@ Water	MXene@ Water	Ultrasonic sonicating	• 0.5 g LiF +15 mL of HCl and stirring for 30 min. • Magnetically stirred at 30 °C for 20 h. • Ultrasonic for 20 min.	Photothermal conversion application
Abdelrazik et al.,[176]		MXene@ Water	Ultrasonic probe sonicating	• 3 g of LiF +3 g of MAX, stirred at 40 °C for two days.	Solar PV/T system application

enhanced from 12.2% to 13.95% when the flow rate is boosted from 0.01 kg/s to 0.07 kg/s, achieving the maximum efficiency of 81.15%. Meanwhile, compared with the MXene@ oil and MXene@ water, the heat transfer coefficient of the MXene@ IL could be improved by 2 and 12.6%, respectively. Simultaneously, Bakthavatchalam et al.[174] confirmed that the thermal efficiency of a PV/T system integrated with MXene@ IL/DEG nanofluid has a significant enhancement of 10.9% when the MXene concentration is in the range from 0.1 wt % to 0.4 wt %.

Moreover, efficient use of abundant solar energy for steam production is an environment-friendly, renewable and sustainable technology for seawater desalination and wastewater purification, permitting strategies to deal with the worldwide long-standing water scarcity problems. Therefore, Zhao et al.[184] proposed a 3D MXene architecture (3DMA) of solar steam generator for enhancing solar thermal conversion efficiency and obtaining effective broadband solar absorption as given in Figure 7A. To ameliorate the 3DMA conversion performance, a wrap-around structure with expandable polyethylene foam (EPF) is inlaid in the MXene as a thermal insulation layer to diminish the heat transfer to the underlying water. Meantime, water channels are shaped neighboring EPE foam to guarantee sufficient water to be provided to the 3DMA surface. Figure 7B displays the fabrication process and SEM images of the 3DMA. Based on the two-step technique method, it is found the pore size from melamine foam (MF) skeleton to the 3DMA reduces gradually. Results from Figure 7C demonstrate that the temperature variation of the bulk water is merely around 3.6°C, which is much lower compared to pure water without any nanomaterials, and it is confirmed that the 3DMA structure contributes to minimizing the heat transfer loss. In addition, as presented in Figure 7D, the efficiency of the 3DMA solar steam could achieve 82.4 and 88.1% when the evaporation rates are 1.309 kg/m^2·h for 1 sun illumination and 6.997 kg/m^2·h for 5 sun illumination, respectively. Yu et al.[185] assembled MXene@ PVA hydrogel materials and applied in the tree-inspired solar steam generation system as exhibited in Figure 7E. It demonstrated that the rapid vapor release and water transport could be realized via these vertically aligned channels within the system. The composite MXene nanomaterial helps to decrease the energy demand of water evaporation through tweaking the interaction between water molecules and hydrophilic polymer networks. It can be observed from Figure 7F that the bulk water temperature is enhanced from 24.1 to 27.8°C on exposure to solar irradiation for 1 h. By comparison, the surface temperature of the TIH could be improved rapidly from 23.6 to 34.7°C within 10 min and reach the consistent value of 35.9°C within 1 h. Furthermore, it is found from Figure 7G that the TIH exhibits much quicker evaporation rate in comparison to the bulk water, implying that the bulk water could provide higher evaporation enthalpy than TIH. Also, the water evaporation enthalpy in TIHs reduces with the growth of PVA concentration, which means that the polymer network is the key element to alter equivalent enthalpy. Li et al.[186] fabricated a novel MXene@ PVA modified cigarette filter (MPCF) nanomaterial to investigate temperature variation on the MPCF model and photo-to-thermal conversion efficiency as exhibited in Figure 7H. The MPCF fabrication process is presented in Figure 7I. The PVA modified CF is infused into the MXene nanosheets to obtain an MPCF, in which the hydrogen bonds between the PVA and MXene could avoid the segregation of MXene from CFs. At the end, 9 pieces of the MPCFs are aggregated by using the solar steam production device as displayed in Figures 7J and 7K. As presented in Figures 7L–7N, the top surface temperatures of the MPCF are 33°C at 2 cm height, 31.5°C at 4 cm height and 31.2°C at 6 cm height, respectively, which are higher compared to the ambient temperature of 23.5°C. This results in thermal energy loss in the forms of radiation and convection produced by temperature variation. In addition, the photo-to-thermal conversion efficiency and ultrahigh solar steam production rate of the MPCF evaporator could achieve 132.9% and 3.38 kg/m^2·h, respectively. Spontaneously, it is notable that the composite MXene can be also utilized to solve the shortage of fresh water and water pollution from brackish water or seawater by the desalination technology. Liu et al.[187] fabricated an ultrathin 2D MXene film to carry out the pervaporation desalination based on the facile filtration approach. Their results reveal that the composite MXene film exhibits a high salt rejection of 99.5% when the water flux rises from 48.2 L/m^2·h to 83.5 L/m^2·h and the water temperature varies from 30 to 65°C. This indicates that water productivity could be effortlessly boosted through the feed temperature and retained at a high desalination efficiency.

Zhang et al.[188] developed a vertically aligned structure of Janus MXene-based aerogel (VA-MXA) for solar desalination application as presented in Figure 8A. The composite Janus VA-MXA has a bottom hydrophilic layer and an upper hydrophobic layer. During the process of the solar desalination, the hydrophilic bottom layer of the Janus VA-MXA could effectively drive seawater to the entire evaporation zone by the vertically aligned channels, by comparison, the hydrophobic upper layer restrains the further upward

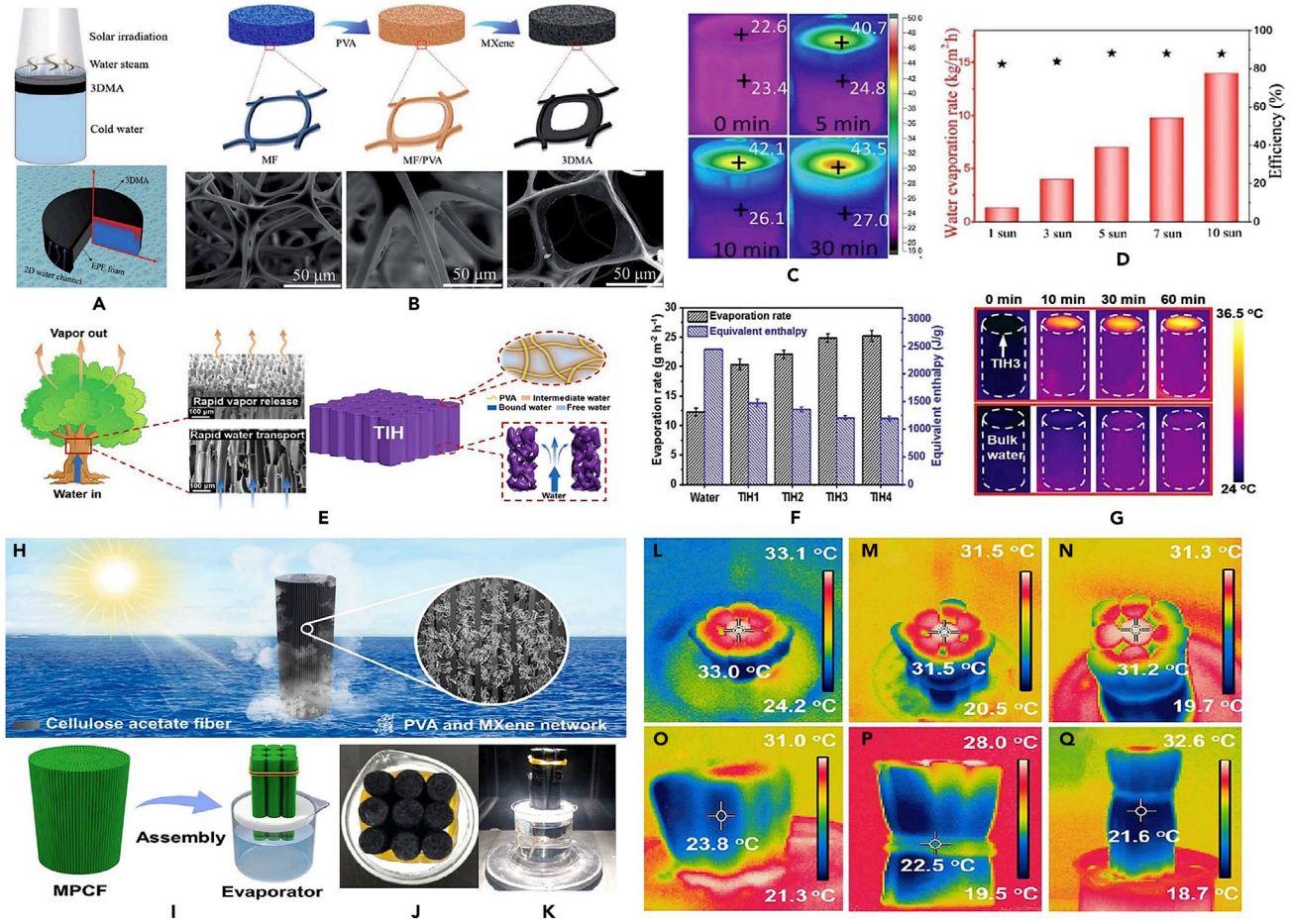

Figure 7. Composite base-MXene steam generation evaporator

(A) 3DMA contacting with water mode and cross-section structure.

(B) 3DMA fabrication process and SEM images.

(C) Temperature variation of the 3DMA surface with EPF for 30 min.

(D) Solar steam efficiency and water evaporation rates of the 3DMA based on different solar illumination intensities.[184] Reproduced with permission from (Zhao et al., 2021), Copyright 2019 The Royal Society of Chemistry.

(E) Schematic diagram of water being transferred from root to top of trunk by tree and SEM images.

(F) Infrared images of bulk water and TIH.

(G) Evaporation rate of water and vaporization enthalpy of bulk water and TIH.[185] Reproduced with permission from (Yu and Wu., 2020), Copyright 2020 Wiley-VCH GmbH, Weinheim.

(H) MPCF.

(I) Fabrication process of MPCF evaporator.

(J) 9 pieces of MPCFs.

(K) assembled MPCF solar steam production device.

(L–N) Top surface temperatures of MPCFs with exposed heights from 2 cm to 6 cm.

(O–Q) Sidewall temperatures of MPCFs with exposed heights from 2 cm to 6 cm.[186] Reproduced with permission from (Li et al., 2022), Copyright 2021 Elsevier.

transportation of water to avoid direct water contact. The SEM images from Figure 8B display that the surface salt accumulations of the Janus VA-MXA and VA-MXA, and reveal that there is no salt either on the surface or inside of the VA-MXA. This is because the continuous water pumping causes fast salt dissolution at the bottom of the hydrophilic layer. However, after solar irradiating for 12 h, several micro-meter thick salt crystals appear on the Janus VA-MXA surface. This indicates that the Janus VA-MXA structure contributes to averting the salt crystallization on the MXene surface and ensures the durability and stability of the Janus VA-MXA during the process of the solar-driven steam production. Herein, the novel Janus VA-MXA guarantees excellent solar steam generation rate and efficiency output reaching 1.46 kg/m^2·h and 87%,

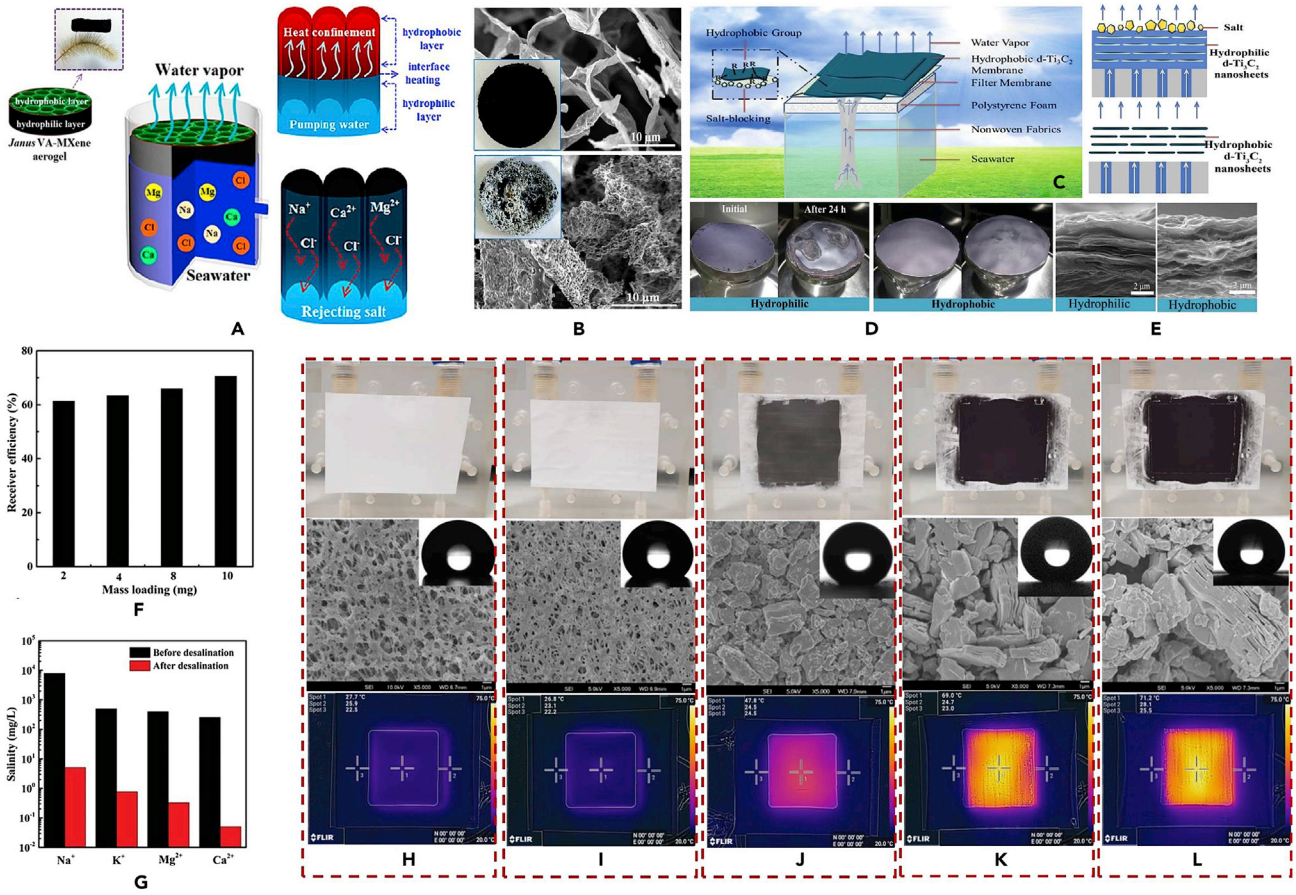

Figure 8. Solar distillation base-composite MXene nanomaterials

(A) Schematic diagram of Janus VA-MXA with bristlegrass, the processes of the solar steam generation and salt rejection.

(B) SEM images.[188] Reproduced with permission from (Zhang et al., 2019), Copyright 2019 American Chemical Society.

(C) Hydrophobic MXene membrane based solar desalination device.

(D) Hydrophilic and hydrophobic MXene films before and after 24-h solar desalination.

(E) SEM images.

(F) Thermal conversion efficiency.

(G) Measured salinity of four primary ions before and after solar desalination.[189] Reproduced with permission from (Zhao et al., 2018), Copyright 2018 The Royal Society of Chemistry.

(H–L) Different MXene@ PVDF films.[190] Reproduced with permission from (Tan et al., 2018), Copyright 2018 Elsevier.

respectively, which are greater than those of normal VA-MXA. Zhao et al.[189] fabricated a long-term stable and highly efficient of solar desalination device with hydrophobic salt-blocking MXene film, which includes a solar absorber base-hydrophobic MXene film, polystyrene foam as floater, vapor evaporator and salt blockeras depicted in Figure 8C. During the procedure of solar desalination by vapor evaporation, the accumulation and deposition of the salt on the MXene film surface result in a gradually slower or non-ideal evaporation rate. There is little alteration in terms of the macroscopic morphology of the MXene film after 24-h desalination as given in Figure 8D. Meanwhile, the SEM images of the hydrophilic and hydrophobic MXene films are shown in Figure 8E. Experimental results from Figure 8F reflect that the solar steam conversion efficiency of the device could reach the maximum value of 71%, and the concentrations of four key ions (K^+, Na^+, and Ca^{2+}, Mg^{2+}) could be definitely decreased in excess of 99.5% rejection rate, satisfying the drinking standard as illustrated in Figure 8G. This implies that the hydrophobic MXene film not only contributes to obtaining freshwater from seawater, but also is suitable for water remediation. Tan et al.[190] utilized the composite MXene@ PVDF/polydimethylsiloxane (PDMS) as a membrane for the solar distillation application to improve the photo-to-thermal conversion efficiency. The photos and FESEM images of the membranes involving pure PVDF film, PDMS-coated PVDF film, MAX phase coated PVDF film and MXene@

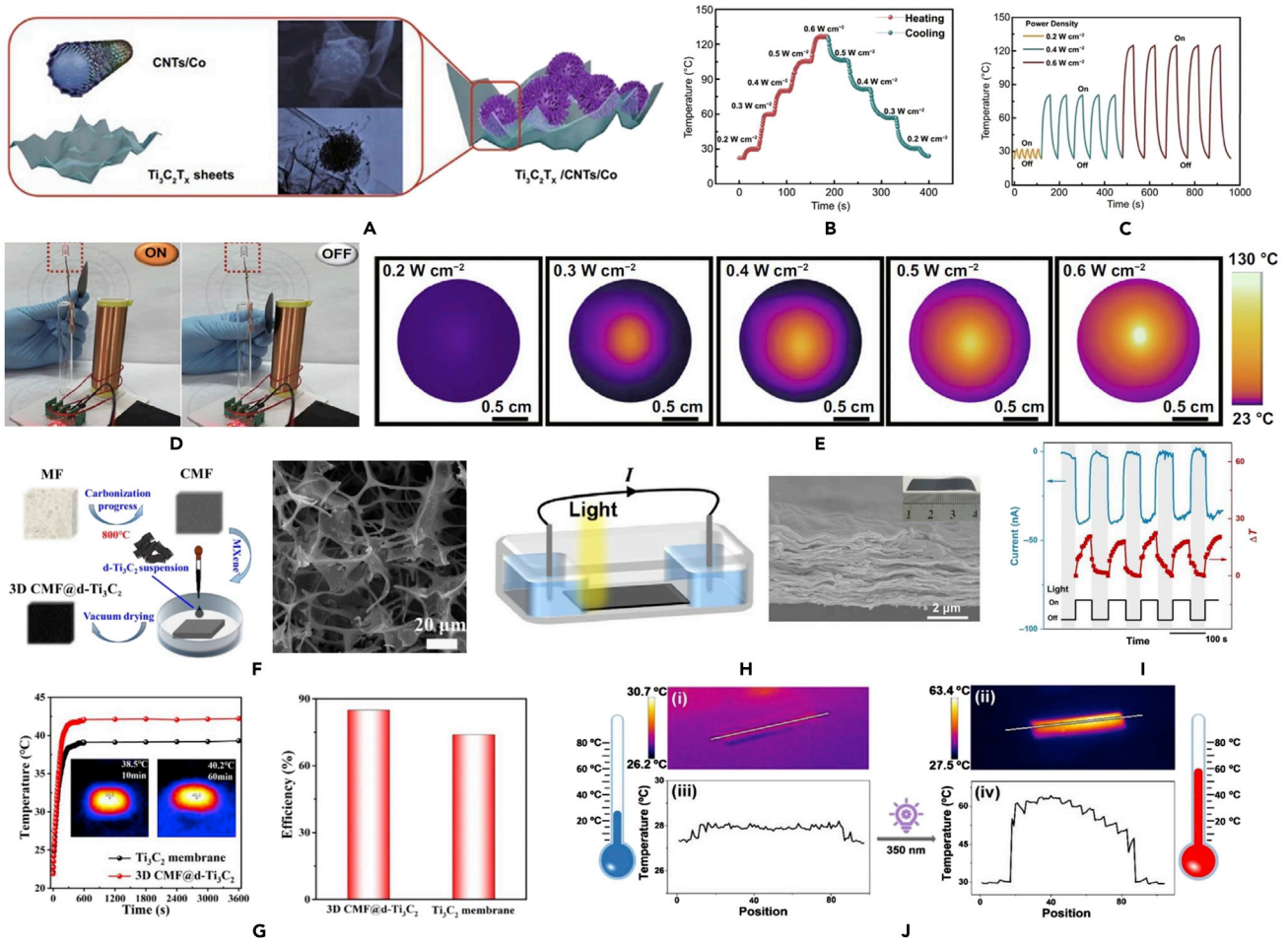

Figure 9. Different composite MXenes

(A) Composite MXene formation process.

(B) Electrical density.

(C) Heating variation at various NIR laser power densities.

(D) LED on and off.

(E) Infrared thermographic photos of the power densities of MXene@ PDMS variation.[191] Reproduced with permission from (Xiang et al., 2021), Copyright 2021 Springer.

(F) Fabrication process and SEM image of 3D MXene@ CMF.

(G) Vapor temperature variation and solar-to-vapor conversion efficiencies between 3D MXene@ CMF and 2D MXene.[192] Reproduced with permission from (Ju et al., 2016), Copyright 2019 World Scientific.

(H) Current production via the MXene film.

(I) Light caused because of temperature variation and current production.

(J) Temperature distribution with the MXene film.[193] Reproduced with permission from (Liu et al., 2020), Copyright 2020 Chinese Chemical Society.

PVDF film are displayed respectively in Figures 8H–8L. Specifically, the thermal images exhibit that both the pristine PVDF and PDMS-coated PVDF membranes exhibit slight growths in temperature of 6°C and 7°C, respectively. by comparison, the MAX@ PVDF and MXene@ PVDF films have significant temperature enhancements of 27°C and 49°C respectively. It is clearly demonstrated that the MXene can improve the photo-to-thermal performance.

Xiang et al.[191] developed an approach for fabricating MXene@ carbon nanotubes/Co nanoparticles (MXene/CNTs/Co) with EMI shielding efficiency, flexibility, excellent electromagnetic wave absorption capacity, hydrophobicity and photo-thermal conversion ability. Figure 9A exhibits the MXene@ CNT/Co formation process by adding the polydimethylsiloxane (PDMS). It is found from Figure 9B that the real-time temperature depends on the light power density, when the power density stepwise is increased from 0.2 to

0.6 W/cm^2, it decreases back to 0.2 W/cm^2. This indicates that the MXene@ PDMS/CNTs/Co film has a controllable light-to-heat conversion performance. In addition, the regular and stable increasing and decreasing temperature cycles corresponding to turning on and off the light over the entire cycling course are described in Figures 9C and 9D, demonstrating that the MXene@ PDMS/CNTs/Co film has the outstanding photo-thermal stability and recyclability. A uniform temperature distribution on the composite MXene film is illustrated in the infrared images in Figure 9E, and it is found that the power density varies from 0.2 to 0.6 W/cm^2. Ju et al.[192] synthesized the MXene@ CMF (carbonized melamine foam) by using the vacuum drying method as presented in Figure 9F, the SEM of 3D MXene@ CMF displays its original interconnected macroporous structure and the MXene nanosheets distribute on the mesh pores and framework. It is revealed from Figure 9G that the absorber and vapor temperatures speedily reach stable high values of 40°C and 42°C respectively, because of the restricted conduction loss of the thermal insulation layer. Moreover, when the water evaporation rate of the 3D MXene@ CMF is defined as 0.25 kg/m^{2}h, the conversion efficiency of the solar steam vapor could achieve 84.6%, which is higher than the 2D MXene film as given in Figure 9G. Liu et al.[193] designed a rectangular MXene film with both sides embedded with polydimethylsiloxane (PDMS) to avoid the solution leakage, and utilized a pair of Ag/AgCl electrodes to analyze the ion transport behavior via the MXene membrane in the horizontal direction as illustrated in Figure 9H. The cross-sectional SEM image from Figure 9H clarifies a highly ordered lamellar structure with a layer spacing of 0.27 nm on the basis of the XRD data. As presented in Figure 9I, the temperature of the illuminated region quickly increases up to 19.91°C (red line) because of the photo-to-thermal influences of MXene composite materials, and the corresponding ionic current enhances sharply to about −37.5 nA (blue line) based on the 200 mW/cm^2 light intensity of partial MXene film. Meanwhile, it can be observed from Figure 9J that the temperature of the MXene film experiences a substantial increase from 28 to 60 °C.

Zhang et al.[194] developed a composite MXene@ SnO_2 membrane to realize water purification and electricity production simultaneously, the MXene sponge material is placed on a ceramic boat and calcined, and maintains 800°C for 2 h to obtain the sponge-like 3D porous MXene framework (SPM) via strengthening the adhesion between the carbon skeleton and MXenn materials. The fabrication process of the MXene@ SnO_2 is exhibited in Figure 10A. Results from Figure 10B reveal that the top surface temperature of the MXene@ SnO_2 material varies from 24.3 to 44.8°C when the time is in the range of 600s to 6000s. By comparison, the temperature of material without adding the MXene@ SnO_2 is sustained at about 24.9°C after 6000s. This means that the solar thermal energy is consumed through the water vapor which has a highly efficiently energy utilization. In addition, the water evaporation rate of MXene@ SnO_2 film maintains almost constant over 12 h of light irradiation, but the evaporation rate of the 3D SPM material is gradually decreased by 65% after 12 h' light irradiation because of MXene surface oxidization as illustrated in Figure 10C. Zhou et al.[195] compounded the MXene@ carbon nanotubes (CNTs) membrane by using vacuum assisted filtration as given in Figure 10D, and the SEM image from Figure 10E indicates the MXene@ CNT composite material has an ultrathin thickness of 2–4 nm and a lateral size of 1–3 mm. As illustrated in Figure 10F, the almost same temperature framework during the repeated heating and cooling cycles specifies the recyclable and stable solar thermal conversion efficiency of MXene@ CNT films. The saturated temperature could be improved from 66.2 to 106.5°C when the solar irradiation intensity is further enhanced from 100 to 250 mW/cm^2 as depicted in Figure 10G. This linear proportional relation of solar radiation intensity to saturated temperature demonstrates that the MXene@ CNT contributes to regulating the photo-to-thermal performance conversion. More importantly, the composite MXene@ CNT material makes it suitable for actual applications, such as aerospace, portable and wearable electronic devices, which is regarded as an effective EMI shielding material because of its excellent durability against these aspects of the mechanical folding and bending, temperature treatment, chemical corrosion and ultrasonic stirring. Liu et al.[196] prepared the MXene@ PET (poly ethylene terephthalate) textiles via dip coating approach as depicted in Figure 10H, and found from Figure 10I that the saturated temperature of the MXene@ PET textiles can be improved sharply 150 °C and maintains a stability status after 1000 s operating, which contributes to providing a superb long-term heating reliability. Moreover, it can be demonstrated from Figure 10J that the overlapped temperature curves including the cycle-1, cycle-5, cycle-10 and cycle-30 at constant 3 V sustain a stable cycle and display superb electro-to-thermal conversion performance for the wearable heaters. Hence, Figure 10K illustrates the MXene@ PET textile application for the wearable heater around the knees, the maximum temperature of knees covered with the MXene@ PET textile could be enhanced by 60°C, whereas the minimum temperature is kept at 35 °C. This means that the photo-to-thermal wearable with MXene@ PET textile could sustain warmth for thermal energy storage application.

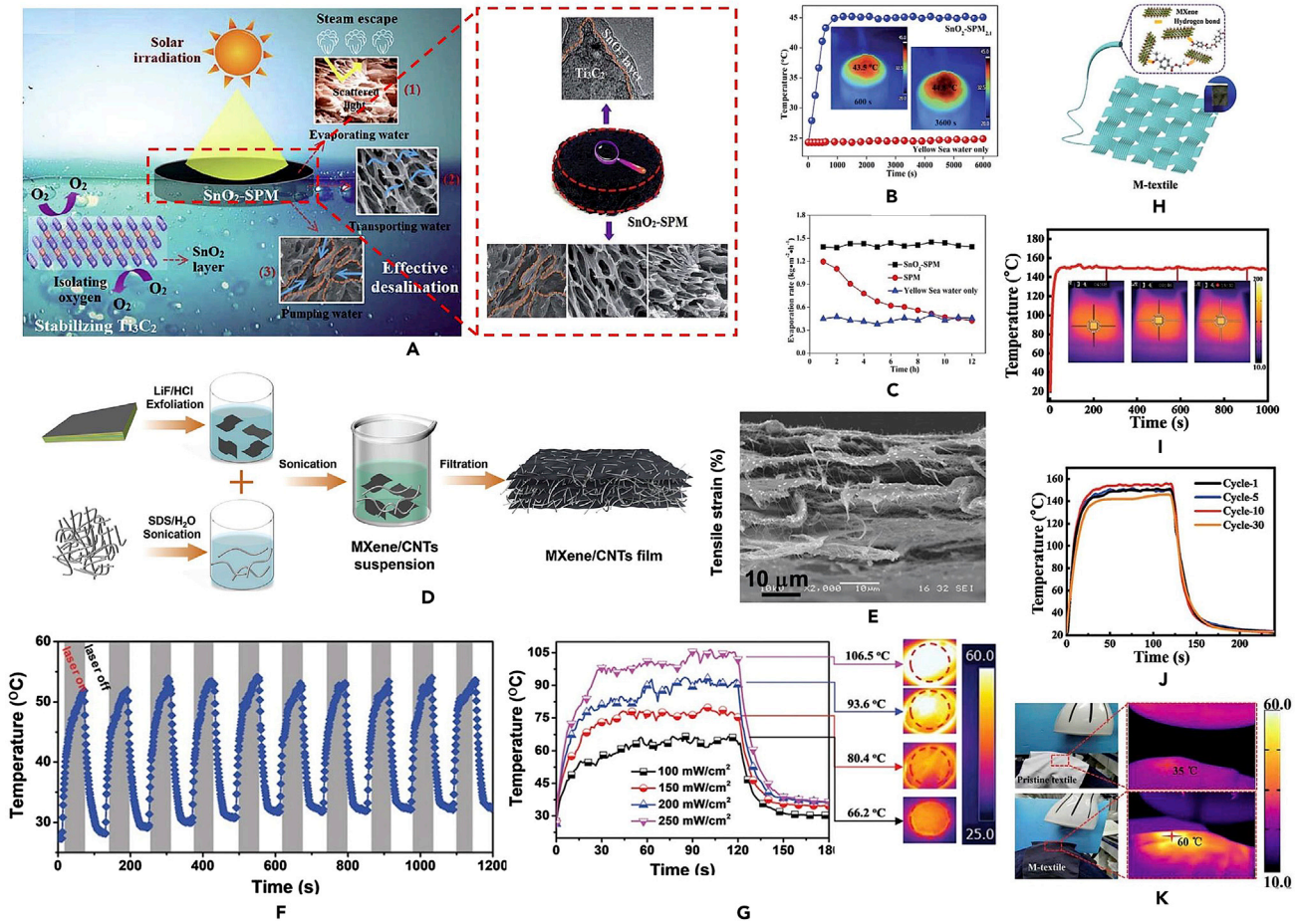

Figure 10. Different Composite MXenes

(A) A normal solar vapor generation system and SEM of preparation process of the SnO_2-SPM.

(B) Temperature of bulk water and SnO_2-SPM under one-sun irradiation.

(C) Evaporation rates comparison for SnO_2-SPM and SPM.[194] Reproduced with permission from (Zhang et al., 2020), Copyright2020 The Royal Society of Chemistry.

(D) Fabrication of flexible MXene@ CNT film.

(E) SEM image.

(F) Temperature profiles of the MXene@ CNT film under repeated on–off light irradiation cycles.

(G) Various irradiated electrical density with the corresponding IR images.[195] Reproduced with permission from (Zhou et al., 2021), Copyright2021 The Royal Society of Chemistry.

(H) Fabrication process of MXene@ PET.

(I) Temperature stability of M-textile-17.3.

(J) Cyclic electrical heating performance of M-textile-17.3.

(K) Digital and IR images.[196] Reproduced with permission from (Liu et al., 2020), Copyright 2020 The Royal Society of Chemistry.

Electro-to-thermal energy conversion

Advanced MXene composite materials can efficiently regulate the power to thermal energy conversion, thereby having a vital influence on sustainable energy utilization. Taking into account the inherent insulating property of pristine MXene, electrically conductive supporting materials are extensively employed to arrange composite MXene material for electro-to-thermal conversion and thermal energy storage. When electric current flows through the conductive MXene, the produced Joule heat is released. Afterward, the released Joule heat is absorbed via the MXene and finally stored in the form of latent heat.[197]

Li et al.[198] fabricated two categories of the bioinspired 2D MXene material as the nano-coating to present the multi-functionality, and found from Figure 11A that when the areal strain is defined in the range from 0 to 800%, the latex balloon varies from 0 to 150 cm^3. The wearable heaters are mostly electrically driven

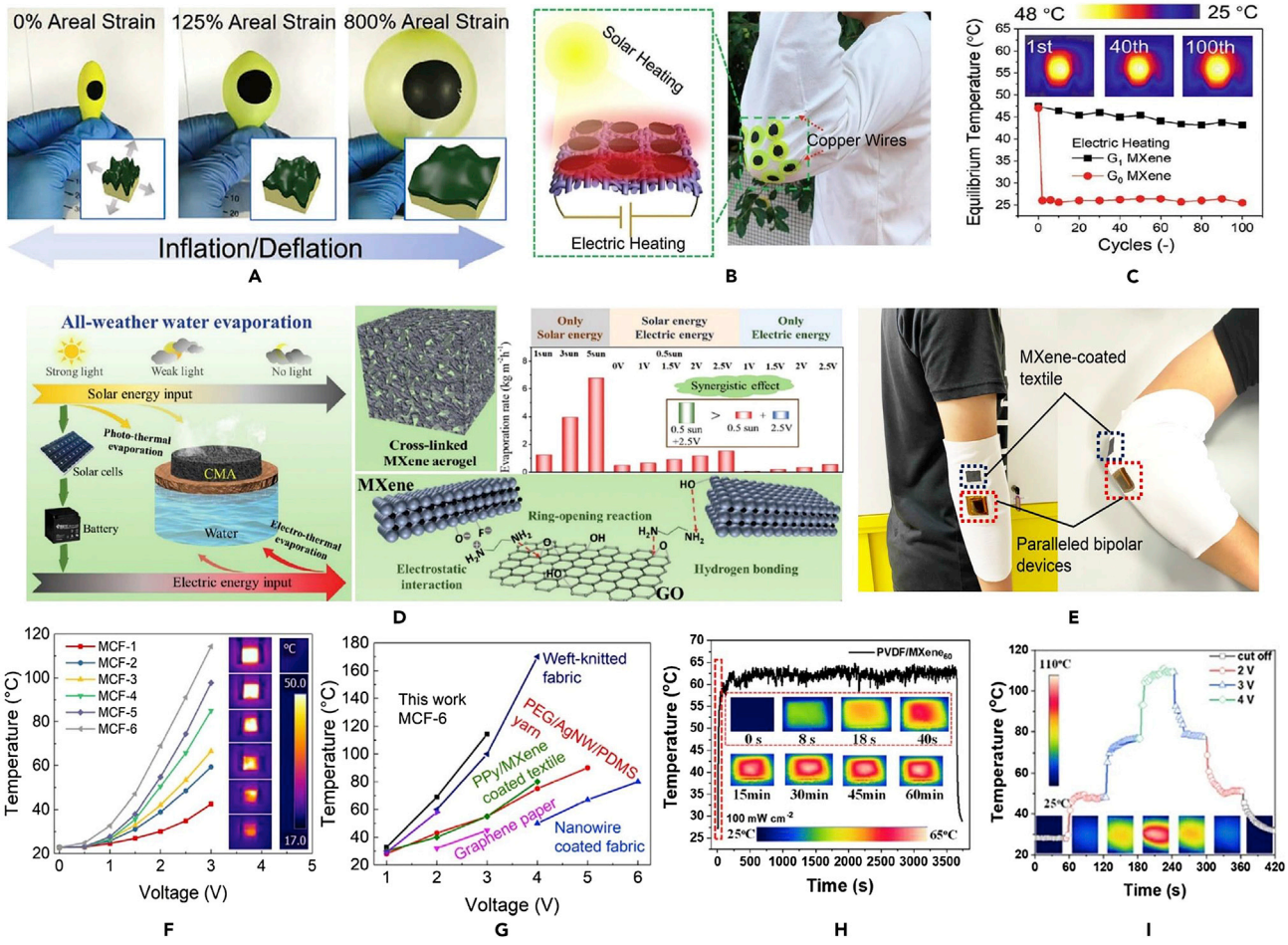

Figure 11. MXene energy conversion

(A) Digital pictures.

(B) Schematic and digital photographs of solar-electric device integrated with T-shirt for wearable thermal management.

(C) Balance temperatures and infrared images of the stretchable MXene heater based on various cycles.[198] Reproduced with permission from (Li et al., 2021), Copyright 2019 Wiley-VCH GmbH, Weinheim.

(D) Synergistic photo-thermal and electro-thermal conversion of CMAs and water evaporation rate and efficiency under all conditions.[199] Reproduced with permission from (Zhao et al., 2020), Copyright 2020 The Royal Society of Chemistry.

(E) Wearable demonstration of the MCF-based self-powered PBTM unit.

(F) Temperature versus voltage curves of MXene-coated cottons and various MCFs at 3 V.

(G) Electrical heating property comparison.[200] Reproduced with permission from (Li et al., 2021), Copyright 2020 Wiley-VCH GmbH, Weinheim.

(H) UV–vis–NIR absorption and reflection spectra of MXene@ PVDF film.

(I) Stepwise increasing and decreasing voltage from 2 to 4 V.[201] Reproduced with permission from (Luo et al., 2021), Copyright 2020 Elsevier.

and suffer from the requirements of steady and constant energy supply, the MXene nanocoatings on elastic substrates can be employed as the stretchable electrodes that can be self-powered by solar illumination and heated on demand as illustrated in Figure 11B. Test results from Figure 11C show that the stretchable MXene heater can heat up to 47.5°C and keep a balance temperature of 43.2°C after 100 cycles, indicating that the MXene heater has a stability for wearable thermal management. Zhao et al.[199] explored an all-weather-available steam production unit that is composed of cross-linked MXene aerogels to investigate the synergistic steam generation driven by integrating power energy with solar radiation as given in Figure 11D. It is demonstrated that the evaporation rate under the combined power energy of 2.5 V and solar illumination of 0.5 sun is greater than that merely 2.5 V or merely solar illumination of 0.5 sun. This results in enhancement of system energy conversion efficiency reaching 88.4% which is higher compared to that of only solar illumination of 0.5 sun (68.6%) and only 2.5 V voltage supply (43.4%). In addition, Li et al.[200] added the MXene@ cotton fabric (CF) heater on an elbow guard to achieve the personal body thermal regulation

including the air permeability and water vapor permeability as described in Figure 11E. The infrared images from Figure 11F show the influence of Joule heating on the electrical heating performance based on various voltages. Moreover, compared to the metal nanowires and graphene, the MXene@ CF represents higher conductivity and Joule heat because of a well-connected MXene flakes on the surface of cotton fiber as illustrated in Figure 11G. Li et al.[150] fabricated a flexible and durable MXene@ polyvinylidene fluoride (PVDF) film to enhance the photo-to-thermal performance, and concluded from Figures 11H and 11I that the MXene@ PVDF has an excellent capability of rapid controllable Joule heating, which contributes to ensuring the reliable EMI shielding performance underneath extremely cold conditions. Hence, these works not only develop novel solutions for the assembly of 2D MXene nanosheets into 3D MXene aerogels achieving highly light-absorbing and electrically conductive, but also provide innovative insights toward designing high-efficiency solar steam generator and person body thermal regulation unit under different complex conditions for practical applications.

Luo et al.[201] exemplified a super-hydrophobic, breathable and elastic smart textile device with a multiple core shell structure, which is made of four portions, including interface layer polydopamine (PDA), cheap and elastic textile substrate, functional layer MXene network and protective layer polydimethylsiloxane (PDMS) as depicted in Figure 12A. This contributes to enhancing the capability of waterproofing and breathability for the MXene@ PDMS smart textile as described in Figure 12B. Herein, it can be observed from Figure 12C that the saturated temperatures of the MXene@ PDMS textile could be boosted by 89.4°C, 61.6°C, 43.5°C and 36.8°C when the voltages are 14, V, 12V, 10V and 8V, respectively. This means that the input voltage can control effectively the saturation temperate of MXene@ PDMS textile. Meanwhile, according to Figure 12D, the maximum values of the working voltage is 12V which is lower compared to the standard safe 36V of the human body, indicating the MXene@ PDMS textile safety in practical application.

Nguyen et al.[202] added the platinum (Pt) into the MXene as a vapor phase infiltration (VPI) material to improve the electrical and thermal conductivities as described in Figure 12E, and discovered from Figures 12F–12H that the electrical conductivities of MXene@ Pt could be enhanced approximately 2.4 times for in-plane structure and 6.6 times for cross-plane structure in comparison with the pure MXene material, respectively. Similarly, the thermal conductivities of the MXene@ Pt could be boosted from 13.6 to 24.5 W/m·K for the in-plane structure and 0.14 to 0.7 W/m·K for cross-plane structure, which are 1.8 times and 5 times compared with the pure MXene materials, respectively. This means that the Pt can increase effectively thermal and electrical conductivities for both cross-plane and in-plane of the MXene. Sang et al.[203] constructed a multi-functional MXene@ polytetrafluoroethylene (PTFE) and polyimide (PI) tape with a sandwich structure utilization a facile "cut and tape" process as exhibited in Figure 12I. Specifically, the MXene film is first cut into the matching shape, then copper foil electrodes are fixed on the surface of the MXene film with conductive silver paste, and finally PTFE and PI tapes are affixed. As depicted in Figure 12J, the sandwich structure displays outstanding flexibility which could be arbitrarily folding bending and swirling. Results from Figures 12 K and 12L indicate that the composite MXene@ PTEF/PI could maintain the saturation temperature at 85°C when the applied voltage is 5V after 13 heating cycles. This indicates that the composite MXene material could provide a stability, long-term and durability of cyclic heating performance. In addition, Liu et al.[204] synthesized the composite 3D MXene@ sliver nanowires (AgNW) material based on the dip coating technique as illustrated in Figure 12M. The electrical heating measure results from Figure 12N demonstrate that the saturation temperature of the MXene@ AgNW could reach 45°C when the voltage is 1V whereas the saturation temperature could reach 215°C when the voltage is 3.5 V during a 30-s operating period. Furthermore, it can be found from Figure 12O that the saturation temperature of the MXene@ AgNW could be enhanced sharply by 224 °C within the 10s. This indicates that the 3D MXene@ AgNW not only sustains the advantages of the air permeability, flexibility and lightweight, but also presents high electro-to-thermal performance and human body thermal regulation.

Thermal energy storage

Energy storage is an important matter and becomes progressively vital because of quickly lessening fossil fuels, and as renewable energy resources are presently intermittent,[205] but its low conversion capacity of storage materials restricts its effectiveness. Herein, highly performance MXene contributes to solve the issue which is ascribed to desirable mechanical, thermal properties.[206] In addition, thermal energy storage based on MXene@ PCM contributes to alleviating the energy crisis and fulfilling the energy

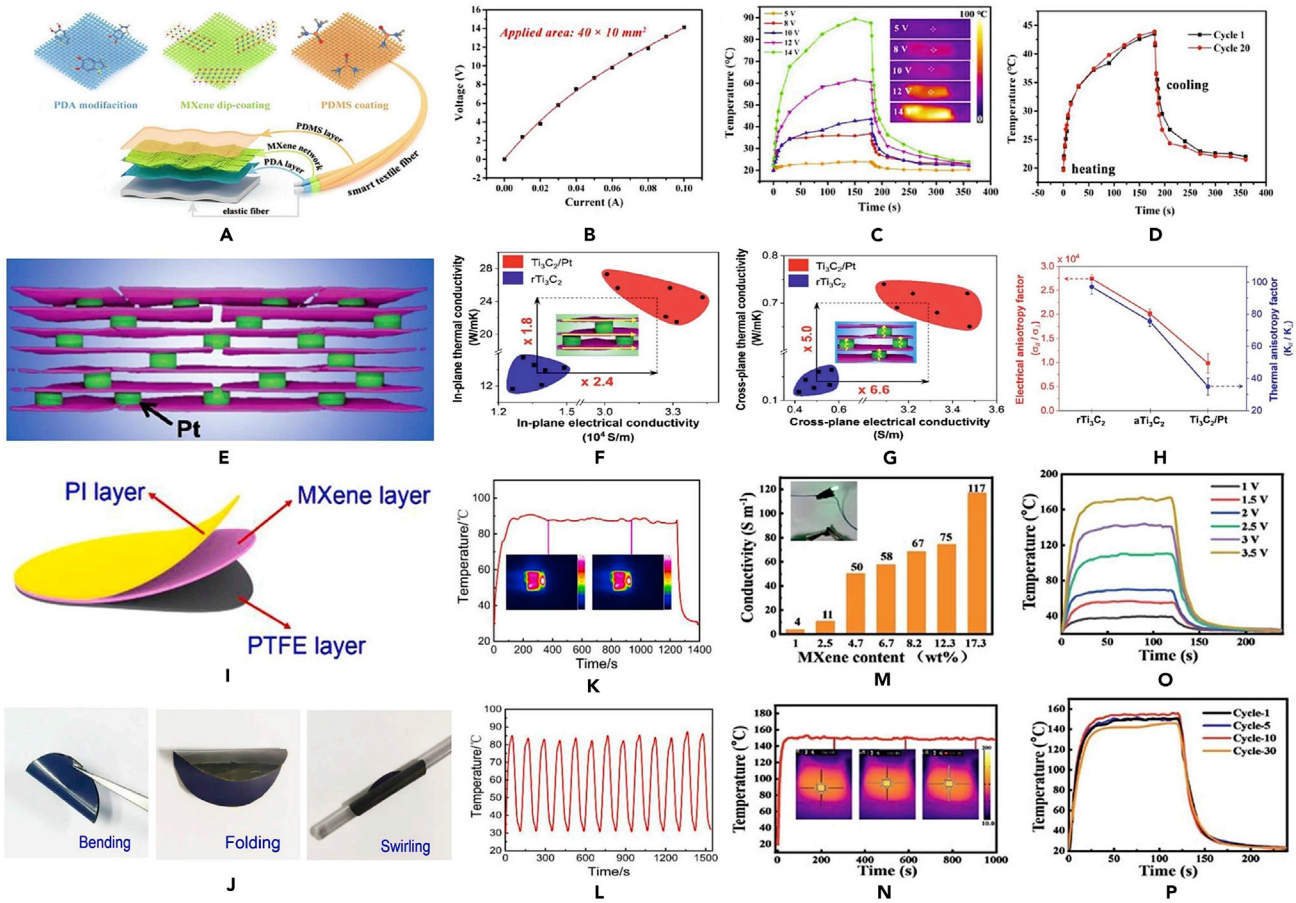

Figure 12. Composite MXene electro-to-thermal energy conversion

(A) Preparation process and structure of MXene@ PM/PDMS material.

(B) Waterproof and breathable properties.

(C) Temperature variation based on different voltages.

(D) Temperature stability variation.[201] Reproduced with permission from (Luo et al., 2021), Copyright 2020 Elsevier.

(E) Fabricating process of MXene@ Pt layer.

(F) In-plane electrical and thermal conductivities variation of MXene@ Pt.

(G) Cross-plane electrical and thermal conductivities variation of MXene@ Pt.

(H) Electrical and thermal anisotropy factors.[202] Reproduced with permission from (Nguyen et al., 2021), Copyright 2021 The Royal Society of Chemistry.

(I) Fabrication process of MXene@ PTFE film.

(J) Various synthesis structures including swirling, bending and folding.

(K) Temperature stability of MXene@ PTFE film at voltage of 5 V.

(L) Electro-to-thermal performance variation of MXene@ PTFE.[203] Reproduced with permission from (Sang et al., 2021), Copyright 2021 Elsevier.

(M) Fabrication process of MXene@ AgNW.

(N) Electric heating performance of MXene@ AgNW at different voltages.

(O) Temperature increasing of MXene@ AgNW.[204] Reproduced with permission from (Liu et al., 2022), Copyright 2022 Elsevier.

requirements.[207] Cao et al.[208] fabricated a shape-stable biomass/MXene phase change composites (SMPCCs) sample to investigate the performance of thermal energy storage by using a one-step method. As presented in Figure 13A, the SMPCCs sample is positioned on stage and exposed under the illumination of infrared lamp which is utilized to assess the light to thermal conversion property. The IR thermal camera recorded the temperature variation from 20 to 80°C. The results in Figure 13B indicate that melting enthalpy varies from 149.9 J/g to 145.5 J/g, resulting in the merely 2.9% of relative enthalpy efficiency loss. This means that the SMPCCs has excellent stability of solar light-to-thermal conversion, which provides powerful potential application in operation of solar energy for long time storage. Meanwhile, it can be observed from Figure 13C and 13 (D) that the intensity and transmittance of the SMPCCs could reach peak values after 20 light-thermal cycles. This indicates that the physical structure and chemical

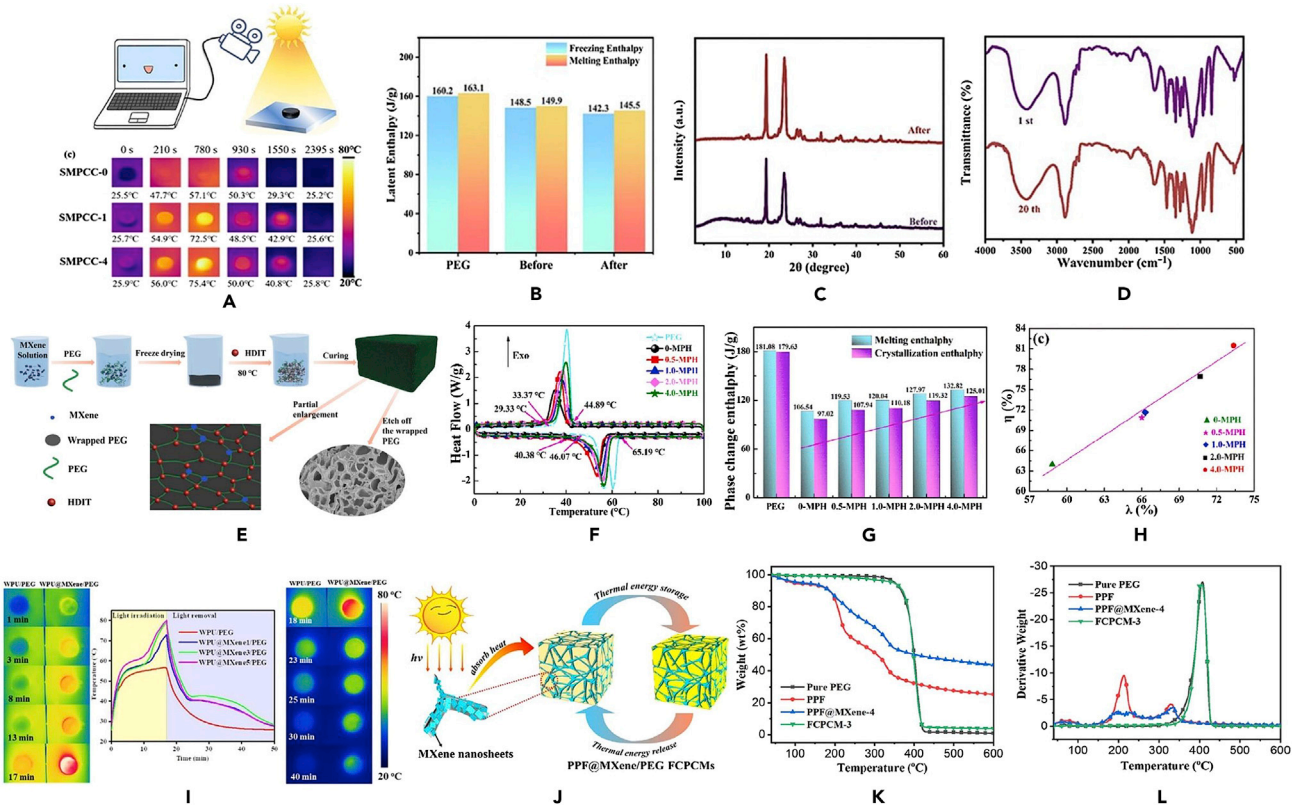

Figure 13. MXene electro-to-thermal energy conversion

(A) Schematic of setup for light-thermal conversion test and IR thermography pictures.

(B) Phase change enthalpy.

(C) Intensity variation curves.

(D) Transmittance variation patterns.[208] Reproduced with permission from (Cao et al., 2022), Copyright 2022 Elsevier.

(E) SSPCMs fabrication process.

(F) Heat flow variation.

(G) Phase change enthalpy variation.

(H) Enthalpy efficiency.[205] Reproduced with permission from (Gong et al., 2021), Copyright 2021 Elsevier.

(I) Storage and release performances of MXene@ WPU/PEG.[209] Reproduced with permission from (Hu et al., 2022), Copyright 2021 Elsevier.

(J) Schematic illustration of MXene@ PEG thermal energy storage.

(K) Temperature-time curves of MXene@ PEG.

(L) UV–vis–NIR absorption spectra of MXene@ PEG.[210] Reproduced with permission from (Sheng et al., 2020), Copyright 2020 Elsevier.

property of SMPCCs are rather stable. Gong et al.[205] developed a MXene@ polyurethane solid-solid phase change material (SSPCM) for improving thermal energy storage as illustrated in Figure 13E. It is found from Figures 13F–13H) that the crystallization and melting of the crystal structures are associated with the processes of the exothermic and endothermic. The melting and crystallization temperatures are in the range from 46.07°C to 65.19°C and from 33.37°C to 44.89°C, respectively. Also, its melting and crystallization enthalpies could reach 181.08 J/g and 179.63 J/g respectively, demonstrating that the materials have high energy storage density. Moreover, the enthalpy efficiencies could reach 81.5 and 76.96%, when the MXenes are 4.0MPH and 2.0 MPH, respectively. Taking into account the economic benefits, the overall performance of 2.0-MPH is superior compared with the 4.0-MPH. Hu et al.[209] compounded the MXene integrated with the water-borne polyurethane (WPU) and polyethylene glycol (PEG) aerogel to enhance thermal energy storage performance. The temperature variation of the MXene@ WPU/PEG material is recorded via infrared thermography camera as shown in Figure 13I, when the solar radiation period is increased, the inflection points in the temperature evolution curves of the MXene@ WPU/PEG occur in a range of 55.5°C–59.6°C, which is attributed to the solid-to-liquid phase change of PEG, demonstrating that the MXene nanosheets possess excellent solar absorption property.

Sheng et al.[210] developed a new bio-based pomelo peel foam (PPF) and PEG composite material which is combined with the MXene to increase the light-to-thermal conversion efficiency and thermal energy storage capability as described in Figure 13J. The DSC and TGA images from Figures 13K and 13L exhibit that the composite phase change material (FCPCMs) has a high latent heat reaching 158.1 J/g and good thermal reliability and thermal energy storage ability. More importantly, the MXene@ PPF skeleton owns efficient light-to-thermal conversion ability, which could be regarded as effective photon captors and molecular heaters for enhancing thermal energy storage and conversion efficiency. Shao et al.[211] proposed a novel material by compounding the MXene-coated melamine foam (MXene@ MF) into the PEG, and found that the phase change enthalpy and conversion efficiency could reach the maximum of 194.1 JG^{-1} and 92.7%, respectively, which indicates that the MXene@ MF/PEG material has the potential to achieve thermal energy storage for the long-term utilization purpose.

MXENE-BASED 3D PRINTING TECHNIQUES

3D printing technology, as a layer-by-layer additive manufacturing, is of huge interest because of its flexibility in light of sophisticated designing, material selections, speedy prototyping, and minimized waste for sustainability. Meanwhile, based on patterning and assembly techniques, the 3D printing techniques mainly includes fused deposition modeling (FDM), direct inkjet and non-digital printing (screen and transfer printing), which are heretofore utilized for nanoparticle assembly and patterning, but there are still some technical difficulties. Specifically, FDM has the mainly obstacles including the restricted selection of printing materials and high volume need of printable feedstock. For inkjet printing, the formulation of printable ink with fluidic properties and appropriate rheological is problematic, because the clogging results in slowing down manufacturing speed. By comparison, the demerits of screen printing technique are high surface roughness and low resolutions. However, because of MXene sheets and existence of hydrogen-bond interaction, MXene derivative materials permit facile shearing by the effect of the external forces, undertaking a novel type of soft matter, suitable for 3D printing.[212,213] Un-like conventional solutions involving vacuum deposition and photolithography, printing technologies have brilliant prospects in terms of low-cost manufacturing, high volume and fast speed, particularly for the fabrication of flexible devices[214] and target applications including transistors, conductive tracks, photodetectors, transparent electrodes, sensors, supercapacitors and batteries.[215] Currently, there are a large of 2D materials which are utilized as the conductive inks including graphene (GR),[216] hexagonal boron nitride (h-BN),[217] black phosphorus (BP),[218] transition metal dichalcogenides (TMDs),[219] but any of the available ink formulation techniques is not able to produce high quality mass scale GR functional ink for practical large scale printed electronic (PE) application. Consequently, it is necessary to develop novel functional ink formulation approaches and materials. By comparison, MXene is a low dimensional non-planar material, which exhibits highly conductive ink formulation for various applications. Specifically, 2D MXene materials could promote their actual demands in the fields of the 3D printing through conquering the existing boundaries of poor conductivity and high expense of alternative functional inks. Thereby, 3D printing technique has the capability of constructing complex 3D architectures owing to shear-thinning inks with tailored rheological behaviors and high viscosity. Herein, a lot of research has been concentrated on highly concentrated MXene ink (~300 mg/mL), high elastic modulus up to ~104 Pa and appropriate shear yield stress of ~102 Pa, which could provide an ideal ink for 3D print well-defined structures like lattices and arrays.[220,221]

MXene-based ink extrusion printing technique

Extrusion is regarded as the most common 3D-printed technique, which is utilized for modeling, prototyping and production applications. Yang et al.[222] utilized the base-MXene ink materials for obtaining the 3D-printed architectures which are ascribed to their high specific surface areas and excellent viscoelastic properties. As shown in Figure 14A, the freestanding 3D printing architectures are developed based on the extrusion printing technique, and the freeze-drying can sustain their dimensions and shape. Consequently, it can be observed from Figure 14B that the successfully fabricate 3D-printed architectures involve a 4-layer of MXene, a 5-layer of University of Manchester logo (UoM) and a 3-layer of bee, which are achieved via a 330 μm nozzle. Moreover, the SEM image from Figure 14C displays that the micro lattice structure has a 326 ± 13 μm of diameter establishing the interlaced configuration without bending. By comparison, the side view presents the boundary between individual printed filament layers without any overlap or internal collapse. This indicates that the viscoelastic property of the MXene ink is extremely appropriate for the 3D-printed freestanding architectures. Moreover, the results from Figures 14D and 14E demonstrate that the 3D printing technique realizes a high areal capacitance of 2.1 F/cm^2 at 1.7 mA/cm^2 and a gravimetric capacitance of 242.5 F/g at 0.2 A/g with a retention of overhead 90% capacitance

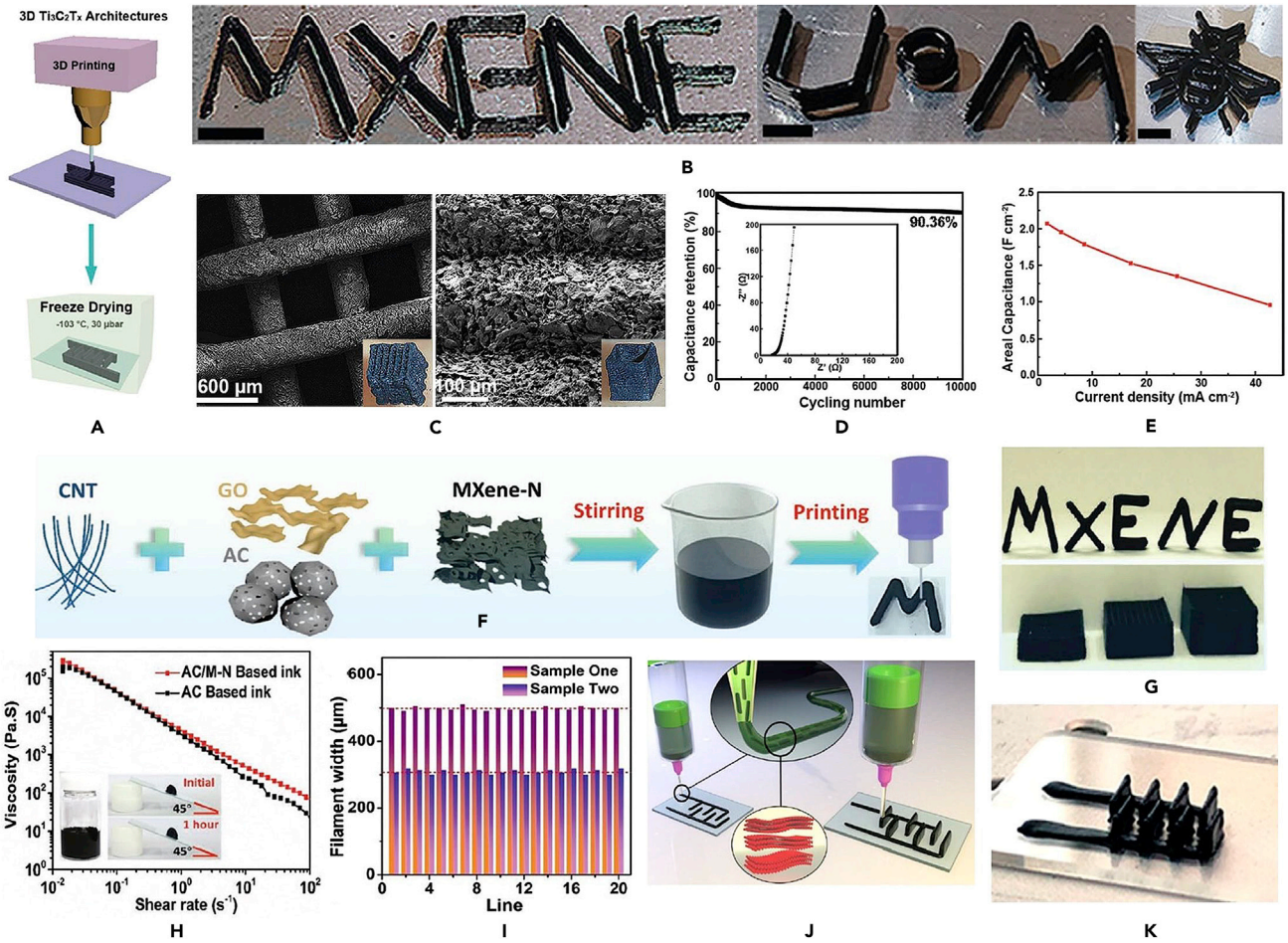

Figure 14. 3D printing based on MXene ink

(A) 3D printing of inks with freeze drying via a 330 μm nozzle.

(B) Various types of outcomes including 4-layer of MXene, 5-layer of University of Manchester (UoM) logo and 3-layer bee.

(C) SEM and digital photos.

(D) Cycling stability test.

(E) Areal capacitance versus different areal current densities.[222] Reproduced with permission from (Yang et al., 2019), Copyright 2020 Elsevier.

(F) Preparation process of MXene binder-free ink.

(G) 3D printing outcome based on the MXene@ GO/AC/CNT ink.

(H) Viscosity variation versus shear rate of the MXene@ GO/AC/CNT ink.

(I) Thickness variation of printing filament via two different nozzles.[74] Reproduced with permission from (Yu et al., 2021), Copyright 2019 Wiley-VCH GmbH, Weinheim.

(J) Diagram of a 3D MSCs printing process.

(K) Photo of the MSC-10 device printed on a glass substrate.[223] Reproduced with permission from (Orangi et al., 2020), Copyright 2019 American Chemical Society.

for 10,000 cycles. Meanwhile, it displays high energy density of 0.0244 m·Wh/cm^2 and high power density of 0.64 mW/cm^2 when the current density is 4.3 mA/cm^2. Yu et al.[79] developed a 3D extrusion printing by using nitrogen-doped MXene (MXene-N) nanosheets based ink to fabricate high areal mass loading electrodes as shown in Figure 14F. The ink is prepared via mixing MXene-N with graphene oxide (GO), carbon nanotubes (CNTs) and carbon (AC) to regulate the viscosity without using any insulating binders, and displays the different types of fine-printed patterns, such as a 15 mm height of "MXENE" rigid scaffold as given in Figure 14G. The results from Figure 14H show that the ideal shear thinning of ink is regarded as the non-Newtonian fluids, the clogging issue can be avoided during extrusion printing procedure, and the composite ink exhibits a high viscosity of above 10^4 Pas when the shear rate is 0.06 s. This indicates that the viscosity of the ink is vital to determining the 3D printing capability. Meanwhile, the influence of nozzle dimension on

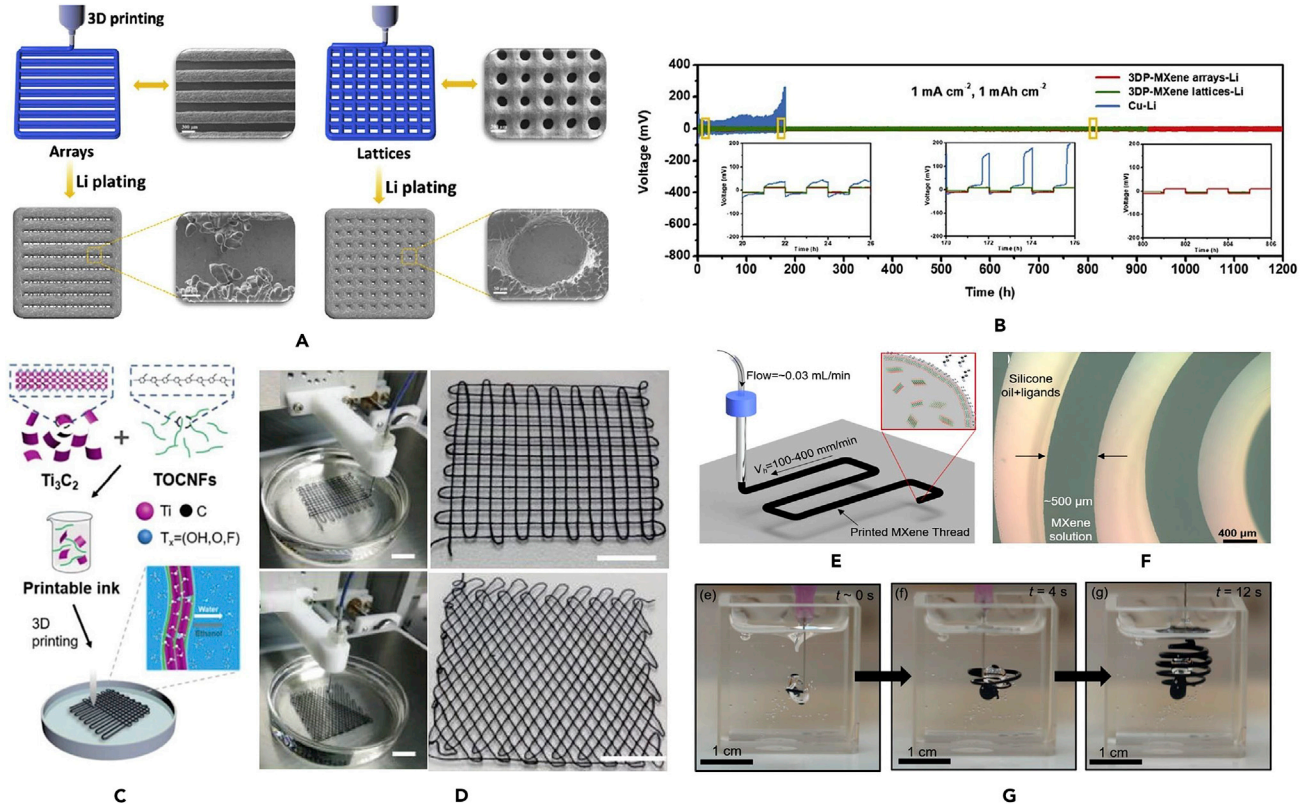

Figure 15. 3D printing

(A) Fabrication process of MXene@ Li-array and Li-lattices.

(B) Comparison of cycling performances.[224] Reproduced with permission from (Shen et al., 2020), Copyright 2020 Elsevier.

(C) Fabrication process of MXene@ TOCNFs ink.

(D) Images of the 3D printing MXene@ TOCNFs with woodpile and fishing net structures.[225] Reproduced with permission from (Cao et al., 2019), Copyright 2019 Wiley-VCH GmbH, Weinheim.

(E) Schematic diagram of 3D printing approach of the MXene@ oil and water.

(F) 3D-printed spiral structure.

(G) Overall 3D printing process.[226] Reproduced with permission from (Cain et al., 2019), Copyright 2019 American Chemical Society.

the extrusion printed filaments is clarified as given in Figure 14I, the 20 printed line width is in the range from 300 to 500 μm when the nozzles' diameters are 190 and 260 μm, respectively. Also, the capacitance retention could reach 96.2% after 5,000 cycles, representing excellent cycling stability. Orangi et al.[223] illustrated a fabrication process of 3D micro-supercapacitors (MSCs) by using the syringes with diameter of 230–600 μm and MXene ink with additive-free and water as shown in Figure 14J. Because of the viscoelastic properties, the multiple layers of MXene ink can be stacked to realize printed electrodes several millimeters in height without collapse as displayed in Figure 14K. So, the MXene@ MSCs ink could achieve the maximum energy density of 51.7 μWh/cm and obtain the outstanding areal capacitance which contributes to enhancing the electrode height and number of deposited layers.

Shen et al.[224] utilized a composite MXene@ lithium (Li) material as printing ink to realize the structure of 3D printing MXene with Li-arrays and Li-lattices as described in Figure 15A. Specifically, the MXene@ Li ink not only facilitates the nucleation of Li and the parallel growth of Li with the filaments, but also enables homogeneous distribution of Li-ion flux and electric field efficiently avoiding the increasing of Li dendrites. Results obtained from Figure 15B indicate that the MXene@ Li-arrays and Li-lattices could produce a low voltage of 10 mV, long cycle stability of 1200 h and high rate capabilities of 20 mA/cm^2. Cao et al.[225] fabricated a hybrid nanomaterial of MXene and TEMPO (2,2,6,6-tetramethylpiperidine-1-oxylradi-cal)-mediated oxidized cellulose nanofibrils (TOCNFs) as an ink (MXene@ TOCNFs) for 3D printing application as depicted in Figure 15C. The composite MXene@ TOCNFs material exhibits a high flexibility, excellent

electrical conductivity, tensile strength and cost-effectively. This contributes to regulating the size and structure, and enhancing the performance and extending application scope. Figure 15D displays the 3D printing MXene structure of the woodpile and fishing net. It is demonstrated that the composite ink has an excellent rheological property, which realizes precise structure and speedily printing. Meanwhile, it can be utilized to arrange multi-dimensional architectures with functional materials for various printing structures. Cain et al.[226] added the surfactants into the MXene ink for improving the viscosity and stability of liquid, and the flow rate of the MXene ink varies from 0.03 to 0.15 mL/min as illustrated in Figure 15E. The detail separation process of the based-MXene tubes, water and oil via the interfacial assembly of MXene sheet surfactants approach is illustrated in Figure 15F. Meanwhile, Figure 15G shows the entire 3D printing process and 3D nature of the printed constructs. This printing approach could fix the interface among MXene, oil and water, which helps to reduce the interfacial surface tension.

MXene-based ink continuous liquid interface production printing technique

Continuous liquid interface production (CLIP) is a proprietary 3D printing approach under the typical process of vat polymerization, which is a brilliant solution to additive manufacturing that capitalizes on the fundamental principle of oxygen-inhibited photopolymerization to produce a continual liquid interface of uncured resin between the exposure window and the growing part. Huang et al.[227] adopted the CLIP method to synthesize the base-MXene hydrogel precursor ink for 3D printing as depicted in Figure 16A. The MXene acts as an effective photo blocker to remarkably eliminate light scattering in the ink and thus enhance the printing quality. Figure 16B presents the 3D printed objects with smooth surfaces based on CLIP method involving a flower and "SCU" letters. In addition, to enhance the stability of 3D printing object, the glycerol is utilized to supersede the water within the MXene when the solvent exchange process is at 70 °C within 33 h as presented in Figure 16C. It is found from Figure 16D that the glycerol allows-NH_2,-OH, and-COOH groups on its molecule, which could form strong hydrogen bonding interaction between the PAM and SA, and exhibit tight adhesion to the surfaces of various materials. Infrared thermal images from Figures 16E and 16F illustrate that the temperature of the MXene@ PAM/SA organogel could be enhanced by 81.2°C after 30 min, by comparison, the temperature of the PAM/SA organogel is only 47.4°C during the same time period, demonstrating that the MXene has an outstanding light-to-thermal conversion performance and provides an appropriate hygroscopicity in terms of the atmospheric water harvesting. Jambhulkar et al.[228] applied the microcontinuous CLIP (μCLIP) method and direct ink writing (DIW) in 3D printing technique to produce a 2D MXene flakes as presented in Figure 16G. Specifically, the μCLIP approach could avoid the nozzle clogging, low viscosity and dyes caused via the effect of coffee ring. Meanwhile, to prevent the capillary effect, the automatic deposition of MXene@ ethanol suspension method based on the DIW is adopted simultaneously because of its high compatibility and high manufacturing flexibility. Results from Figure 16H reflect that the deposition of 10 mg/mL ink presents relatively more uneven morphologies compared to 20 and 50 mg/mL inks, which is clear and smooth from the 3D surface mapping. This indicates that the higher interaction between nanoparticles in concentrated dispersions is conduced to unpredictable island formation within the micro channel and nanoparticle agglomerations. In the meantime, it can be observed from Figures 16I and 16J that the particle thickness grows with the particle concentrations and layer numbers. In summary, the hybrid 3D printing approach has a massive potential for scalable, digital, rapid and low price manufacturing of hierarchical structures, particularly for micro patterning and aligning 2D nanoparticles not easily accessible via traditional processing solutions.

Other MXene-based ink printing techniques

Yuan et al.[229] combined the freeze-drying and dip-coating approach with the 3D printing technique to fabricate the MXene@ melamine sponge material for achieving the microwave shielding and transmitting functions simultaneously as shown in Figure 17A. To be more specific, a dimension of 50 × 10 × 0.5 mm 3D printed resin base is utilized to support the MXene@ melamine sponge (MMS) as a base unit as shown in Figure 17B. The digital photo of the composite MMS on a green plant indicates the composite sponge is lightweight in Figure 17C. Yu et al.[230] prepared a MXene@ NiCoP (NCPM) material as an ink formulation for the 3D printing as exhibited in Figure 17D. Also, a square-shaped box with a dimension of 10 × 10 × 3 mm^3 is constructed by a layer-by- layer printing method, where NCPM-based ink is injected from a nozzle at a constant speed of 2 mm/s. It can be disclosed from Figure 17E that the device consists of a printed AC negative electrode and an NCPM positive electrode in a KOH aqueous electrolyte, and the cycling performance and specific capacitance are constant, indicating outstanding cycling stability. The areal energy density and volumetric energy density of the 3D-printed MXene@ NCPM material could reach 0.9 m·Wh/cm^3 and 2.2 m·Wh/cm^3, respectively, which are evidently superior to other materials as

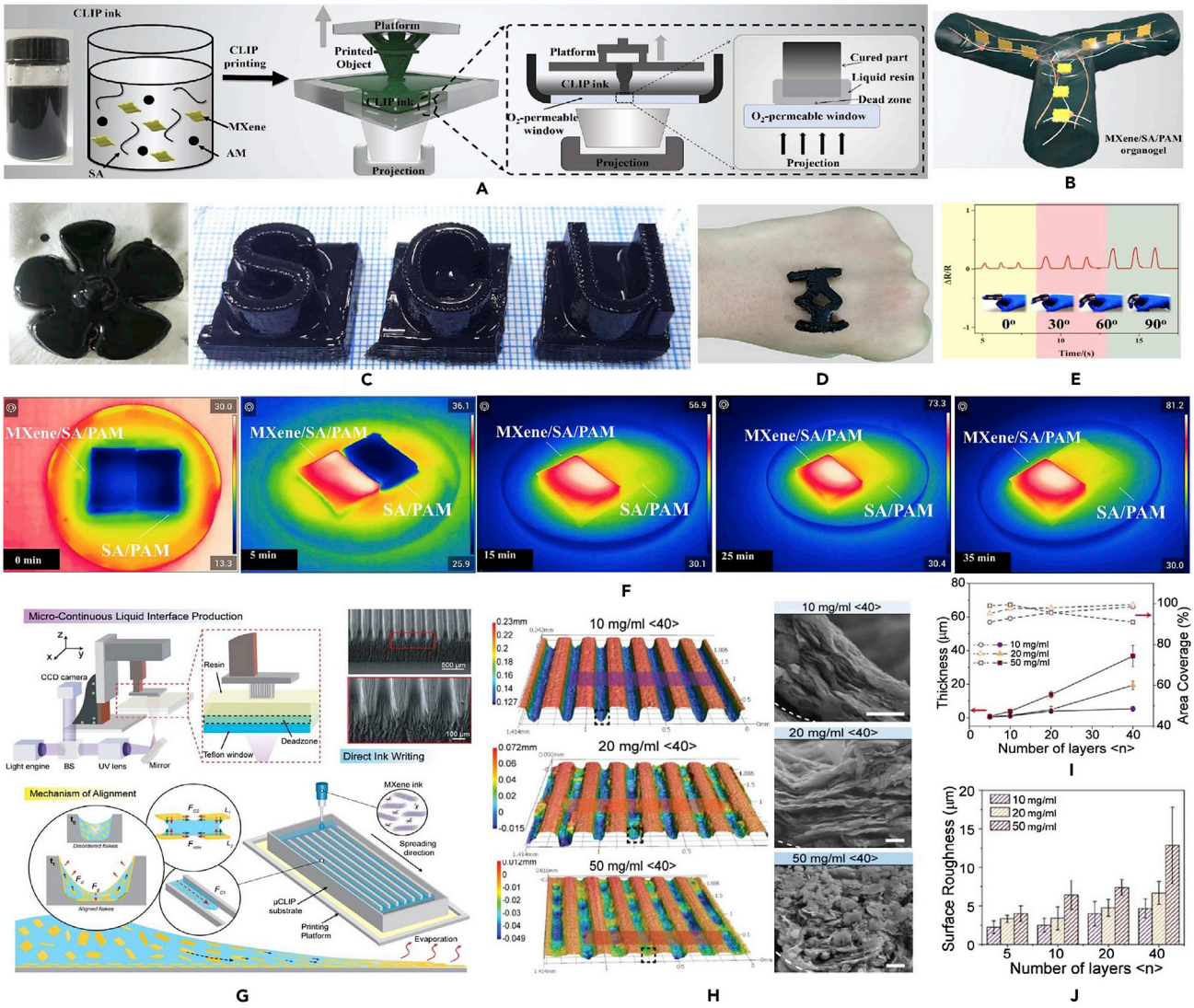

Figure 16. CLIP 3D printing technique

(A) CLIP process.

(B) CLIP-printed flower and SCU letters.

(C) MXene@ PAM/SA organogel.

(D) Chemistry structure of MXene@ PAM/SA organogel.

(E) Temperature variation comparison between MXene@ PAM/SA and PAM/SA organogels.

(F) 3D printing integrated with μCLIP and DIW technique.[227] Reproduced with permission from (Huang et al., 2021), Copyright 2020 Elsevier.

(G) 3D printing surface mapping and SEM images.

(H) MXene particle thickness variation with number of layers.

(I) Surface roughness variation with number of layers.[228] Reproduced with permission from (Jambhulkar et al., 2021), Copyright 2021 American Chemical Society.

illustrated in Figure 17F. To overcome the poor electrochemical performance of a bare 3D-printed carbon electrode, Kumar et al.[231] combined the fused deposition modeling (FDM) with dip-coating method to realize the 3D-printed MXene@ nanocarbon electrodes (CEs) as shown in Figure 17G. An SEM image of MXene@ CEs is described in Figure 17H, and it is observed that the surface of the dip-coated 3D-CEs could be attached to the surface of MXene layers. It is demonstrated that the modified 3D printing method contributes to enhancing the catalytic property of the electrodes and coat a variety of substrates, which could be applied for different electrochemical utilization in the future. Wei et al.[232] adopted a 3D printed method for a Lithium (Li)– sulfur battery by using the nitrogen-doped porous MXene (N-p MXene). Figure 17I

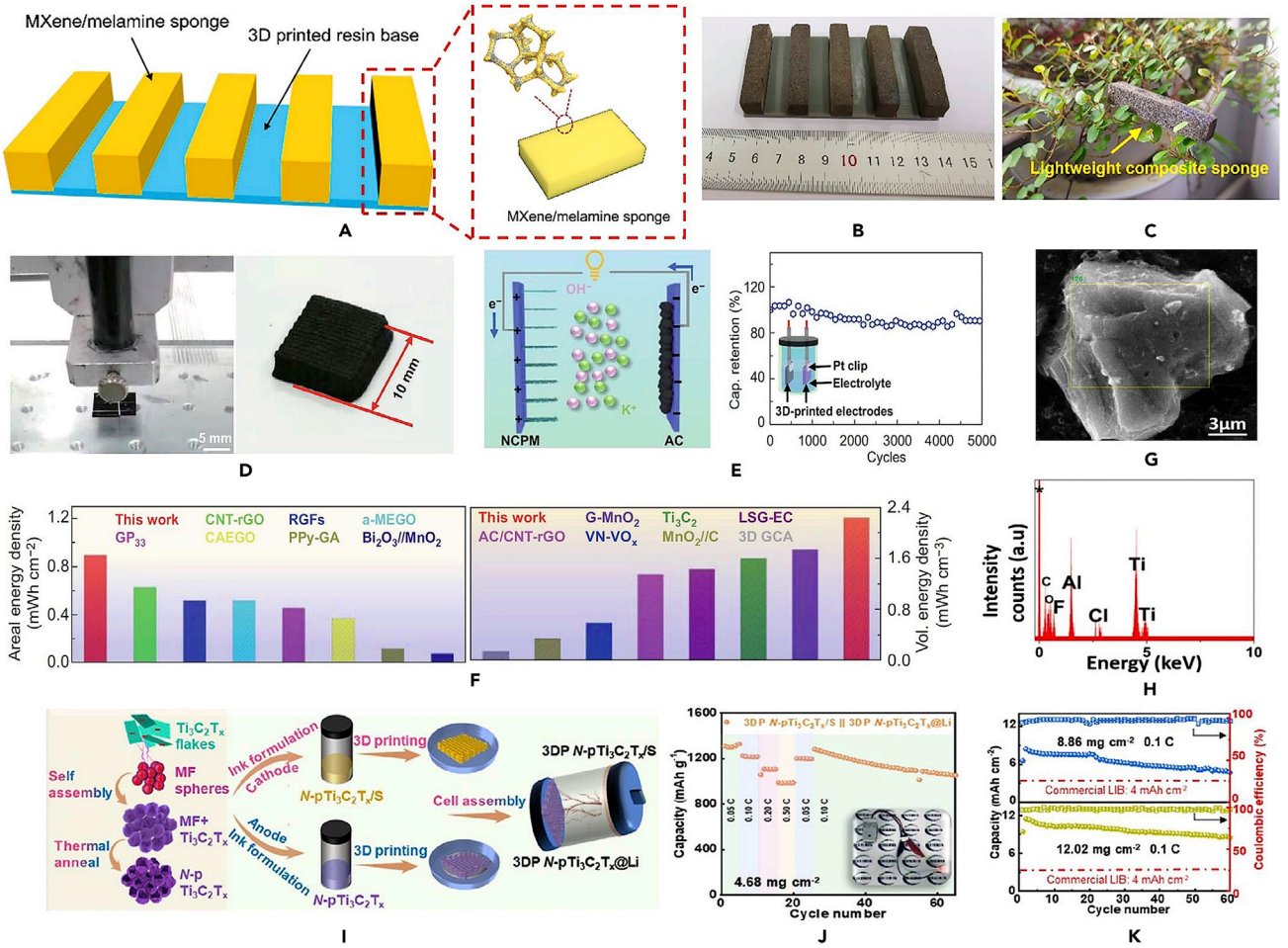

Figure 17. Other MXene-based ink printing

(A) Fabrication process of the MXene@ melamine sponge.

(B) Actual photo of 3D printing with MMS.

(C) MMS on a green plant.[229] Reproduced with permission from (Yuan et al., 2021), Copyright 2021 Elsevier.

(D) 3D printing MXene@ NCPM.

(E) 3D-printed NCPM components.

(F) Comparison of areal and volumetric energy densities.[230] Reproduced with permission from (Yu et al., 2020), Copyright 2019 Wiley-VCH GmbH, Weinheim.

(G) FDM 3D-printed with dip-coating method.

(H) SEM image of 3D-printed nanocarbon electrodes (3D-CEs).[231] Reproduced with permission from (Kumar et al., 2021), Copyright 2021 American Chemical Society.

(I) Preparation process of N-p MXene.

(J) Rate performance.

(K) Cyclic performances.[232] Reproduced with permission from (Jambhulkar et al., 2021), Copyright 2020 Elsevier.

describes the fabrication process of the N-p MXene@ Li as the ink, which includes continuous stages of material preparation, ink formulation and 3D printing cell assembly. It can be seen from Figure 17J that the capacities of the N-p MXene@ Li could reach 988.2, 1110, 1217 and 1300 mAh/g when the cycle numbers are 0.5, 0.2, 0.1 and 0.05C, respectively. Moreover, as presented in Figure 17K, the 3D-printed with N-p MXene@ Li ink could provide a high areal capacity of 8.47 mAh/cm ^{2} when the sulfur loading is 12.02 mg/cm ^{2}. This N-p MXene@ Li material can also offer adequate space for massive Li deposition, so it could be widely applied for energy conversion and storage utilizations in practical engineering.

In this section, the recent development of 3D printed techniques has been summarized based on different MXene-based inks, and the vital characteristics of these techniques are illustrated in Table 3. Each category

Table 3. 3D printed techniques

Printing techniques		Reference	Ink material	Configuration	Key findings
MXene-based ink extrusion printing technique		Yang et al.,[222]	MXene	Symmetric, stereo-3D	• To achieve the 2.1 F/cm^{2}of areal capacitance with 0.244 m·Wh/cm^{2}of energy density and 0.64 mW/cm^2 of power density.
		Yu et al.,[74]	MXene-N@ AC-CNT	Symmetric, stereo-3D	• The areal capacitance is 3.4 F/cm^2 for one-layer, 5.2 F/cm^2 for two-layer and 8.2 F/cm2 for three-layer electrode. • The volumetric energy density is 0.83 m·Wh/cm^2.
		Orangi et al.,[223]	MXene@ superabsorbent polymer	Symmetric, planar	• To achieve 1035 F/cm^2 of areal capacitance with 51.7 μm·Wh/cm^2 of energy density.
		Shen et al.,[224]	MXene@ Li	Symmetric, stereo-3D	• To realize a 20 mA/cm^{2}of capability rate and 1200 h of stability cycling.
		Cao et al.,[225]	MXene@ TOCNFs	Symmetric, planar	• To display high sensitivity, flexibility and outstanding durability.
		Cain et al.,[226]	MXene@ water-oil	Asymmetric, planar	• To lower the interfacial surface tension.
MXene-based ink continuous liquid interface production printing technique		Huang et al.,[227]	MXene@ SA-PAM	Symmetric, stereo-3D	• To boost structural stability and satisfactory adhesion to various surfaces.
		Jambhulkar et al.,[228]	MXene	Symmetric, planar	• To achieve multi-layer material and multi-scale additive manufacturing
Other techniques	DIW	Yu et al.,[230]	MXene@ NiCoP	Symmetric, stereo-3D	• To exhibit a 1.4 V of voltage with 5000 cycles of long operating. • To reach 2.2 mWh/cm^{3}of volumetric energy density and 0.89 mWh/cm^2 of ultrahigh areal capacitance.
	Dip-coating technique	Kumar et al.,[231]	MXene@ nanocarbon	Symmetric, planar	• To enhance the catalytic surface properties of MXene@ nanocarbon electrodes.
	DIW	Wei et al.,[232]	MXene-N	Symmetric, stereo-3D	• To achieve 0.5 mA/cm^2 of current density with long operation of 1600 h.

of the mentioned 3D printed techniques has its own merits and demerits. Specifically, the MXene-based ink extrusion printing technique is straightforward for fabricating 3D designs through layer-by-layer stacking of the MXene-based ink on the basis of programmed patterns. The prior condition for this technique is gaining MXene-based inks that retain a unique shear-thinning rheological behavior that prompt them to be printable. The continuous liquid interface production (CLIP) 3D-printed technique has attracted huge attention because of fast printing speed (>500 mm/h), high surface smoothness and extraordinary relationship between the slicing thickness and speed of the device. By comparison, laser-based 3D printing employs a highly focused laser beam with ultrahigh energy to produce complete fusion and melt a printed material and obtain pre-designed 3D architectures by moving the laser point along a programmed route. In sum, 3D printing technique could provide tremendous flexibility that is completed different from traditional fabrication techniques. However, lots of difficulties need to be solved before 3D printing technique could be ubiquitously applied for fabrication. Most of 3D printing techniques permit controllable patterning of highly ordered large pore, then very few solutions could handle the distribution of pores within the scope of sub-micron, which also vitally effect device performance. Meanwhile, the qualification of the MXene is conducive to averting vaporization and speedily solidifying. Furthermore, it is demonstrated that the modified 3D printing method like the modified dip-coating method contributes to enhancing the catalytic property of the electrodes and coating a variety of substrates, which could be applied for different utilizations in the future.

LIMITATIONS OF THE STUDY AND FORWARD-LOOKING UTILIZATION OF COMPOSITE MXENE NANOMATERIALS

This review highlights the recent advances in 2D layered MXene derivative nanomaterial for synthetic technique, thermal energy storage and conversion as well as MXene-based 3D printing techniques. The thermal and electrical conversion performances of the MXene-based composite nanomaterial are enhanced because of large specific surface area, hydrophilicity, high electrical conductivity and stability. Until now, MXenes have already presented potential in some areas, like EMI, thermal energy conversion and storage applications. Despite the numerous advantages of these materials, there are still many challenges hindering their particular applications. Meanwhile, novel applications are emerging where MXene exceed other nanomaterials, like hydrogen energy storage, radio frequency field applications, carbon dioxide capture and remediation of environmental pollution.

Crucial observations

The great conductivity, unique morphology, thermoelectric and magnetic properties assist the MXene as the promising materials to achieve plenty of applications including the wearable device, catalysis, photo-to-thermal therapy, surface plasmon technology, and environmental pollution regulation. However, the understanding of the MXene structure and performance are still in the infancy stage; in the meantime, there are many issues in the aspects of the theory, trial, application, cost and 3D printed technique.

- The thermal stabilities of MXenes generally depend on their dimension, composition materials, synthetic method and environment. The bigger size of MXene contributes to boosting their thermal stabilities. Current research normally supports the opinion that single MXene could be oxidized into TiO_2 during delamination and storage under ambient air condition. This would affect the chemical stabilities of MXene for long term utilization, particularly in photo-to-thermal utilizations. To solve the oxidation issue, the roadmap of 2D MXene materials has been established including photo-to-thermal conversion as a vital landmark. Based on state-of-the-art thoughts, the existing difficulties could be overcome to make MXene one of the prominent photo-to-thermal materials for wide-ranging utilizations.
- The versatile composition of MXene ensures high quality, complexity and reproducibility. Even small alterations during the synthesis process period change the degree of etching, exfoliation and intercalation, as well as surface terminations of flakes, which impacts their stable and physical properties. Consequently, a more profound understanding of the synthesis method contributes to obtaining a better regulating, and guarantee reproducibility in the number of stacked sheets with known flake dimension and interlayer spacing.
- It is still problematic in terms of the exposure of MXene to ambient air because of deficiency of chemical inertness; nevertheless, scientists are discovering some novel solutions to address this instability of MXene based on adjusting the precursor of MAX phase. Consequently, dynamic and thermodynamic stabilities of MXene dominate the synthesis probability or difficulty, whereas etching and post-treatment methods contribute to regulating the surface chemistry. In addition, the mechanical properties of most reported MXene composite materials are inferior, considerably preventing the practical application in many regions. The enhancement of the MXene material mechanical property, such as Young's modulus, fracture toughness, hardness and tensile strength, contributes to improving the actual applications.
- As for 3D MXene structures, their morphology, pore-size, conductivity and hydrophilicity properties have a significant influence on their thermal energy conversion and storage abilities. Therefore, the effects of each parameter in different fields of the application are required to be investigated via high accuracy processing. Moreover, most 3D porous structures for thermal energy conversion and storage are measured in half-cell units. Despite being a practical approach for assessing the potential, the actual capabilities of volumetric and electricity as well as actual demands rely heavily on the full-cell composition and designs, which are yet to be discovered.
- The unique rheological properties realized via the 2D MXene inks integrated with the sustainability solution contributes to accelerating to discover other demands organized 3D architectures, meanwhile, the strategy contributes to expanding to combine other structural and functional materials into MXene-based 3D printable inks. This means that the exploration of innovative MAX phases and related to 2D materials must be investigated for future research, which assists to achieve

well-stability and cost-effectively ink materials. Even if the chemical reliability and quality of the MXene material are enhanced, the synthesis cost of the composite MXene material still maintains a high value. Decreasing the fabrication expense through modification in the chemical usage or MXene properties should be investigated to form an eco-friendly, cost and sustainability process.

To sum up, addition of the MXene into different materials results in various alterations in terms of synthesis circumstances including the surface termination of flake, exfoliation, intercalation and etching degree, indicating that the stability, physical properties and process ability are affected. As a result, a more profound investigation of the synthesis method is necessary to obtain better regulating and guarantee reproducibility in the MXene stacked sheets between flake size and interlayer spacing. When the chemical quality and reliability need to be enhanced, the synthetic methods of the MXene composite materials are quite expensive and less environmentally friendly; also, very few researches could adopt the fluorine-free syntheses approach. Moreover, conventional PCM (paraffin wax) in thermal energy utilization contributes to absorbing or releasing an amount of heat during phase transition with a wide-ranging of temperature, however, 0.21–0.24 W/m·K of low thermal conductivity of paraffin wax has become a demerit in thermal energy applications causing a dramatically decelerating for energy charging and discharging rates. Introduction of the MXene into PCM is conducive to boosting significantly thermal energy capacity and stability. Therefore, it is necessary to select proper PCM category based on various application scenarios for making it better in performance in light of energy stability and storage capacity. At an applied level, although the colloidal stability and anti-oxidation ability of the MXenes have considerably been enhanced over the past few years, the MXene inks stability still presents issues for industrial application because of its short shelf life. In the meantime, scalability is another problem. Despite several changes having been made, the highly toxic hydrofluoric acid is still the mainstream etching agent to generate the MXenes, making the industrialization of the MXene inks highly challenging, which is a fast-emerging arena that needs efforts on both theoretical and experimental areas. Meanwhile, the batch size of the MXene is still on a gram level, hence, there is a long way to go before it achieves industrially relevant quantities accordingly. For example, it is not applied to achieve the MXene printing by using the roll-to-roll approaches owing to high industrialization. Moreover, the combination of various and patterned and printing technologies contributes to providing quicker production speed and more multifaceted printed structure based on various feature sizes and demands on MXene-based inks. Furthermore, high power of 3D printing technology in terms of the new composite material construction assembly and multi-functionality need to be further discovered, which can assist with enhancing the performance of device and lowering manufacturing expense.

Forward-looking utilizations of composite MXene nanomaterials

In addition, the MXene exhibits a great future in different fields because of its advantages like high-performance solid-state 2D materials, light weight, high density and calorific value, high surface area, high adsorption energy capacity, charge transfer ability between MXene and CO_2 and more multiple adsorption spaces. These contribute to opening novel research window to achieve more energy conversion, energy storage and environmental protection, such as hydrogen energy storage, radio frequency field applications, CO_2 capture and remediation of environmental pollution by using the MXene-based materials.

Hydrogen energy storage

Hydrogen is regarded as a preferable choice to phase out the utilization of fossil fuels because of its light weight, high gravimetric energy density and high calorific value. Meanwhile, it can also prevent global warming because there is no direct GHG emission and fossil fuel combustion. Nevertheless, the hydrogen energy storage solutions have security threat issues, making the solid-state storing method an attractive alternative selection. Storing hydrogen in solid state is safer, more practical and economical compared with that in liquid or gaseous phases. Hu et al.[233] found that the merits of MXene as hydrogen storage media include the effectiveness for hydrogen storage in carbon-based materials, high gravimetric hydrogen storage capacity, and high surface area per weight. Herein, MXene is utilized as the hydrogen energy storage media at moderate temperature and pressure. Kumar et al.[234] utilized the MXene nanoparticle materials for the hydrogen energy storage to obtain the maximum capacity of the hydrogen energy storage of 8.55 wt %, which is far higher than the gravimetric capacity of metal-based complex hydrides. Therefore, further investigation on employing the MXene as a hydrogen storage media should be implemented for enhancing hydrogen energy storage capacity and adsorption properties. In addition, the interaction of MXene surface with the molecular-atomic hydrogen is a vital parameter to attain the optimum hydrogen storage and adsorption ability; also, the

interlayer spacing among MXene sheets, the role of functional groups and fundamental topographical properties of the MXene multiple-layers needs to be explored for future research.

Radio frequency field applications

To develop the wearable and portable electronic devices, the MXene is utilized as a novel antenna instead of the traditional metal antenna at high frequencies, particularly used in fifth-generation (5G) network. To be more specific, the MXene antenna is manufactured by using the microstrip patch based on the spray-coating fabrication approach, which has the characteristics of the micro-meter-thin and flexible. Also, the target frequencies are in the range from 5.6 GHz to 16.4 GHz.[235] The radiation efficiency of a 5.5 μm thick MXene patch could achieve 99% at 16.4 GHz, which is the same as that of a typical 35 μm thickness copper patch antenna at approximately 7% of the copper weight and 15% of the thickness. Furthermore, Habib et al.[236] demonstrated that MXene sustains a high dielectric loss, which is ascribed to rapid heating in radio frequency field, and the structure of MXene is conducive to achieving 303 K/s of extraordinary heating rate because of the dependent of frequency and concentration. Herein, future work will focus on investigating the MXene in various polymer matrices for radio frequency response via experimental testing approach.

Carbon dioxide capture

Carbon dioxide capture is the important direction for the employment of carbon sources and mitigation of the GHG effect to attain value-added products or fuels. More concentration should be focused on the development of new materials with high CO_2 adsorption capacity and conversion rate. The MXene is regarded as a potential material for CO_2 capture because of its high efficiency.[237] It is found that the abatement capacity of CO_2 is in the range from 2.34 to 8.25 mol/kg, which is quite competitive to other nowadays-existent material solutions.[238] This is ascribed to the structure of MXene which possess high surface area, high adsorption energy capacity, charge transfer ability between the MXene and CO_2 and more multiple adsorption spaces. The merits could enhance CO_2 capture capacity and reduce energy consumption of CO_2 desorption. In addition, it is revealed that the surface of the MXene results in exothermic activation of CO_2 molecule when the pressure of CO_2 is low, which contributes to selecting the appropriate thickness of MXene.[239] This implies that adjusting the surface structure of MXene would be a beneficial approach for the enhancement of CO_2 capture capacity. Shamsabadi et al.[240] found that the composite MXene@ polyurethane material exhibits a comparable efficiency of CO_2 separation. This implies that the method would supply a favorable route for the enhancement of CO_2 capture and separation via composite MXene derivative materials. Based on above-mentioned methods, in terms of the structure of MXene as the solid absorbent, the size, ratio and distribution of pores in MXene should be investigated in the future, and those involve other MXene-based derived types of solid absorbent.

Remediation of environmental pollution

It is of utmost importance to perform the remediation of environmental pollution by using the MXene materials,[241] such as thorium removal,[242] uranium removal[243] and radionuclide removal[244] as well as effective management. Specifically, thorium is a type of toxic element to the environment because of its radioactive properties although it sustains at a trace level as well as results in irreversible risk to human being body. Furthermore, heavy metal ions are the most vital pollutants in soil and water which are attributed to high toxicity to human beings and other living organisms. In parallel, the compatible nature of the MXene toward the environment renders the distinctive features, such as the outstanding chemical compatibility, high thermal stability, high cost-effective merit for production and widespread resistance to withstand intensified radiations. The future potential applications of MXenes are illustrated in Table 4.

Recycled of MXene composite materials

The MXene composite materials, known for their excellent quality, durability, low weight, high thermal and electrical conductivity and high strength, are broadly being utilized in renewable energy and industries, transport, construction, aerospace and automotive. However, recycling and disposal of the MXene composite materials are currently huge challenges that are being progressively addressed, as they should with any extensively employed material. Formerly, there are very restricted recycling processes for the MXene composite materials because of economic and technological limitations, but research and development (R&D) activities are on the rise. It is necessary to properly dispose the recycling and waste disposal

Table 4. Future potential applications

Reference	Materials	Application fields		Key findings
Hu et al.,[233]	Ti_2C	Hydrogen storage		• Binding energy is 0.272 eV. • The hydrogen storage capacity could achieve the maximum value of 8.6 wt %. • The temperature scope could be controlled in the range from 300 K to 400 K.
Han et al.,[235]	MXene	Radio frequency communication		• MXene antennas has a high power radiation at frequency from 5.6 to 16.4 GHz. • The radiation efficiency of MXene antennas with 5.5 μm thickness could reach 99%.
Habib et al.,[236]	MXene@ polymer	Radio frequency communication		• The heat of radio frequency could be produced quickly for intermediate loading ranging from 10 to 1000 S/m.
Chen et al.,[237]	MXene	CO_2 capture		• The capture capacity of CO_2 based on MXene could realize 44.2 m mol/g.
	V_2CT_x@ polymer	CO_2 sensing		• MXene-based CO_2 sensor has high sensitivity characteristic because of high tenability and thermal conductivity.
	MXene@ Pt	CO_2 conversion		• Pt nanoparticles integrated with MXene displays merely 18% conversion rate.
	M_2XO_2			• The best electro-catalysts of M_2XO_2 for CO_2 could reach 0.52 V.
	MXene@ ZnO-Fe			• The CO2 conversion efficiency by using MXene@ ZnO-Fe reaches about 88%.
	MXene@ C_3N_4			• The maximum CO_2conversion rate could reach 5.19 μmol/g·h.
Morales-Garcia et al.,[238,239]	M_2C	CO_2 elimination and capture		• The amount of CO_2 could be eliminated in the range from 2.34 to 8.25 mol/kg. • The adsorption energy of MXene for $CO_2$is about −3.69 eV. • The effect of MXene thickness on absorption energy of CO_2 is less.
Kumar et al.,[241]	MXene	Toxic pollutants removal	Heavy metal removal	• The Chromium removal efficiency is controlled from 62 to 225 mg/g. • The Uranium (VI) removal efficiency is controlled from 140 to 470 mg/g. • The Lead removal efficiency is in the range from 140 to 2560 mg/g.
	MXene		Uranium removal	• The efficacy of uranium removal is 480 mg/g when the pH is setup to be 3.
	MXene		Dyes removal	• The removal efficiency of methylene blue ranges from 77 to 189 mg/g.
Li et al.,[242]	MXene@ hydrated		Thorium removal	• The maximum removal efficiency of Thorium can realize 213.2 mg/g.
He et al.,[244]	MXene@ Ca^{2+}		Uranium and Phosphate removal	• The maximum removal efficiency of Uranium and Phosphate is 823.6 mg/g when the temperature reaches 298 K.

at the end of the useful life of MXene composite materials. A large number of technologies have been employed including thermal, mechanical and chemical recycling; however, they are on the brink of being fully commercialized. Herein, wide-ranging investigation and development are being implemented to attain better recycling technologies for the MXene composite materials. This is conducive to achieving the sustainable development of the MXene composites materials in the aspect of engineering applications. Consequently, continual research is required to determine definitive solutions to effectively recycle the MXene composites materials to extend the service life in the future.

Energy efficiency of energy storage or degradation mechanisms

Although the MXene composite materials exhibits some merits on chemical and physical characteristics, the MXene composite materials start to degrade causing a series of complicated reactions, such as chain scission, oxidation and rupture of backbones. These could cause the reduction of thermal energy efficiency and flame retardant efficiency because of thermal degradation and insufficient heat supply. Therefore, adequate heat supply contributes to maintaining thermal degradation of the MXene composite materials and obtaining amount of fuel to feed the flame. In addition, the oxidizability of the MXenes would result in phase transition and microstructure alterations, especially those of temperature and light could exacerbate this degradation procedure owing to the shielding influence of the dense structure on the exterior moisture. This oxidation action is also an effective solution of fabricating MXene composites without the requirement to add any foreign objects. In particular, when the pressure environment and high temperature derived from hydrothermal procedure, boost not only MXene phase transition, but also rich and change structural evolution. Hence, it is predictable that the wide variety of MXene composite materials available in various environments could provide crucial possibilities for future development.

Conclusions

In this article, the state-of-the-art perspectives on the MXene derivative nanomaterials are retrospected in light of the composite types, synthetic methods, thermal energy utilization and 3D-printed techniques. Various MXene derivative nanomaterials (like MXene@ PCM, MXene@ polymer, MXene@ oil, MXene@ ionic liquid, MXene@ graphene oxide and MXene@ water) are synthesized by different solutions including the direct vacuum impregnation method, freeze-drying method, multi-layered casting method, two-step technique method and Toluene diluted method. These are conducive to obtaining high stability MXene liquid and avoiding the surface oxidized and degraded in base solution. Meanwhile, the photo-to-thermal and electrical-to-thermal energy conversions, and thermal energy storage characters of the MXene-based derivative materials are illustrated as well. In addition, the advanced 3D printed technique with the unique rheological properties achieved by the 2D MXene inks is explored to control structural modeling and incorporate other functional and structural materials. Accordingly, some critical outcomes are exemplified as follows:

- For averting the oxidation reaction of the MXene, it is huge challenging, particularly when they are moved from laboratory to industry for producing commercial products. Presently, there are different solutions, such as synthesis of minimal defective layered MXene, polymeric composites of MXens, organic media or organic dispersions of MXene and storage conditions for aqueous dispersion, which are utilized to improve the oxidation stabilities and mechanical strengths of the MXenes. The raw material plays the vital effects on the stabilities and conductive properties of the MXenes. Moreover, the oxidation kinetics of the MXenes aqueous dispersion relies on the temperature variation, concentration of colloidal dispersions, PH, and storage environment conditions. Consequently, investigation on the mechanisms and oxidation kinetics of the MXene could boost the MXene oxidation stability.
- The addition of different materials like PCM, polymer, oil, ionic liquid, graphene oxide and water into the MXene contributes to obtaining outstanding thermal and electrical conductivities, high specific surface area, chemical tenability, high optical and mechanical properties. Meanwhile, the solar energy conversion efficiency can be dramatically improved when the proper amount of MXene is added into the system, this can be widely applied to thermal management and storage systems. The synthesis methods of the composite MXene nanomaterials, involving the direct vacuum impregnation method, freeze-drying method, two-step technique and toluene dilution

method, play the vital roles in stable chemistry structure, high thermal physical properties and energy conversion efficiency.

- The MXene composite derivative materials could achieve efficient photo-to-thermal and electro-to-thermal energy conversions and thermal energy storage, their photo-to-thermal and electro-to-thermal energy conversion efficiencies could reach 80–90%, meantime, the capacity of thermal energy storage can be improved approximately 20–40% compared to the conventional types. Furthermore, the synthesis approaches not only form novel solutions for the assembly of 2D MXene nanosheets into 3D MXene aerogels achieving highly light-absorbing and electrically conductive, but also provide innovative insights into designing high-efficient solar steam generators and personal thermal regulation units. It is indicated that the 3D MXene not only sustains the advantages of the air permeability, flexibility and lightweight, but also presents high electro-to-thermal conversion efficiency and effective human body thermal regulation.
- Although the MXene composite materials exhibit some merits on chemical and physical characteristics, the MXene composite materials degrade causing a series of complicated reactions, such as chain scission, oxidation and rupture of backbones. These could cause the reductions of thermal energy efficiency and flame retardant efficiency because of thermal degradation and insufficient heat supply. Therefore, adequate heat supply contributes to maintaining the thermal degradation of the MXene composite materials and obtaining amount of fuel to feed the flame. In addition, the oxidizability of the MXenes would result in phase transition and microstructure alterations, especially those of temperature and light could exacerbate this degradation procedure owing to the shielding influence of the dense structure on the exterior moisture. This oxidation action is also an effective solution of fabricating MXene composites without the requirement to add any foreign objects. In particular, when the pressure environment and high temperature derived from hydrothermal procedure, boost not only the MXene phase transition, but also rich and change structural evolution. Hence, it is predictable that the wide variety of the MXene composite materials available in various environments could provide crucial possibilities for future development.
- The flame-retardant efficiency of the MXene composite material is closely associated with the dispersion of nanosheets in the matrix. Moreover, surface amendment of composite material is an encouraging solution to attain a well-dispersed material with boosted flame retardancy. It has been demonstrated that the MXene has an excellent flame-retardant additive for different types of polymer materials. In the meantime, higher efficiency and more cost-effectively utilization could be achieved via simplicity blending with other categories of flame retardants. Typically, a synergistic influence would always appear between various flame retardants, contributing to producing a much higher flame retardancy in comparison to the sum of the single element influence.
- 3D printing technology, as a layer-by-layer additive manufacturing, is of considerable interest because of its speedy prototyping, material selections, complicated designing, as well as minimized waste for sustainability. Meanwhile, traditional ink-based 3D printing techniques, like fused deposition modeling, binder jetting, and DIW of soft materials, are the key methods within the scope of the laboratory scale fabrication, which contribute to printing a wide range of materials. However, the printable materials have the limit for useful traditional ink-based 3D printing method. Herein, high shear-thinning and viscosity MXene-based inks with tailored rheological behaviors are the prerequisites to build complex 3D architectures, and the shear-thinning behavior could guarantee the MXene-based ink to move over the nozzle underneath an applied stress.
- The MXene exhibits a great future in different fields because of its advantages such as high-performance solid-state 2D materials, light weight, high density and calorific value, high surface area, high adsorption energy capacity, charge transfer ability between MXene and CO_2 and more multiple adsorption spaces. These contribute to opening novel research areas for achieving high performance energy conversion and energy storage, and excellent environmental protection, such as hydrogen energy storage, radio frequency fields applications, CO_2 capture and remediation of environmental pollution by using the MXene-based materials.

ACKNOWLEDGMENTS

This work was financially supported by the 'Taishan' Scholar Program of Shandong Province, China (tsqn 2022) and Talent Scientific Research Foundation of Shandong Jianzhu University (X22058Z).

AUTHOR CONTRIBUTIONS

Y.C. and R.Z. designed, conceived, and drafted the work. J.Z. and T.H. performed the whole-genome sequencing and sequence assembly. Y.C. analyzed the data and interpreted the results. All authors modified the manuscript and approved the final version.

DECLARATION OF INTERESTS

The authors declare no competing interests.

REFERENCES

1. Schneider, C.R., Zaval, L., and Markowitz, E.M. (2021). Positive emotions and climate change. Current Opinion in Behavioral Sciences *42*, 114–120.
2. Yuan, J., Ma, J., Sun, Y., Zhou, T., Zhao, Y., and Yu, F. (2020). Microbial degradation and other environmental aspects of microplastics/plastics. Sci. Total Environ. *715*, 136968.
3. Kozarcanin, S., Liu, H., and Andresen, G.B. (2019). 21st century climate change impacts on key properties of a large-scale renewable-based electricity system. Joule *3*, 992–1005.
4. Abdolhosseinzadeh, S., Sadighikia, S., and Alkan Gürsel, S. (2018). Scalable synthesis of sub-nanosized platinum-reduced graphene oxide composite by an ultraprecise photocatalytic method. ACS Sustainable Chem. Eng. *6*, 3773–3782.
5. Zhao, L., Tian, H., Silver, S.H., Kahn, A., Ren, T.L., and Rand, B.P. (2018). Ultrasensitive heterojunctions of graphene and 2D perovskites reveal spontaneous iodide loss. Joule *2*, 2133–2144.
6. Kelly, A.G., Hallam, T., Backes, C., Harvey, A., Esmaeily, A.S., Godwin, I., Coelho, J., Nicolosi, V., Lauth, J., Kulkarni, A., et al. (2017). All-printed thin-film transistors from networks of liquid-exfoliated nanosheets. Science *356*, 69–73.
7. Zhang, H. (2015). Ultrathin two-dimensional nanomaterials. ACS Nano *9*, 9451–9469.
8. Kara, A., Enriquez, H., Seitsonen, A.P., Lew Yan Voon, L., Vizzini, S., Aufray, B., and Oughaddou, H. (2012). A review on silicene — new candidate for electronics. Surf. Sci. Rep. *67*, 1–18.
9. Kharadi, M.A., Malik, G.F.A., Khanday, F.A., Shah, K.A., Mittal, S., and Kaushik, B.K. (2020). Review—silicene: from material to device applications. ECS J. Solid State Sci. Technol. *9*, 115031.
10. Xiao, X., Wang, H., Urbankowski, P., and Gogotsi, Y. (2018). Topochemical synthesis of 2D materials. Chem. Soc. Rev. *47*, 8744–8765.
11. Ang, W.L., Sturala, J., Antonatos, N., Sofer, Z., and Bonanni, A. (2021). Effect of surface chemistry on bio-conjugation and bio-recognition abilities of 2D germanene materials. Nanoscale *13*, 1893–1903.
12. Zhang, S., Yao, F., Yang, L., Zhang, F., and Xu, S. (2015). Sulfur-doped mesoporous carbon from surfactant-intercalated layered double hydroxide precursor as high-performance anode nanomaterials for both Li-ion and Naion batteries. Carbon *93*, 143–150.
13. Shi, L., and Zhao, T. (2017). Recent advances in inorganic 2D materials and their applications in lithium and sodium batteries. J. Mater. Chem. *5*, 3735–3758.
14. Duan, X., Xu, J., Wei, Z., Ma, J., Guo, S., Liu, H., and Dou, S. (2017). Atomically thin transition-metal dichalcogenides for electrocatalysis and energy storage. Small Methods *1*, 1700156.
15. Chhowalla, M., Liu, Z., and Zhang, H. (2015). Two-dimensional transition metal dichalcogenide (TMD) nanosheets. Chem. Soc. Rev. *44*, 2584–2586.
16. Tan, X., Wu, Y., Lin, X., Zeb, A., Xu, X., Luo, Y., and Liu, J. (2020). Application of MOF-derived transition metal oxides and composites as anodes for lithium-ion batteries. Inorg. Chem. Front. *7*, 4939–4955.
17. Liu, Q., Hu, Z., Li, W., Zou, C., Jin, H., Wang, S., Chou, S., and Dou, S.X. (2021). Sodium transition metal oxides: the preferred cathode choice for future sodium-ion batteries. Energy Environ. Sci. *14*, 158–179.
18. Abdolhosseinzadeh, S., Jiang, X., Zhang, H., Qiu, J., and Zhang, C.J. (2021). Perspectives on solution processing of two-dimensional MXenes. Mater. Today *48*, 214–240.
19. Gogotsi, Y., and Anasori, B. (2019). The rise of MXenes. ACS Nano *13*, 8491–8494.
20. Yu, L., Liu, B., Wang, Y., Yu, F., and Ma, J. (2021). Recent progress on MXene-derived material and its' application in energy and environment. J. Power Sources *490*, 229250.
21. Alhabeb, M., Maleski, K., Anasori, B., Lelyukh, P., Clark, L., Sin, S., and Gogotsi, Y. (2017). Guidelines for synthesis and processing of two-dimensional titanium carbide ($Ti_3C_2T_x$ MXene). Chem. Mater. *29*, 7633–7644.
22. Naguib, M., Kurtoglu, M., Presser, V., Lu, J., Niu, J., Heon, M., Hultman, L., Gogotsi, Y., and Barsoum, M.W. (2011). Two-dimensional nanocrystals produced by exfoliation of Ti_3AlC_2. Adv. Mater. *23*, 4248–4253.
23. Naguib, M., Come, J., Dyatkin, B., Presser, V., Taberna, P.L., Simon, P., Barsoum, M.W., and Gogotsi, Y. (2012). MXene: a promising transition metal carbide anode for lithium-ion batteries. Electrochem.Commun. *16*, 61–64.
24. Naguib, M., Mashtalir, O., Carle, J., Presser, V., Lu, J., Hultman, L., Gogotsi, Y., and Barsoum, M.W. (2012). Two-dimensional transition metal carbide. ACS Nano *6*, 1322–1331.
25. Naguib, M., Mochalin, V.N., Barsoum, M.W., and Gogotsi, Y. (2014). Two-dimensional materials: 25th Anniversary Article: MXenes: a new family of two-dimensional materials. Adv. Mater. *26*, 982.
26. Mashtalir, O., Naguib, M., Mochalin, V.N., Dall'Agnese, Y., Heon, M., Barsoum, M.W., and Gogotsi, Y. (2013). Intercalation and delamination of layered carbides and carbonitrides. Nat. Commun. *4*, 1716–1717.
27. Halim, J., Lukatskaya, M.R., Cook, K.M., Lu, J., Smith, C.R., Näslund, L.Å., May, S.J., Hultman, L., Gogotsi, Y., Eklund, P., and Barsoum, M.W. (2014). Transparent conductive two-dimensional titanium carbide epitaxial thin films. Chem. Mater. *26*, 2374–2381.
28. Ghidiu, M., Lukatskaya, M.R., Zhao, M.Q., Gogotsi, Y., and Barsoum, M.W. (2014). Conductive two-dimensional titanium carbide "clay" with high volumetric capacitance. Nature *516*, 78–81.
29. Mashtalir, O., Lukatskaya, M.R., Zhao, M.Q., Barsoum, M.W., and Gogotsi, Y. (2015). Amine-assisted delamination of Nb_2C MXene for Li ion energy storage devices. Adv. Mater. *27*, 3501–3506.
30. Naguib, M., Unocic, R.R., Armstrong, B.L., and Nanda, J. (2015). Large-scale delamination of multi-layers transition metal carbides and carbonitrides "MXenes". Dalton Trans. *44*, 9353–9358.

31. Anasori, B., Xie, Y., Beidaghi, M., Lu, J., Hosler, B.C., Hultman, L., Barsoum, M.W., Kent, P.R.C., Gogotsi, Y., and Barsoum, M.W. (2015). Two-dimensional, ordered, double transition metals carbides (MXenes). ACS Nano *9*, 9507–9516.

32. Dillon, A.D., Ghidiu, M.J., Krick, A.L., Griggs, J., May, S.J., Gogotsi, Y., Barsoum, M.W., and Fafarman, A.T. (2016). Highly conductive optical quality solution-processed films of 2D titanium carbide. Adv. Funct. Mater. *26*, 4162–4168.

33. Hantanasirisakul, K., Zhao, M., Urbankowski, P., Halim, J., Anasori, B., Kota, S., Ren, C.E., Barsoum, M.W., and Gogotsi, Y. (2016). Fabrication of $Ti_3C_2T_x$ MXene transparent thin films with tunable optoelectronic properties. Adv. Electron. Mater. *2*, 1600050.

34. Urbankowski, P., Anasori, B., Makaryan, T., Er, D., Kota, S., Walsh, P.L., Zhao, M., Shenoy, V.B., Barsoum, M.W., and Gogotsi, Y. (2016). Synthesis of two-dimensional titanium nitride Ti_4N_3 (MXene). Nanoscale *8*, 11385–11391.

35. Tao, Q., Dahlqvist, M., Lu, J., Kota, S., Meshkian, R., Halim, J., Palisaitis, J., Hultman, L., Barsoum, M.W., Persson, P.O.Å., and Rosen, J. (2017). Two-dimensional $Mo_{1.33}C$ MXene with divacancy ordering prepared from parent 3D laminate with in-plane chemical ordering. Nat. Commun. *8*, 14949–14957.

36. Zhang, C.J., Pinilla, S., McEvoy, N., Cullen, C.P., Anasori, B., Long, E., Park, S.H., Seral-Ascaso, A., Shmeliov, A., Krishnan, D., et al. (2017). Oxidation stability of colloidal two-dimensional titanium carbides (MXenes). Chem. Mater. *29*, 4848–4856.

37. Li, T., Yao, L., Liu, Q., Gu, J., Luo, R., Li, J., Yan, X., Wang, W., Liu, P., Chen, B., et al. (2018). Fluorine-free synthesis of high-purity $Ti_3C_2T_x$ (T=OH, O) via Alkali treatment. Angew. Chem. Int. Ed. Engl. *57*, 6115–6119.

38. Alhabeb, M., Maleski, K., Mathis, T.S., Sarycheva, A., Hatter, C.B., Uzun, S., Levitt, A., and Gogotsi, Y. (2018). Selective etching of silicon from Ti_3SiC_2 (MAX) to obtain 2D titanium carbide (MXene). Angew. Chem. Int. Ed. Engl. *57*, 5444–5448.

39. Gund, G.S., Park, J.H., Harpalsinh, R., Kota, M., Shin, J.H., Kim, T.i., Gogotsi, Y., and Park, H.S. (2019). MXene/polymer hybrid materials for flexible AC-filtering electrochemical capacitors. Joule *3*, 164–176.

40. Li, J., Levitt, A., Kurra, N., Juan, K., Noriega, N., Xiao, X., Wang, X., Wang, H., Alshareef, H.N., and Gogotsi, Y. (2019). MXene-conducting polymer electrochromic microsupercapacitors. Energy Storage Mater. *20*, 455–461.

41. Shang, T., Lin, Z., Qi, C., Liu, X., Li, P., Tao, Y., Wu, Z., Li, D., Simon, P., and Yang, Q. (2019). 3D macroscopic architectures from self-assembled MXene hydrogels. Adv. Funct. Mater. *29*, 1903960.

42. Natu, V., Pai, R., Sokol, M., Carey, M., Kalra, V., and Barsoum, M.W. (2020). 2D $Ti_3C_2T_z$ MXene synthesized by water-free etching of Ti_3AlC_2 in polar organic solvents. Chem *6*, 616–630.

43. Miao, J., Zhu, Q., Li, K., Zhang, P., Zhao, Q., and Xu, B. (2021). Self-propagating fabrication of 3D porous MXene-rGO film electrode for high-performance supercapacitors. J. Energy Chem. *52*, 243–250.

44. Quyen, V.T., Ha, L.T.T., Thanh, D.M., Le, Q.V., Viet, N.M., Nham, N.T., and Thang, P.Q. (2021). Advanced synthesis of MXene-derived nanoflower-shaped TiO_2@Ti_3C_2 heterojunction to enhance photocatalytic degradation of Rhodamine B. Environ. Technol. Innovat. *21*, 101286.

45. Huang, J.J., Liu, X.Q., Meng, F.F., He, L.Q., Wang, J.X., Wu, J.C., Lu, X.H., Tong, Y.X., and Fang, P.P. (2020). A facile method to produce $MoSe_2$/MXene hybrid nanoflowers with enhanced electrocatalytic activity for hydrogen evolution. J. Electroanal. Chem. *856*, 113727.

46. Li, Y., Deng, X., Tian, J., Liang, Z., and Cui, H. (2018). Ti_3C_2 MXene-derived Ti_3C_2/TiO_2 nanoflowers for noble-metal-free photocatalytic overall water splitting. Appl. Mater. Today *13*, 217–227.

47. Dong, Y., Wu, Z.S., Zheng, S., Wang, X., Qin, J., Wang, S., Shi, X., and Bao, X. (2017). Ti_3C_2 MXene-derived sodium/potassium titanate nanoribbons for high-performance sodium/potassium ion batteries with enhanced capacities. ACS Nano *11*, 4792–4800.

48. Lian, P., Dong, Y., Wu, Z.S., Zheng, S., Wang, X., Wang, S., Sun, C., Qin, J., Shi, X., and Bao, X. (2017). Alkalized Ti_3C_2 MXene nanoribbons with expanded interlayer spacing for high-capacity sodium and potassium ion batteries. Nano Energy *40*, 1–8.

49. Xu, G., Niu, Y., Yang, X., Jin, Z., Wang, Y., Xu, Y., and Niu, H. (2018). Preparation of $Ti_3C_2T_x$ MXene-derived quantum dots with white/blue-emitting photoluminescence and electrochemiluminescence. Adv. Opt. Mater. *6*, 1800951.

50. Mao, H., Gu, C., Yan, S., Xin, Q., Cheng, S., Tan, P., Wang, X., Xiu, F., Liu, X., Liu, J., et al. (2020). MXene Quantum dot/polymer hybrid structures with tunable electrical conductance and resistive switching for nonvolatile memory devices. Adv. Electron. Mater. *6*, 1900493.

51. Lim, G.P., Soon, C.F., Morsin, M., Ahmad, M.K., Nayan, N., and Tee, K.S. (2020). Synthesis, characterization and antifungal property of $Ti_3C_2T_x$ MXene nanosheets. Ceram.Int. *46*, 20306–20312.

52. Ding, L., Wei, Y., Wang, Y., Chen, H., Caro, J., and Wang, H. (2017). A two-dimensional lamellar membrane: MXene nanosheet stacks. Angew. Chem. Int. Ed. Engl. *56*, 1825–1829.

53. Zhao, Q., Zhu, Q., Miao, J., Zhang, P., Wan, P., He, L., and Xu, B. (2019). Flexible 3D porous MXene foam for high-performance lithium-ion batteries. Small *15*, 1904293.

54. Bu, F., Zagho, M.M., Ibrahim, Y., Ma, B., Elzatahry, A., and Zhao, D. (2020). Porous MXenes: synthesis, structures, and applications. Nano Today *30*, 100803.

55. Yue, Y., Liu, N., Liu, W., Li, M., Ma, Y., Luo, C., Wang, S., Rao, J., Hu, X., Su, J., et al. (2018). 3D hybrid porous MXene-sponge network and its application in piezoresistive sensor. Nano Energy *50*, 79–87.

56. Shui, W., Li, J., Wang, H., Xing, Y., Li, Y., Yang, Q., Xiao, X., Wen, Q., and Zhang, H. (2020). $Ti_3C_2T_x$ MXene sponge composite as broadband terahertz absorber. Adv. Optical Mater. *8*, 2001120.

57. Zhang, X., Shao, B., Guo, A., Sun, Z., Zhao, J., Cui, F., and Yang, X. (2021). MnO_2 nanoshells/$Ti_3C_2T_x$ MXene hybrid film as supercapacitor electrode. Appl. Surf. Sci. *560*, 150040.

58. Zhang, Z., Weng, L., Rao, Q., Yang, S., Hu, J., Cai, J., and Min, Y. (2019). Highly-dispersed iron oxide nanoparticles anchored on crumpled nitrogen-doped MXene nanosheets as anode for Li-ion batteries with enhanced cyclic and rate performance. J. Power Sources *439*, 227107.

59. Seredych, M., Shuck, C.E., Pinto, D., Alhabeb, M., Precetti, E., Deysher, G., Anasori, B., Kurra, N., and Gogotsi, Y. (2019). High-temperature behavior and surface chemistry of carbide MXenes studied by thermal analysis. Chem. Mater. *31*, 3324–3332.

60. Hart, J.L., Hantanasirisakul, K., Lang, A.C., Anasori, B., Pinto, D., Pivak, Y., van Omme, J.T., May, S.J., Gogotsi, Y., and Taheri, M.L. (2019). Control of MXenes' electronic properties through termination and intercalation. Nat. Commun. *10*, 522.

61. Yun, T., Kim, H., Iqbal, A., Cho, Y.S., Lee, G.S., Kim, M.K., Kim, S.J., Kim, D., Gogotsi, Y., Kim, S.O., and Koo, C.M. (2020). Electromagnetic shielding of monolayer MXene assemblies. Adv. Mater. *32*.

62. Iqbal, A., Sambyal, P., and Koo, C.M. (2020). 2D MXenes for electromagnetic shielding: a review. Adv. Funct. Mater. *30*, 2070307.

63. Iqbal, A., Shahzad, F., Hantanasirisakul, K., Kim, M.K., Kwon, J., Hong, J., Kim, H., Kim, D., Gogotsi, Y., and Koo, C.M. (2020). Anomalous absorption of electromagnetic waves by 2D transition metal carbonitride Ti_3CNT_x (MXene). Science *369*, 446–450.

64. Choi, G., Shahzad, F., Bahk, Y.M., Jhon, Y.M., Park, H., Alhabeb, M., Anasori, B., Kim, D.S., Koo, C.M., Gogotsi, Y., and Seo, M. (2018). Enhanced terahertz shielding of MXenes with nano-metamaterials. Adv. Opt. Mater. *6* (5), 1701076.

65. Li, G., Amer, N., Hafez, H.A., Huang, S., Turchinovich, D., Mochalin, V.N., Hegmann, F.A., and Titova, L.V. (2020). Dynamical control over terahertz electromagnetic interference shielding with 2D $Ti_3C_2T_y$

MXene by ultrafast optical pulses. Nano Lett. *20*, 636–643.

66. Yang, Q., Huang, Z., Li, X., Liu, Z., Li, H., Liang, G., Wang, D., Huang, Q., Zhang, S., Chen, S., and Zhi, C. (2019). A wholly degradable, rechargeable Zn-Ti_3C_2 MXene capacitor with superior anti-self-discharge function. ACS Nano *13*, 8275–8283.

67. Zhang, C.J., Anasori, B., Seral-Ascaso, A., Park, S.H., McEvoy, N., Shmeliov, A., Duesberg, G.S., Coleman, J.N., Gogotsi, Y., and Nicolosi, V. (2017). Transparent, flexible, and conductive 2D titanium carbide (MXene) films with high volumetric capacitance. Adv. Mater. *29*, 1702678.

68. Kim, S.J., Koh, H.J., Ren, C.E., Kwon, O., Maleski, K., Cho, S.Y., Anasori, B., Kim, C.K., Choi, Y.K., Kim, J., et al. (2018). Metallic $Ti_3C_2T_x$ MXene gas sensors with ultrahigh signal-to-noise ratio. ACS Nano *12*, 986–993.

69. Park, T.H., Yu, S., Koo, M., Kim, H., Kim, E.H., Park, J.E., Ok, B., Kim, B., Noh, S.H., Park, C., et al. (2019). Shape-adaptable 2D titanium carbide (MXene) heater. ACS Nano *13*, 6835–6844.

70. Ahn, S., Han, T.H., Maleski, K., Song, J., Kim, Y.H., Park, M.H., Zhou, H., Yoo, S., Gogotsi, Y., and Lee, T.W. (2020). A 2D titanium carbide MXene flexible electrode for high-efficiency light-emitting diodes. Adv. Mater. *32*, 2000919.

71. Lee, S., Kim, E.H., Yu, S., Kim, H., Park, C., Park, T.H., Han, H., Lee, S.W., Baek, S., Jin, W., et al. (2020). Alternating-current MXene polymer light-emitting diodes. Adv. Funct. Mater. *30*, 2070212.

72. Rasool, K., Helal, M., Ali, A., Ren, C.E., Gogotsi, Y., and Mahmoud, K.A. (2016). Antibacterial activity of $Ti_3C_2T_x$ MXene. ACS Nano *10*, 3674–3684.

73. Zhang, F., Jia, Z., Wang, C., Feng, A., Wang, K., Hou, T., Liu, J., Zhang, Y., and Wu, G. (2020). Sandwich-like silicon/$Ti_3C_2T_x$ MXene composite by electrostatic self-assembly for high performance lithium ion battery. Energy *195*, 117047.

74. Yu, L., Fan, Z., Shao, Y., Tian, Z., Sun, J., and Liu, Z. (2019). Versatile N-doped MXene ink for printed electrochemical energy storage application. Adv. Energy Mater. *9*, 1901839.

75. Rosenkranz, A., Grützmacher, P.G., Espinoza, R., Fuenzalida, V.M., Blanco, E., Escalona, N., Gracia, F.J., Villarroel, R., Guo, L., Kang, R., et al. (2019). Multi-layer $Ti_3C_2T_x$ -nanoparticles (MXenes) as solid lubricants role of surface terminations and intercalated water. Appl. Surf. Sci. *494*, 13–21.

76. Qin, L., Tao, Q., Liu, X., Fahlman, M., Halim, J., Persson, P.O., Rosen, J., and Zhang, F. (2019). Polymer-MXene composite films formed by MXene-facilitated electrochemical polymerization for flexible solid-state microsupercapacitors. Nano Energy *60*, 734–742.

77. Wang, H., Wu, Y., Yuan, X., Zeng, G., Zhou, J., Wang, X., and Chew, J.W. (2018). Clay-inspired MXene-based electrochemical devices and photo-electrocatalyst: state-of-the-art progresses and challenges. Adv. Mater. *30*, 1704561.

78. Zha, X.J., Zhao, X., Pu, J.H., Tang, L.S., Ke, K., Bao, R.Y., Bai, L., Liu, Z.Y., Yang, M.B., and Yang, W. (2019). Flexible anti-biofouling MXene/cellulose fibrous membrane for sustainable solar-driven water purify cation. ACS Appl. Mater. Interfaces *11*, 36589–36597.

79. Bao, Z., Bing, N., Zhu, X., Xie, H., and Yu, W. (2021). $Ti_3C_2T_x$ MXene contained nanofluids with high thermal conductivity, super colloidal stability and low viscosity. Chem. Eng. J. *406*, 126390.

80. Lu, X., Huang, H., Zhang, X., Lin, P., Huang, J., Sheng, X., Zhang, L., and Qu, J.p. (2019). Novel light-driven and electro-driven polyethylene glycol/two-dimensional MXene form-stable phase change material with enhanced thermal conductivity and electrical conductivity for thermal energy storage. Compos. B Eng. *177*, 107372.

81. Aslfattahi, N., Saidur, R., Arifutzzaman, A., Sadri, R., Bimbo, N., Sabri, M.F.M., Maughan, P.A., Bouscarrat, L., Dawson, R.J., Said, S.M., et al. (2020). Experimental investigation of energy storage properties and thermal conductivity of a novel organic phase change material/MXene as a new class of nanocomposites. J. Energy Storage *27*, 101115.

82. Jin, X., Wang, J., Dai, L., Liu, X., Li, L., Yang, Y., Cao, Y., Wang, W., Wu, H., and Guo, S. (2020). Flame-retardant poly (vinyl alcohol)/MXene multilayered films with outstanding electromagnetic interference shielding and thermal conductive performances. Chem. Eng. J. *380*, 122475.

83. Lim, S., Park, H., Yang, J., Kwak, C., and Lee, J. (2019). Stable colloidal dispersion of octylated Ti_3C_2-MXenes in a nonpolar solvent. Colloids Surf. A Physicochem.Eng. Asp. *579*, 123648.

84. Cheng, Z., Chang, G., Xue, B., Xie, L., and Zheng, Q. (2023). Hierarchical Ni-plated melamine sponge and MXene film synergistically supported phase change materials towards integrated shape stability, thermal management and electromagnetic interference shielding. J. Mater. Sci. Technol. *132*, 132–143.

85. Aslfattahi, N., Samylingam, L., Abdelrazik, A.S., Arifutzzaman, A., and Saidur, R. (2020). MXene based new class of silicone oil nanofluids for the performance improvement of concentrated photovoltaic thermal collector. Sol. Energy Mater. Sol. Cell. *211*, 110526.

86. Luo, S., Patole, S., Anwer, S., Li, B., Delclos, T., Gogotsi, O., Zahorodna, V., Balitskyi, V., and Liao, K. (2020). Tensile behaviors of $Ti_3C_2T_x$ (MXene) films. Nanotechnology *31*, 395704.

87. Wan, S., Li, X., Wang, Y., Chen, Y., Xie, X., Yang, R., Tomsia, A.P., Jiang, L., and Cheng, Q. (2020). Strong sequentially bridged MXene sheets. Proc. Natl. Acad. Sci. USA *117*, 27154–27161.

88. Liang, B., Liao, X., Zhu, Q., Yu, M., Li, J., Geng, B., Liu, K., Jia, D., Yang, Z., and Zhou, Y. (2021). Spark plasma sintering and improved fracture toughness of silicoboron carbonitride ceramics with the integration of 2D MXene. Ceram.Int. *47*, 27730–27735.

89. Fei, M., Lin, R., Lu, Y., Zhang, X., Bian, R., Cheng, J., Luo, P., Xu, C., and Cai, D. (2017). MXene-reinforced alumina ceramic composites. Ceram.Int. *43*, 17206–17210.

90. Wozniak, J., Petrus, M., Cygan, T., Jastrzębska, A., Wojciechowski, T., Ziemkowska, W., and Olszyna, A. (2019). Silicon carbide matrix composites reinforced with two-dimensional titanium carbide—manufacturing and properties. Ceram.Int. *45*, 6624–6631.

91. Firestein, K.L., von Treifeldt, J.E., Kvashnin, D.G., Fernando, J.F.S., Zhang, C., Kvashnin, A.G., Podryabinkin, E.V., Shapeev, A.V., Siriwardena, D.P., Sorokin, P.B., and Golberg, D. (2020). Young's modulus and tensile strength of Ti3C2 MXene nanosheets as revealed by in situ TEM probing, AFM nanomechanical mapping, and theoretical calculations. Nano Lett. *20*, 5900–5908.

92. Yu, W., Li, X., Vallet, M., and Tian, L. (2019). High temperature damping behavior and dynamic Young's modulus of magnesium matrix composite reinforced by Ti_2AlC MAX phase particles. Mech. Mater. *129*, 246–253.

93. Monastyreckis, G., Mishnaevsky, L., Hatter, C., Aniskevich, A., Gogotsi, Y., and Zeleniakiene, D. (2020). Micromechanical modeling of MXene-polymer composites. Carbon *162*, 402–409.

94. Ye, Z., Ji, C., Yu, T., Sun, R., Zeng, X., and Cao, B. (2022). Enhanced interfacial heat-transfer of Al_2O_3-MXene-silicone composite via an electrostatic self-assembly strategy. Int. J. Heat Mass Tran. *199*, 123430.

95. Chen, X., Li, R., Li, B., Wang, J., Wang, T., Yan, F., and Zhang, G. (2021). Achieving ultra-high ductility and fracture toughness in molybdenum via Mo_2TiC_2 MXene addition. Materials Science and Engineering: A *818*, 141422.

96. Luo, S., Xiang, T., Dong, J., Su, F., Ji, Y., Liu, C., and Feng, Y. (2022). A double crosslinking MXene/cellulose nanofiber layered film for improving mechanical properties and stable electromagnetic interference shielding performance. J. Mater. Sci. Technol. *129*, 127–134.

97. Hatam-Lee, S.M., Esfandiar, A., and Rajabpour, A. (2021). Mechanical behaviors of titanium nitride and carbide MXenes: a molecular dynamics study. Appl. Surf. Sci. *566*, 150633.

98. Palisaitis, J., Persson, I., Halim, J., Rosen, J., and Persson, P.O.Å. (2018). On the structural stability of MXene and the role of transition metal adatoms. Nanoscale *10*, 10850–10855.

99. Kajiyama, S., Szabova, L., Iinuma, H., Sugahara, A., Gotoh, K., Sodeyama, K., Tateyama, Y., Okubo, M., and Yamada, A. (2017). Enhanced Li-ion accessibility in MXene titanium carbide by steric chloride termination. Adv. Energy Mater. *7*, 1601873.

100. Li, Z., Wang, L., Sun, D., Zhang, Y., Liu, B., Hu, Q., and Zhou, A. (2015). Synthesis and thermal stability of two-dimensional carbide MXene Ti_3C_2. Mater. Sci. Eng., B *191*, 33–40.

101. Wang, K., Zhou, Y., Xu, W., Huang, D., Wang, Z., and Hong, M. (2016). Fabrication and thermal stability of two-dimensional carbide Ti_3C_2 nanosheets. Ceram.Int. *42*, 8419–8424.

102. Li, J., Du, Y., Huo, C., Wang, S., and Cui, C. (2015). Thermal stability of two-dimensional Ti_2C nanosheets. Ceram.Int. *41*, 2631–2635.

103. Bhat, A., Anwer, S., Bhat, K.S., Mohideen, M.I.H., Liao, K., Qurashi, A., et al. (2021). Prospects challenges and stability of 2D MXenes for clean energy conversion and storage applications.npj 2D Mater. Appl *61*, 1–21.

104. Zhang, C.J., Ma, Y., Zhang, X., Abdolhosseinzadeh, S., Sheng, H., Lan, W., Pakdel, A., Heier, J., and Nüesch, F. (2020). Two-dimensional transition metal carbides and nitrides (MXenes): synthesis, properties, and electrochemical energy storage applications. Energy Environ. Mater. *3*, 29–55.

105. Iqbal, A., Hong, J., Ko, T.Y., and Koo, C.M. (2021). Improving oxidation stability of 2D MXenes: synthesis, storage media, and conditions. Nano Converg. *8*, 9–22.

106. Kim, D., Ko, T.Y., Kim, H., Lee, G.H., Cho, S., and Koo, C.M. (2019). Nonpolar Organic Dispersion of 2D $Ti_3C_2T_x$ MXene flakes via simultaneous interfacial chemical grafting and phase transfer method. ACS Nano *13*, 13818–13828.

107. Xia, F., Lao, J., Yu, R., Sang, X., Luo, J., Li, Y., and Wu, J. (2019). Ambient oxidation of Ti_3C_2 MXene initialized by atomic defects. Nanoscale *11*, 23330–23337.

108. Shuck, C.E., Han, M., Maleski, K., Hantanasirisakul, K., Kim, S.J., Choi, J., Reil, W.E.B., and Gogotsi, Y. (2019). Effect of Ti_3AlC_2 MAX phase on structure and properties of resultant $Ti_3C_2T_x$ MXene. ACS Appl. Nano Mater. *2*, 3368–3376.

109. Shekhirev, M., Shuck, C.E., Sarycheva, A., and Gogotsi, Y. (2021). Characterization of MXenes at every step, from their precursors to single flakes and assembled films. Prog.Mater.Sci. *120*, 100757.

110. Lee, G.S., Yun, T., Kim, H., Kim, I.H., Choi, J., Lee, S.H., Lee, H.J., Hwang, H.S., Kim, J.G., Kim, D.W., et al. (2020). Mussel inspired highly aligned $Ti_3C_2T_x$ MXene film with synergistic enhancement of mechanical strength and ambient stability. ACS Nano *14*, 11722–11732.

111. Huang, S., and Mochalin, V.N. (2019). Hydrolysis of 2D transition-metal carbides (MXenes) in colloidal solutions. Inorg. Chem. *58*, 1958–1966.

112. Zhao, X., Vashisth, A., Blivin, J.W., Tan, Z., Holta, D.E., Kotasthane, V., Shah, S.A., Habib, T., Liu, S., Lutkenhaus, J.L., et al. (2020). pH, nanosheet concentration, and antioxidant affect the oxidation of $Ti_3C_2T_x$ and Ti_2CT_x MXene dispersions. Adv. Mater. Interfaces *7*, 2000845.

113. Zhan, X., Si, C., Zhou, J., and Sun, Z. (2020). MXene and MXene-based composites: synthesis, properties and environment-related applications. Nanoscale Horiz. *5*, 235–258.

114. Gong, K., Zhou, K., Qian, X., Shi, C., and Yu, B. (2021). MXene as emerging nanofillers for high-performance polymer composites: a review. Compos. B Eng. *217*, 108867.

115. George, S.M., and Kandasubramanian, B. (2020). Advancements in MXene-Polymer composites for various biomedical applications. Ceram.Int. *46*, 8522–8535.

116. Faruk, M.O., Ahmed, A., Adak, B., Marzana, M., Hossain, M.M., and Mukhopadhyay, S. (2021). High performance 2D MXene based conducting polymer hybrids: synthesis to emerging applications. J. Mater. Chem. C *9*, 10193–10215.

117. Ma, C., Ma, M., Si, C., Ji, X., and Wan, P. (2021). Flexible MXene-based composites for wearable devices. Adv. Funct. Mater. *31*, 2009524.

118. Mahmud, S.T., Hasan, M.M., Bain, S., Rahman, S.T., Rhaman, M., Hossain, M.M., and Ordu, M. (2022). Multilayer MXene heterostructures and nanohybrids for multifunctional applications: a review. ACS Materials Lett. *4*, 1174–1206.

119. Liu, H., Fu, R., Su, X., Wu, B., Wang, H., Xu, Y., and Liu, X. (2021). MXene confined in shape-stabilized phase change material combining enhanced electromagnetic interference shielding and thermal management capability. Compos. Sci. Technol. *210*, 108835.

120. Wang, Y., Yang, J., Chen, Z., and Hu, Y. (2019). A new flexible and ultralight carbon foam/$Ti_3C_2T_X$ MXene hybrid for high-performance electromagnetic wave absorption. RSC Adv. *9*, 41038–41049.

121. Seok, S.H., Choo, S., Kwak, J., Ju, H., Han, J.H., Kang, W.S., Lee, J., Kim, S.Y., Lee, D.H., Lee, J., et al. (2021). Synthesis of high quality 2D carbide MXene flakes using a highly purified MAX precursor for ink applications. Nanoscale Adv. *3*, 517–527.

122. Abdelrazik, A.S., Al-Sulaiman, F.A., Saidur, R., and Ben-Mansour, R. (2019). Evaluation of the effects of optical filtration and nanoPCM on the performance of a hybrid photovoltaic-thermal solar collector. Energy Convers.Manag. *195*, 139–156.

123. Nižetić, S., Jurčević, M., Arıcı, M., Arasu, A.V., and Xie, G. (2020). Nano-enhanced phase change materials and fluids in energy applications: a review. Renew. Sustain. Energy Rev. *129*, 109931.

124. Nourafkan, E., Asachi, M., Jin, H., Wen, D., and Ahmed, W. (2019). Stability and photo-thermal conversion performance of binary nanofluids for solar absorption refrigeration systems. Renew. Energy *140*, 264–273.

125. Zhou, Y., Sheng, D., Liu, X., Lin, C., Yang, Y., Ji, F., Dong, L., Xu, S., and Yang, Y. (2018). Synthesis and properties of crosslinking halloysite nanotubes/polyurethane-based solid-solid phase change materials. Sol. Energy Mater. Sol. Cell. *174*, 84–93.

126. Fang, Y., Liu, S., Li, X., Hu, X., Wu, H., Lu, X., and Qu, J. (2022). Biomass porous potatoes/MXene encapsulated PEG-based PCMs with improved photo-to-thermal conversion capability. Sol. Energy Mater. Sol. Cell. *237*, 111559.

127. Lu, X., Huang, J., Wong, W.Y., and Qu, J.p. (2019). A novel bio-based polyurethane/wood powder composite as shape-stable phase change material with high relative enthalpy efficiency for solar thermal energy storage. Sol. Energy Mater. Sol. Cell. *200*, 109987.

128. Atinafu, D.G., Dong, W., Huang, X., Gao, H., Wang, J., Yang, M., and Wang, G. (2018). One-pot synthesis of light-driven polymeric composite phase change materials based on N-doped porous carbon for enhanced latent heat storage capacity and thermal conductivity. Sol. Energy Mater. Sol. Cell. *179*, 392–400.

129. Gök, Ö., Alkan, C., and Konuklu, Y. (2019). Developing a poly (ethylene glycol)/cellulose phase change reactive composite for cooling application. Sol. Energy Mater. Sol. Cell. *191*, 345–349.

130. Zhang, Y., Wang, J., Qiu, J., Jin, X., Umair, M.M., Lu, R., Zhang, S., and Tang, B. (2019). Ag-graphene/PEG composite phase change materials for enhancing solar-thermal energy conversion and storage capacity. Appl. Energy *237*, 83–90.

131. Zhang, H., Yuan, Y., Sun, Q., and Cao, X. (2017). Enhanced thermal energy storage performance of polyethylene glycol by using interfacial interaction of copper-based metal oxide. Adv. Eng. Mater. *19*, 1600601.

132. Yang, J., Yu, P., Tang, L.S., Bao, R.Y., Liu, Z.Y., Yang, M.B., and Yang, W. (2017). Hierarchically interconnected porous scaffolds for phase change materials with improved thermal conductivity and efficient solar-to-electric energy conversion. Nanoscale *9*, 17704–17709.

133. Lin, P., Xie, J., He, Y., Lu, X., Li, W., Fang, J., Yan, S., Zhang, L., Sheng, X., and Chen, Y. (2020). MXene aerogel-based phase change materials toward solar energy conversion. Sol. Energy Mater. Sol. Cell. *206*, 110229.

134. Fan, X., Liu, L., Jin, X., Wang, W., Zhang, S., and Tang, B. (2019). MXene $Ti_3C_2T_x$ for phase change composite with superior photothermal storage capability. J. Mater. Chem. *7*, 14319–14327.

135. Mo, Z., Mo, P., Yi, M., Hu, Z., Tan, G., Selim, M.S., Chen, Y., Chen, X., Hao, Z., and Wei, X. (2021). $Ti_3C_2T_x$@ Polyvinyl alcohol

foam-supported phase change materials with simultaneous enhanced thermal conductivity and solar-thermal conversion performance. Sol. Energy Mater. Sol. Cell. *219*, 110813.

136. Zhou, B., Li, Q., Xu, P., Feng, Y., Ma, J., Liu, C., and Shen, C. (2021). An asymmetric sandwich structural cellulose-based film with self-supported MXene and AgNW layers for flexible electromagnetic interference shielding and thermal management. Nanoscale *13*, 2378–2388.

137. Zhou, B., Zhang, Z., Li, Y., Han, G., Feng, Y., Wang, B., Zhang, D., Ma, J., and Liu, C. (2020). Flexible, robust, and multifunctional electromagnetic interference shielding film with alternating cellulose nanofiber and MXene layers. ACS Appl. Mater. Interfaces *12*, 4895–4905.

138. Xu, H., Yin, X., Li, X., Li, M., Liang, S., Zhang, L., and Cheng, L. (2019). Lightweight Ti_2CT_x MXene/poly (vinyl alcohol) composite foams for electromagnetic wave shielding with absorption-dominated feature. ACS Appl. Mater. Interfaces *11*, 10198–10207.

139. Liu, R., and Li, W. (2018). High-thermal-stability and high-thermal-conductivity $Ti_3C_2T_x$ MXene/poly (vinyl alcohol) (PVA) composites. ACS Omega *3*, 2609–2617.

140. Xie, F., Jia, F., Zhuo, L., Lu, Z., Si, L., Huang, J., Zhang, M., and Ma, Q. (2019). Ultrathin MXene/aramid nanofiber composite paper with excellent mechanical properties for efficient electromagnetic interference shielding. Nanoscale *11*, 23382–23391.

141. Lei, C., Zhang, Y., Liu, D., Wu, K., and Fu, Q. (2020). Metal-level robust, folding endurance, and highly temperature-stable MXene-based film with engineered aramid nanofiber for extreme-condition electromagnetic interference shielding applications. ACS Appl. Mater. Interfaces *12*, 26485–26495.

142. Ma, Z., Kang, S., Ma, J., Shao, L., Zhang, Y., Liu, C., Wei, A., Xiang, X., Wei, L., and Gu, J. (2020). Ultraflexible and mechanically strong double-layered aramid nanofiber–$Ti_3C_2T_x$ MXene/silver nanowire nanocomposite papers for high-performance electromagnetic interference shielding. ACS Nano *14*, 8368–8382.

143. Zhan, Z., Song, Q., Zhou, Z., and Lu, C. (2019). Ultrastrong and conductive MXene/cellulose nanofiber films enhanced by hierarchical nano-architecture and interfacial interaction for flexible electromagnetic interference shielding. J. Mater. Chem. C *7*, 9820–9829.

144. Cao, W.T., Chen, F.F., Zhu, Y.J., Zhang, Y.G., Jiang, Y.Y., Ma, M.G., and Chen, F. (2018). Binary strengthening and toughening of MXene/cellulose nanofiber composite paper with nacre-inspired structure and superior electromagnetic interference shielding properties. ACS Nano *12*, 4583–4593.

145. Chen, J., Huang, X., Sun, B., Wang, Y., Zhu, Y., and Jiang, P. (2017). Vertically aligned and interconnected boron nitride nanosheets for advanced flexible nanocomposite thermal interface materials. ACS Appl. Mater. Interfaces *9*, 30909–30917.

146. Lin, Z.H., Yang, Y., Wu, J.M., Liu, Y., Zhang, F., and Wang, Z.L. (2012). $BaTiO_3$ nanotubes-based flexible and transparent nanogenerators. J. Phys. Chem. Lett. *3*, 3599–3604.

147. Wang, D., Lin, Y., Hu, D., Jiang, P., and Huang, X. (2020). Multifunctional 3D-MXene/PDMS nanocomposites for electrical, thermal and triboelectric applications. Compos. Appl. Sci. Manuf. *130*, 105754.

148. Yang, Y., Cao, Z., He, P., Shi, L., Ding, G., Wang, R., and Sun, J. (2019). $Ti_3C_2T_x$ MXene-graphene composite films for wearable strain sensors featured with high sensitivity and large range of linear response. Nano Energy *66*, 104134.

149. Liu, Y., Li, E., Yan, Y., Lin, Z., Chen, Q., Wang, X., Shan, L., Chen, H., and Guo, T. (2021). A one-structure-layer PDMS/MXenes based stretchable triboelectric nanogenerator for simultaneously harvesting mechanical and light energy. Nano Energy *86*, 106118.

150. Li, Y., Zhou, B., Shen, Y., He, C., Wang, B., Liu, C., Feng, Y., and Shen, C. (2021). Scalable manufacturing of flexible, durable $Ti_3C_2T_x$ MXene/Polyvinylidene fluoride film for multifunctional electromagnetic interference shielding and electro/photo-thermal conversion applications. Compos. B Eng. *217*, 108902.

151. Luo, J.Q., Zhao, S., Zhang, H.B., Deng, Z., Li, L., and Yu, Z.Z. (2019). Flexible, stretchable and electrically conductive MXene/natural rubber nanocomposite films for efficient electromagnetic interference shielding. Compos. Sci. Technol. *182*, 107754.

152. Xu, H., Zheng, D., Liu, F., Li, W., and Lin, J. (2020). Synthesis of an MXene/polyaniline composite with excellent electrochemical properties. J. Mater. Chem. *8*, 5853–5858.

153. VahidMohammadi, A., Moncada, J., Chen, H., Kayali, E., Orangi, J., Carrero, C.A., and Beidaghi, M. (2018). Thick and freestanding MXene/PANI pseudocapacitive electrodes with ultrahigh specific capacitance. J. Mater. Chem. *6*, 22123–22133.

154. Zhang, C., Xu, S., Cai, D., Cao, J., Wang, L., and Han, W. (2020). Planar supercapacitor with high areal capacitance based on Ti_3C_2 /polypyrrole composite film. Electrochim. Acta *330*, 135277.

155. Chen, W., Liu, P., Liu, Y., and Liu, Z. (2022). Recent advances in two-dimensional $Ti_3C_2T_x$ MXene for flame retardant polymer materials. Chem. Eng. J. *446*, 137239.

156. Wang, X., Kalali, E.N., Wan, J.T., and Wang, D.Y. (2017). Carbon-family materials for flame retardant polymeric materials. Prog.Polym.Sci. *69*, 22–46.

157. He, W., Song, P., Yu, B., Fang, Z., and Wang, H. (2020). Flame retardant polymeric nanocomposites through the combination of nanomaterials and conventional flame retardants. Prog.Mater.Sci. *114*, 100687.

158. Wang, N.N., Wang, H., Wang, Y.Y., Wei, Y.H., Si, J.Y., Yuen, A.C.Y., Xie, J.S., Yu, B., Zhu, S.E., Lu, H.D., et al. (2019). Robust, lightweight, hydrophobic, and fire-retarded polyimide/MXene aerogels for effective oil/water separation. ACS Appl. Mater. Interfaces *11*, 40512–40523.

159. Hai, Y., Jiang, S., Zhou, C., Sun, P., Huang, Y., and Niu, S. (2020). Fire-safe unsaturated polyester resin nanocomposites based on MAX and MXene: a comparative investigation of their properties and mechanism of fire retardancy. Dalton Trans. *49*, 5803–5814.

160. Li, L., Cao, Y., Liu, X., Wang, J., Yang, Y., and Wang, W. (2020). Multifunctional MXene-based fireproof electromagnetic shielding films with exceptional anisotropic heat dissipation capability and joule heating performance. ACS Appl. Mater. Interfaces *12*, 27350–27360.

161. Wei, S., Xie, Y., Xing, Y., Wang, L., Ye, H., Xiong, X., Wang, S., and Han, K. (2019). Two-dimensional graphene Oxide/MXene composite lamellar membranes for efficient solvent permeation and molecular separation. J. Membr. Sci. *582*, 414–422.

162. Yan, J., Ren, C.E., Maleski, K., Hatter, C.B., Anasori, B., Urbankowski, P., Sarycheva, A., and Gogotsi, Y. (2017). Flexible MXene/graphene films for ultrafast supercapacitors with outstanding volumetric capacitance. Adv. Funct. Mater. *27*, 1701264.

163. He, Y., Shen, Z., Yue, G., Gao, Y., Huo, J., Dong, C., Mao, Y., and Tan, F. (2022). A dye-sensitized solar cells with enhanced efficiency based on a "pillared effect" of $CoMoP_2$ @Mxene@ CNTs composite counter electrode. J. Alloys Compd. *922*, 166279.

164. Cai, Y.Z., Fang, Y.S., Cao, W.Q., He, P., and Cao, M.S. (2021). MXene-CNT/PANI ternary material with excellent super capacitive performance driven by synergy. J. Alloys Compd. *868*, 159159.

165. Wang, X., Luo, D., Wang, J., Sun, Z., Cui, G., Chen, Y., Wang, T., Zheng, L., Zhao, Y., Shui, L., et al. (2021). Strain engineering of a MXene/CNT hierarchical porous hollow microsphere electrocatalyst for a high-efficiency lithium polysulfide conversion process. Angew. Chem. Int. Ed. Engl. *60*, 2371–2378.

166. Hu, Z., Liu, Z., Huang, B., Gao, Y., Song, F., Younus, H.A., Wang, X., and Zhang, S. (2022). MXene supported transition metal nanoparticles accelerate sulfur reduction reaction kinetics. J. Mater. Chem. *10*, 13758–13768.

167. Wen, Q., and Yang, M. (2022). Platinum nanoparticles modified MXene for highly sensitive detection of pyruvate. Mater.Lett. *322*, 132496.

168. Hussein, A.M., Kadirgamma, K., Kadirgamma, K., Noor, M.M., and Aik, L.K. (2018). Palm oil based nanofluids for

enhancing heat transfer and rheological properties. Heat Mass Tran. *54*, 3163–3169.

169. Hoffmann, J.F., Vaitilingom, G., Henry, J.F., Chirtoc, M., Olives, R., Goetz, V., and Py, X. (2018). Temperature dependence of thermophysical and rheological properties of seven vegetable oils in view of their use as heat transfer fluids in concentrated solar plants. Sol. Energy Mater. Sol. Cell. *178*, 129–138.

170. Samylingam, L., Aslfattahi, N., Saidur, R., Yahya, S.M., Afzal, A., Arifutzzaman, A., Tan, K.H., and Kadirgama, K. (2020). Thermal and energy performance improvement of hybrid PV/T system by using olein palm oil with MXene as a new class of heat transfer fluid. Sol. Energy Mater. Sol. Cell. *218*, 110754.

171. Parashar, N., Aslfattahi, N., Yahya, S.M., and Saidur, R. (2021). An artifcial neural network approach for the prediction of dynamic viscosity of MXene-palm oil nanofuid using experimental data. J. Therm. Anal. Calorim. *144*, 1175–1186.

172. Rubbi, F., Habib, K., Saidur, R., Aslfattahi, N., Yahya, S.M., and Das, L. (2020). Performance optimization of a hybrid PV/T solar system using Soybean oil/MXene nanofluids as a new class of heat transfer fluids. Sol. Energy *208*, 124–138.

173. Das, L., Habib, K., Saidur, R., Aslfattahi, N., Yahya, S.M., and Rubbi, F. (2020). Improved thermophysical properties and energy efficiency of aqueous ionic liquid/MXene nanofluid in a hybrid PV/T solar system. Nanomaterials *10*, 1372–1426.

174. Bakthavatchalam, B., Habib, K., Saidur, R., Aslfattahi, N., Yahya, S.M., Rashedi, A., and Khanam, T. (2021). Optimization of thermophysical and rheological properties of MXene ionanofluids for hybrid solar photovoltaic/thermal systems. Nanomaterials *11*, 320.

175. Wang, H., Li, X., Luo, B., Wei, K., and Zeng, G. (2021). The MXene/water nanofluids with high stability and photo-thermal conversion for direct absorption solar collectors: a comparative study. Energy *227*, 120483.

176. Abdelrazik, A.S., Tan, K.H., Aslfattahi, N., Arifutzzaman, A., Saidur, R., and Al-Sulaiman, F.A. (2020). Optical, stability and energy performance of water-based MXene nanofluids in hybrid PV/thermal solar systems. Sol. Energy *204*, 32–47.

177. Xu, C., Wang, L., Liu, Z., Chen, L., Guo, J., Kang, N., Ma, X.L., Cheng, H.M., and Ren, W. (2015). Large-area high-quality 2D ultrathin Mo_2C superconducting crystals. Nat. Mater. *14*, 1135–1141.

178. Yang, C., Jiang, Q., Li, W., He, H., Yang, L., Lu, Z., and Huang, H. (2019). Ultrafine Pt nanoparticle-decorated 3D hybrid architectures built from reduced graphene oxide and MXene nanosheets for methanol oxidation. Chem. Mater. *31*, 9277–9287.

179. Geng, D., Zhao, X., Li, L., Song, P., Tian, B., Liu, W., Chen, J., Shi, D., Lin, M., Zhou, W., and Loh, K.P. (2016). Controlled growth of ultrathin Mo_2C superconducting crystals on liquid Cu surface. 2D Mater. *4*, 011012.

180. Hu, S., Li, S., Xu, W., Zhang, J., Zhou, Y., and Cheng, Z. (2019). Rapid preparation, thermal stability and electromagnetic interference shielding properties of two-dimensional Ti_3C_2 MXene. Ceram.Int. *45*, 19902–19909.

181. Natu, V., Sokol, M., Verger, L., and Barsoum, M.W. (2018). Effect of edge charges on stability and aggregation of $Ti_3C_2T_z$ MXene colloidal suspensions. J. Phys. Chem. C *122*, 27745–27753.

182. Omomo, Y., Sasaki, T., Wang, L., and Watanabe, M. (2003). Redoxable nanosheet crystallites of MnO2 derived via delamination of a layered manganese oxide. J. Am. Chem. Soc. *125*, 3568–3575.

183. Wang, D., Fang, Y., Yu, W., Wang, L., Xie, H., and Yue, Y. (2021). Significant solar energy absorption of MXene $Ti_3C_2T_x$ nanofluids via localized surface plasmon resonance. Sol. Energy Mater. Sol. Cell. *220*, 110850.

184. Zhao, X., Zha, X.J., Pu, J.H., Bai, L., Bao, R.Y., Liu, Z.Y., Yang, M.B., and Yang, W. (2019). Macroporous three-dimensional MXene architectures for highly efficient solar steam generation. J. Mater. Chem. *7*, 10446–10455.

185. Yu, Z., and Wu, P. (2020). Biomimetic MXene-polyvinyl alcohol composite hydrogel with vertically aligned channels for highly efficient solar steam generation. Adv. Mater. Technol. *5*, 2000065.

186. Li, W., Tian, X., Li, X., Liu, J., Li, C., Feng, X., Shu, C., and Yu, Z.Z. (2022). An environmental energy-enhanced solar steam evaporator derived from MXene-decorated cellulose acetate cigarette filter with ultrahigh solar steam generation efficiency. J. Colloid Interface Sci. *606*, 748–757.

187. Liu, G., Shen, J., Liu, Q., Liu, G., Xiong, J., Yang, J., and Jin, W. (2018). Ultrathin two-dimensional MXene membrane for pervaporation desalination. J. Membr. Sci. *548*, 548–558.

188. Zhang, Q., Yi, G., Fu, Z., Yu, H., Chen, S., and Quan, X. (2019). Vertically aligned Janus MXene-based aerogels for solar desalination with high efficiency and salt resistance. ACS Nano *13*, 13196–13207.

189. Zhao, J., Yang, Y., Yang, C., Tian, Y., Han, Y., Liu, J., Yin, X., and Que, W. (2018). A hydrophobic surface enabled salt-blocking 2D Ti_3C_2 MXene membrane for efficient and stable solar desalination. J. Mater. Chem. *6*, 16196–16204.

190. Tan, Y.Z., Wang, H., Han, L., Tanis-Kanbur, M.B., Pranav, M.V., and Chew, J.W. (2018). Photothermal-enhanced and fouling-resistant membrane for solar-assisted membrane distillation. J. Membr. Sci. *565*, 254–265.

191. Xiang, Z., Shi, Y., Zhu, X., Cai, L., and Lu, W. (2021). Flexible and waterproof 2D/1D/0D construction of MXene based nanocomposites for electromagnetic wave absorption, EMI shielding, and photothermal conversion. Nano-Micro Lett. *13*, 150.

192. Ju, M., Yang, Y., Zhao, J., Yin, X., Wu, Y., and Que, W. (2019). Macroporous 3D MXene architecture for solar-driven interfacial water evaporation. J. Adv. Dielect. *09*, 1950047.

193. Liu, P., Zhou, T., Teng, Y., Fu, L., Hu, Y., Lin, X., Kong, X.Y., Jiang, L., and Wen, L. (2021). Light-induced heat driving active ion transport based on 2D MXene nanofluids for enhancing osmotic energy conversion. CCS Chem. *3*, 1325–1335.

194. Zhang, Q., Fu, Z., Yu, H., and Chen, S. (2020). Nanoplating of a SnO_2 thin-film on MXene-based sponge for stable and efficient solar energy conversion. J. Mater. Chem. *8*, 8065–8074.

195. Zhou, B., Li, Y., Li, Z., Ma, J., Zhou, K., Liu, C., Shen, C., and Feng, Y. (2021). Fire/heat-resistant, anti-corrosion and folding $Ti_2C_3T_x$ MXene/single-walled carbon nanotube films for extreme-environmental EMI shielding and solar-thermal conversion applications. J. Mater. Chem. C *9*, 10425–10434.

196. Liu, X., Jin, X., Li, L., Wang, J., Yang, Y., Cao, Y., and Wang, W. (2020). Air-permeable, multifunctional, dual-energydriven MXene-decorated polymeric textile-based wearable heaters with exceptional electrothermal and photothermal conversion performance. J. Mater. Chem. *8*, 12526–12537.

197. Chen, X., Tang, Z., Gao, H., Chen, S., and Wang, G. (2020). Phase change materials for electro-thermal conversion and storage: from fundamental understanding to engineering design. iScience *23*, 101208.

198. Li, K., Chang, T.H., Li, Z., Yang, H., Fu, F., Li, T., Ho, J.S., and Chen, P.Y. (2021). Biomimetic MXene textures with enhanced light-to-heat conversion for solar steam generation and wearable thermal management. Compos. B Eng. *217*, 108902.

199. Zhao, X., Peng, L.M., Tang, C.Y., Pu, J.H., Zha, X.J., Ke, K., Bao, R.Y., Yang, M.B., and Yang, W. (2020). All-weather-available, continuous steam generation based on the synergistic photo-thermal and electro-thermal conversion by MXene-based aerogel. Mater.Horiz. *7*, 855–865.

200. Li, J., Chen, J., Wang, H., and Xiao, X. (2021). All-MXene cotton-based supercapacitor-powered human body thermal management system. Chemelectrochem *8*, 607–655.

201. Luo, J., Gao, S., Luo, H., Wang, L., Huang, X., Guo, Z., Lai, X., Lin, L., Li, R.K., and Gao, J. (2021). Superhydrophobic and breathable smart MXene-based textile for multifunctional wearable sensing electronics. Chem. Eng. J. *406*, 126898.

202. Nguyen, V.P., Lim, M., Kim, K.S., Kim, J.H., Park, J.S., Yuk, J.M., and Lee, S.M. (2021). Drastically increased electrical and thermal conductivities of Pt-infiltrated MXenes. J. Mater. Chem. *9*, 10739–10746.

203. Sang, M., Liu, G., Liu, S., Wu, Y., Xuan, S., Wang, S., Xuan, S., Jiang, W., and Gong, X. (2021). Flexible PTFE/MXene/PI soft electrothermal actuator with electromagnetic-interference shielding property. Chem. Eng. J. *414*, 128883.

204. Liu, X., Du, X., Li, L., Cao, Y., Yang, Y., Wang, W., and Wang, J. (2022). Multifunctional AgNW@MXene decorated polymeric textile for highly-efficient electro-/photothermal conversion and triboelectric nanogenerator. Compos. Appl. Sci. Manuf. *156*, 106883.

205. Gong, S., Ding, Y., Li, X., Liu, S., Wu, H., Lu, X., and Qu, J. (2021). Novel flexible polyurethane/MXene composites with sensitive solar thermal energy storage behavior. Compos. Appl. Sci. Manuf. *149*, 106505.

206. Jamil, F., Ali, H.M., and Janjua, M.M. (2021). MXene based Adv. Mater. for thermal energy storage: a recent review. J. Energy Storage *35*, 102322.

207. Xiong, D., Shi, Y., and Yang, H.Y. (2021). Rational design of MXene-based films for energy storage: progress, prospects. Mater. Today *46*, 183–211.

208. Cao, Y., Li, W., Huang, D., Zhang, J., Lin, P., Zhang, L., Sheng, X., Chen, Y., and Lu, X. (2022). One-step construction of novel phase change composites supported by a biomass/MXene gel network for efficient thermal energy storage. Sol. Energy Mater. Sol. Cell. *241*, 111729.

209. Hu, W.w., Shi, X.y., Gao, M.h., Huang, C.h., Huang, T., Zhang, N., Yang, J.h., Qi, X.d., and Wang, Y. (2021). Light-actuated shape memory and self-healing phase change composites supported by MXene/waterborne polyurethane aerogel for superior solar-thermal energy storage. Compos.Commun. *28*, 100980.

210. Sheng, X., Dong, D., Lu, X., Zhang, L., and Chen, Y. (2020). MXene-wrapped bio-based pomelo peel foam/polyethylene glycol composite phase change material with enhanced light-to-thermal conversion efficiency, thermal energy storage capability and thermal conductivity. Compos. Appl. Sci. Manuf. *138*, 106067.

211. Shao, Y.w., Hu, W.w., Gao, M.h., Xiao, Y.y., Huang, T., Zhang, N., Yang, J.h., Qi, X.d., and Wang, Y. (2021). Flexible MXene-coated melamine foam based phase change material composites for integrated solar-thermal energy conversion/storage, shape memory and thermal therapy functions. Compos. Appl. Sci. Manuf. *143*, 106291.

212. Hu, G., Kang, J., Ng, L.W.T., Zhu, X., Howe, R.C.T., Jones, C.G., Hersam, M.C., and Hasan, T. (2018). Functional inks and printing of two-dimensional materials. Chem. Soc. Rev. *47*, 3265–3300.

213. Truby, R.L., and Lewis, J.A. (2016). Printing soft matter in three dimensions. Nature *540*, 371–378.

214. Zhang, Y.Z., Wang, Y., Jiang, Q., El-Demellawi, J.K., Kim, H., and Alshareef, H.N. (2020). MXene printing and patterned coating for device applications. Adv. Mater. *32*, 1908486.

215. Sreenilayam, S.P., Ul Ahad, I., Nicolosi, V., and Brabazon, D. (2021). MXene materials based printed flexible devices for healthcare, biomedical and energy storage applications. Mater. Today *43*, 99–131.

216. Vuorinen, T., Niittynen, J., Kankkunen, T., Kraft, T.M., and Mäntysalo, M. (2016). Inkjet-printed graphene/PEDOT: PSS temperature sensors on a skin-conformable polyurethane substrate. Sci. Rep. *6*, 35289.

217. Aki, D., Ulag, S., Unal, S., Sengor, M., Ekren, N., Lin, C.C., Yılmazer, H., Ustundag, C.B., Kalaskar, D.M., and Gunduz, O. (2020). 3D printing of PVA/hexagonal boron nitride/bacterial cellulose composite scaffolds for bone tissue engineering. Mater.Des. *196*, 109094.

218. Xing, R., Xia, Y., Huang, R., Qi, W., Su, R., and He, Z. (2020). Three-dimensional printing of black phosphorous/polypyrrole electrode for energy storage using thermoresponsive ink. Chem. Commun. *56*, 3115–3118.

219. McManus, D., Dal Santo, A., Selvasundaram, P.B., Krupke, R., LiBassi, A., and Casiraghi, C. (2018). Photocurrent study of all-printed photodetectors on paper made of different transition metal dichalcogenide nanosheets. Flex. Print. Electron. *3*, 034005.

220. Jadhav, A., and Jadhav, V.S. (2022). A review on 3D printing: an additive manufacturing technology. Mater.Today Proc. *62*, 2094–2099.

221. Chandwani, L., Sharma, H., and Kumar, P. (2020). A review on 3D printing technology. Int. J. Eng. Sci. *2*, 3072–3074.

222. Yang, W., Yang, J., Byun, J.J., Moissinac, F.P., Xu, J., Haigh, S.J., Domingos, M., Bissett, M.A., Dryfe, R.A.W., and Barg, S. (2019). 3D printing of freestanding MXene architectures for current-collector-free supercapacitors. Adv. Mater. *31*, 1902725.

223. Orangi, J., Hamade, F., Davis, V.A., and Beidaghi, M. (2020). 3D printing of additive-free 2D $Ti_3C_2T_x$ (MXene) ink for fabrication of micro-supercapacitors with ultra-high energy densities. ACS Nano *14*, 640–650.

224. Shen, K., Li, B., and Yang, S. (2020). 3D printing dendrite-free lithium anodes based on the nucleated MXene arrays. Energy Storage Mater. *24*, 670–675.

225. Cao, W., Ma, C., Mao, D., Zhang, J., Ma, M., and Chen, F. (2019). MXene-reinforced cellulose nanofibril inks for 3D-printed smart fibres and textiles. Adv. Funct. Mater. *29*, 1905898.

226. Cain, J.D., Azizi, A., Maleski, K., Anasori, B., Glazer, E.C., Kim, P.Y., Gogotsi, Y., Helms, B.A., Russell, T.P., and Zettl, A. (2019). Sculpting liquids with two-dimensional materials: the assembly of $Ti_3C_2T_x$ MXene sheets at liquid-liquid interfaces. ACS Nano *13*, 12385–12392.

227. Huang, B., Zhou, Z., Wei, L., Song, Q., Yu, W., Zhou, Y., Hu, R., Zhang, W., and Lu, C. (2021). $Ti_3C_2T_x$ MXene as a novel functional photo blocker for stereolithographic 3D printing of multifunctional gels via continuous liquid interface production. Compos. B Eng. *225*, 109261.

228. Jambhulkar, S., Liu, S., Vala, P., Xu, W., Ravichandran, D., Zhu, Y., Bi, K., Nian, Q., Chen, X., and Song, K. (2021). Aligned $Ti_3C_2T_x$ MXene for 3D micropatterning via additive manufacturing. ACS Nano *15*, 12057–12068.

229. Yuan, W., Liu, H., Wang, X., Huang, L., Yin, F., and Yuan, Y. (2021). Conductive MXene/melamine sponge combined with 3D printing resin base prepared as an electromagnetic interference shielding switch. Compos. Appl. Sci. Manuf. *143*, 106238.

230. Yu, L., Li, W., Wei, C., Yang, Q., Shao, Y., and Sun, J. (2020). 3D Printing of NiCoP/Ti_3C_2 MXene architectures for energy storage devices with high areal and volumetric energy density. Nano-Micro Lett. *12*, 143.

231. Akshay Kumar, K., Ghosh, K., Alduhaish, O., and Pumera, M. (2021). Dip-coating of MXene and transition metal dichalcogenides on 3D-printed nanocarbon electrodes for the hydrogen evolution reaction. Electrochem.Commun. *122*, 106890.

232. Wei, C., Tian, M., Fan, Z., Yu, L., Song, Y., Yang, X., Shi, Z., Wang, M., Yang, R., and Sun, J. (2021). Concurrent realization of dendrite-free anode and high-loading cathode via 3D printed N-Ti_3C_2 MXene framework toward advanced Li–S full batteries. Energy Storage Mater. *41*, 141–151.

233. Hu, Q., Sun, D., Wu, Q., Wang, H., Wang, L., Liu, B., Zhou, A., and He, J. (2013). MXene: a new family of promising hydrogen storage medium. J. Phys. Chem. A *117*, 14253–14260.

234. Kumar, P., Singh, S., Hashmi, S., and Kim, K.H. (2021). MXenes: emerging 2D materials for hydrogen storage. Nano Energy *85*, 105989.

235. Han, M., Liu, Y., Rakhmanov, R., Israel, C., Tajin, M.A.S., Friedman, G., Volman, V., Hoorfar, A., Dandekar, K.R., and Gogotsi, Y. (2021). Solution-processed $Ti_3C_2T_x$ MXene antennas for radio-frequency communication. Adv. Mater. *33*, 2003225.

236. Habib, T., Patil, N., Zhao, X., Prehn, E., Anas, M., Lutkenhaus, J.L., Radovic, M., and Green, M.J. (2019). Heating of $Ti_3C_2T_x$ MXene/polymer composites in response to radio frequency fields. Sci. Rep. *9*, 16489.

237. Chen, J., Li, H., Guo, S., Yang, Z., Sun, S., Zeng, J., Gou, H., Chen, Y., Wang, F., Lin, Y., et al. (2022). CO_2 capture and conversion to value-added products promoted by MXene-based materials. Orphanet J. Rare Dis. *17*, 394–410.

238. Morales-García, Á., Fernández-Fernández, A., Viñes, F., and Illas, F. (2018). CO_2 abatement using two-dimensional MXene carbides. J. Mater. Chem. *6*, 3381–3385.

239. Morales-García, Á., Mayans-Llorach, M., Viñes, F., and Illas, F. (2019). Thickness biased capture of CO_2 on carbide MXenes. Phys. Chem. Chem. Phys. *21*, 23136–23142.

240. Shamsabadi, A.A., Isfahani, A.P., Salestan, S.K., Rahimpour, A., Ghalei, B., Sivaniah, E., and Soroush, M. (2020). Pushing rubbery polymer membranes to be economic for CO_2 separation: embedment with $Ti_3C_2T_x$ MXene Nanosheets. ACS Appl. Mater. Interfaces *12*, 3984–3992.

241. Kumar, J.A., Prakash, P., Krithiga, T., Amarnath, D.J., Premkumar, J., Rajamohan, N., Vasseghian, Y., Saravanan, P., and Rajasimman, M. (2022). Methods of synthesis, characteristics, and environmental applications of MXene: a comprehensive review. Chemosphere *286*, 131607.

242. Li, S., Wang, L., Peng, J., Zhai, M., and Shi, W. (2019). Efficient thorium (IV) removal by two dimensional Ti_2CT_x MXene from aqueous solution. Chem. Eng. J. *366*, 192–199.

243. Zou, X., Liu, H., Xu, H., Wu, X., Han, X., Kang, J., and Reddy, K.M. (2021). A simple approach to synthesis Cr_2CT_x MXene for efficient hydrogen evolution reaction. Mater. Today Energy *20*, 100668.

244. He, Z., Huang, D., Yue, G., Zhu, J., and Zhao, P. (2021). Ca^{2+} induced 3D porous MXene gel for continuous removal of phosphate and uranium. Appl. Surf. Sci. *570*, 150804.